AN INTEGRATED SEISMIC HAZARD FRAMEWORK FOR LIQUEFACTION TRIGGERING ASSESSMENT OF EARTHFILL DAMS' FOUNDATION SOILS

A THESIS SUBMITTED TO
THE GRADUATE SCHOOL OF NATURAL AND APPLIED SCIENCES
OF
MIDDLE EAST TECHNICAL UNIVERSITY

BY

SEVİNÇ ÜNSAL ORAL

IN PARTIAL FULFILLMENT OF THE REQUIREMENTS
FOR
THE DEGREE OF MASTER OF SCIENCE
IN
CIVIL ENGINEERING

FEBRUARY 2009

Approval of the thesis:

AN INTEGRATED SEISMIC HAZARD FRAMEWORK FOR LIQUEFACTION TRIGGERING ASSESSMENT OF EARTHFILL DAMS' FOUNDATION SOILS

submitted by **SEVİNÇ ÜNSAL ORAL** in partial fulfillment of the requirements for the degree of **Master of Science in Civil Engineering Department**, **Middle East Technical University** by,

Prof. Dr. Canan Özgen
Dean, Graduate School of **Natural and Applied Sciences** _____

Prof. Dr. Güney Özcebe
Head of Department, **Civil Engineering** _____

Assoc Prof Dr. Kemal Önder Çetin
Supervisor, **Civil Engineering Dept., METU** _____

Prof. Dr. M. Yener Özkan
Co-Supervisor, **Civil Engineering Dept., METU** _____

Examining Committee Members:

Prof. Dr. Orhan Erol
Civil Engineering Dept., METU _____

Assoc. Prof. Dr. Kemal Önder Çetin
Civil Engineering Dept., METU _____

Prof. Dr. M. Yener Özkan
Civil Engineering Dept., METU _____

Dr. Kartal Toker
Civil Engineering Dept., METU _____

Assist. Prof. Dr. Nihat Sinan Işık
Techical Education Faculty, Gazi University _____

Date: 10.02.2009

I hereby declare that all information in this document has been obtained and presented in accordance with academic rules and ethical conduct. I also declare that, as required by these rules and conduct, I have fully cited and referenced all material and results that are not original to this work.

Name, Last name: SEVİNÇ ÜNSAL ORAL

Signature :

ABSTRACT

AN INTEGRATED SEISMIC HAZARD FRAMEWORK FOR LIQUEFACTION TRIGGERING ASSESSMENT OF EARTHFILL DAMS' FOUNDATION SOILS

Ünsal Oral, Sevinç
M.Sc., Department of Civil Engineering
Supervisor: Assoc. Prof Dr. Kemal. Önder Çetin
Co-Supervisor: Prof. Dr. M. Yener Özkan

February 2009, 150 pages

Within the confines of this study, seismic soil liquefaction triggering potential of a dam foundation is assessed within an integrated probabilistic seismic hazard assessment framework. More specifically, the scheme presented hereby directly integrates effective stress-based seismic soil liquefaction triggering assessment with seismic hazard analysis framework, supported by an illustrative case. The proposed methodology successively, i) processes the discrete stages of probabilistic seismic hazard workflow upon seismic source characterization, ii) numerically develops the target elastic acceleration response spectra for typical rock sites, covering all the earthquake scenarios that are re-grouped with respect to earthquake magnitude and distance, iii) matches the strong ground motion records selected from a database with the target response spectra for every defined scenario, and iv) performs 2-D equivalent linear seismic response analyses of a 56 m high earth fill dam founded on 24 m thick alluvial deposits. Results of seismic response analyses are presented in the form of annual

probability of excess pore pressure ratios and seismically-induced lateral deformations exceeding various threshold values. For the purpose of assessing the safety of the dam slopes, phi-c reduction based slope stability analyses were also performed representing post-liquefaction conditions. After having integrated this phi-c reduction analyses results into the probabilistic hazard framework, annual probabilities of factor of safety of slopes exceeding various threshold values were estimated. As the concluding remark, probability of liquefaction triggering, induced deformations and factor of safeties are presented for a service life of 100 years. It is believed that the proposed probabilistic seismic performance assessment methodology which incorporates both phi-c reduction based failure probabilities and seismic soil liquefaction-induced deformation potentials, provides dam engineers a robust methodology to rationally quantify the level of confidence with their decisions regarding if costly mitigation of dam foundation soils against seismic soil liquefaction triggering hazard and induced risks is necessary.

Keywords: Seismic hazard, liquefaction, earthfill dams, dynamic analysis,

ÖZ

BARAJ TEMELLERİNDE SIVILAŞMA TETİKLENMESİ BELİRLEMESİ İÇİN TÜMLEŞİK SİSMİK TEHLİKE ANALİZİ YAKLAŞIMI

Ünsal Oral, Sevinç
Yüksek Lisans, İnşaat Mühendisliği Bölümü
Tez Yöneticisi: Doç. Dr. Kemal Önder Çetin
Y. Tez Yöneticisi: Prof. Dr. M. Yener Özkan

Şubat 2009, 150 sayfa

Bu çalışmanın kapsamında, baraj temellerinin zemin sıvılaşması tetiklenme potansiyelini sismik tehlike analizi çerçevesinde belirlemek için tümleşik bir yaklaşım geliştirilmiştir. Sunulan tezin örnek bir problemle desteklenmiş akış şeması, efektif gerilme tabanlı sismik zemin sıvılaşması potansiyeli belirlemesiyle olasılıksal sismik tehlike analizini doğrudan tümleştirmektedir. Önerilen yöntem sırasıyla, i) sismik kaynak tanımlaması sonrasında olasılıksal sismik tehlike analizi akışının tanımlı parçalarını işlemekte, ii) tipik kaya sahalar icin deprem büyüklüğü ve kaynak-saha mesafesine göre yeniden gruplandırılmış her senaryo kümesi için hedef elastik ivme tepki spektrumlarını oluşturmakta, iii) deprem veritabanlarından seçilmiş kayıtları hedef tepki spektrumlarıyla eşlemekte, ve iv) 24 m kalınlığındaki alüvyon çökeltisi üzerinde yer alan 56 m yüksekliğindeki bir toprak dolgu baraj için iki boyutlu eşdeğer lineer sismik tepki analizlerini gerçekleştirmektedir. Sismik tepki analizlerinin sonuçları, aşırı

boşluk suyu basıncı oranının ve yanal deformasyonların belirli bir eşik değere karşılık gelen senelik aşılma olasılıklarını ifade eden risk eğrileri şeklinde ifade edilmektedir. Bununla birlikte, sıvılaşma ve meydana gelecek yanal deformasyonların olasılıksal ifadesi yüz senelik ekonomik ömür içerisinde sunulmuştur. Önerilen olasılıksal sismik performans belirleme yönteminin, baraj mühendislerinin, potansiyel olarak sıvılaşabilir temel zeminlerini sıyırma kararlarını rasyonel ve niceleştirilmiş bir şekilde vermelerine yardımcı olacağına inanılmaktadır.

Anahtar Kelimeler: Sismik tehlike, Zemin sıvılaşması, Toprak dolgu baraj, dinamik analiz.

To my family

ACKNOWLEDGEMENTS

I would like to express my sincere thanks to my supervisor Assoc. Prof. Dr. Kemal Önder Çetin for his constant encouragement and support throughout my study. Without his ambition, creative ideas, clear expression and concern of the detail, this thesis would not have been possible.

I wish to thank Prof. Dr. M. Yener Özkan for his invaluable suggestions.

I wish to thank to Anıl Yunatcı for his technical support and valuable help.

I wish to thank my husband Yaşar Zahit Oral for his unwavering support during my studies. His dear love and infinite patience were certainly fundamental to my success.

I would like to thank to my parents Nazmiye and İlyas Ünsal, and my sister Seçil Ünsal. Their unconditional love, continued encouragement and belief in my abilities nurtured me throughout this process. Essentially words are not enough to thank my family for their endless support.

Finally, I would like to thank all my friends, for their friendship and fellowship in nearby or kilometers away. I feel lucky to have their friendship.

TABLE OF CONTENTS

LIST OF TABLES

TABLE

LIST OF FIGURES

FIGURE

LIST OF ABBREVIATIONS

CRR	Cyclic Resistance Ratio
CSR	Cyclic Stress Ratio
CSR_{eq}	Equivalent Cyclic Resistance Ratio
a_{max}	Peak Horizontal Ground Surface Acceleration
g	Acceleration of Gravity
σ_v	Total Vertical Stress
σ'_v	Effective Vertical Stress
r_d	Nonlinear Shear Mass Participation Factor
FS	Factor of Safety
DWF_M	Duration Weighting Factor
FC	Fines Content
K_σ	Over burden Correction Factor
P_L	Probability of Liquefaction
Φ	Standard Cumulative Normal Distribution
Φ^{-1}	Inverse of the Standard Cumulative Normal Distribution
$N_{1,60}$	Normalized Standard Penetration Resistance Value
$N_{1,60,cs}$	Fines-Corrected Standard Penetration Resistance
M_w	Moment Magnitude
M_o	Seismic Moment
M_{min}	Minimum Magnitude Earthquake
M_{max}	Maximum Magnitude Earthquake
PSHA	Probabilistic Seismic Hazard Analysis
μ	Rigidity of the Crust
A	Area of the Fault
D	Average Slip on the Fault

$\mathbf{S}$	Slip Rate
$\mathbf{f_m(m)}$	Magnitude Density Function
$\mathbf{N(M_{min})}$	Activity Rate
$\mathbf{r_{jb}}$	Rupture Distance
$\mathbf{V_S}$	Shear Wave Velocity
$\mathbf{\sigma^2_e}$	Earthquake-to-Earthquake Component of the Variability
$\mathbf{Y}$	Peak Horizontal Acceleration in g
OBE	Operating Basis Earthquake
MCE	Maximum Credible Earthquake
$\mathbf{E}$	Elastic Modulus
$\mathbf{K}$	Bulk Modulus
$\mathbf{G}$	Shear Modulus
$\mathbf{\nu}$	Poisson's Ratio
$\mathbf{\Delta e_{ij}}$	Incremental Strain Tensor
$\mathbf{u_i}$	Displacement Rate
$\mathbf{\Delta t}$	Time Step
$\mathbf{\varepsilon}$	Axial Strain
$\mathbf{\varepsilon^e}$	Elastic Axial Strain
$\mathbf{\varepsilon^p}$	Plastic Axial Strain
$\mathbf{\gamma}$	Shear Strain
$\mathbf{\sigma}$	Normal Stress
$\mathbf{\tau}$	Shear Stress
$\mathbf{S_a}$	Spectral Acceleration
$\mathbf{\ddot{u}_{max}}$	Maximum Crest Acceleration
$\mathbf{k_y}$	Critical Yield Acceleration
$\mathbf{k_m}$	Maximum Rock Acceleration
$\mathbf{d}$	Damping Ratio
$\mathbf{k}$	Seismic Coefficient

CHAPTER 1

INTRODUCTION

1.1 Research Statement

Earthquakes are probably one of the most frightening naturally occurring hazards encountered. They typically occur with little warnings and have devastating effects, resulting in hundreds to thousands of deaths and injuries, and millions to billions of dollars worth of property damage.

The consequences of a dam failure during an earthquake are very serious, because the water released from the reservoir could cause severe flooding downstream. A number of earth dams have failed or suffered large displacements during past earthquakes. Therefore, seismic performance of embankment dams has been a topic of considerable interest since early 20^{th} century. In parallel to the understanding of its importance, the available methods have improved from simple pseudo-static to more complicated finite element or difference analyses.

After some earthquakes, the damage was associated to large reduction in the stiffness and strength of saturated cohesionless soils (liquefaction). Primary cause of the damage or failure was explained by the build-up of pore water pressures in the embankment and the possible loss of strength due to these high pore pressures (Seed et al. 1978). Almost failure of Van Norman (San Fernando) dams during the 1971 San Fernando earthquake, California can be referred as a vivid example of liquefaction-induced damage. The crest of the upper dam slides towards downstream for about 1.5 m accompanied by almost catastrophic failure of the upstream slope, which had been founded on liquefiable alluvial soils.

Within the scope of this study, seismic soil liquefaction triggering potential of a dam foundation is assessed within an integrated probabilistic seismic hazard assessment framework. More specifically, the scheme presented hereby directly integrates effective stress-based seismic soil liquefaction triggering assessment with seismic hazard analysis framework for a 56 m high earthfill dam, founded on 24 m thick alluvial deposits.

1.2 Research Significance

Liquefaction of soils, continues to be a major cause of damage and loss of life after earthquakes (e.g.; the 1964 Alaska, 1964 Niigata, 1983 Nihonkai-Chubu, 1989 Loma Prieta, 1993 Kushiro-Oki, 1994 Northridge, 1995 Hyogoken-Nambu (Kobe), 1999 Kocaeli and 1999 Ji-Ji earthquakes). In the last 40 years, liquefaction engineering assessment of earthfill dams has evolved from one step simple, mostly deterministic assessment to multi step engineering evaluations of i) "triggering" or initiation of soil liquefaction, to a more rigorous methodology additionally including the assessment of ii) post-liquefaction strength and overall post liquefaction stability, iii) expected liquefaction induced deformations and displacements, iv) the consequences of these deformations and displacements, v) engineered mitigation, if necessary. Within the confines of this manuscript, it is intended to develop a methodology for the probabilistically-based seismic soil liquefaction triggering-induced risk assessment of a 56 m high earthfill dam, founded on 24 m thick alluvial deposits.

Results of seismic response analyses are presented in the form of annual probability of excess pore pressure ratios and lateral deformations exceeding certain threshold values. For the purpose of assessing the safety of the dam slopes, phi-c reduction based slope stability analyses were also performed for post liquefaction conditions. By using these phi-c reduction results within a probabilistic framework, annual probabilities of factor of safety of slopes exceeding various threshold values were estimated. As the concluding remark,

probability of liquefaction triggering, induced deformations and factor of safeties are presented for a service life of 100 years. It is believed that the proposed probabilistic seismic performance assessment methodology, which incorporates both ϕ-c reduction based failure probabilities and seismic soil liquefaction-induced deformation potentials, provides dam engineers to rationally quantify the level of confidence with their decisions regarding if costly mitigation of dam foundation soils against seismic soil liquefaction triggering hazard and induced risks is necessary.

1.3 Thesis Organization and Scope

This thesis is composed of seven main sections. Contents of each chapter are summarized as follows:

In the first chapter, the research statement and introductory comments are presented.

Chapter 2 presents a general literature overview for the: i) definition of embankment dams, ii) seismic response of earthfill dams and iii) seismic soil liquefaction engineering.

Chapter 3 summarizes available information about the seismic hazard assessment methodology; source characterization, attenuation relationships and general framework for assessing design earthquake motions.

Chapter 4 describes the steps followed as part of the 2-D effective stress based seismic response analyses of a earthfill dam including i) mesh generation, constitutive model basics and model parameter , ii) static analysis of the earthfill dam, and iii) dynamic response analyses.

In chapter 5, the post processing of the numerical analyses results are presented to illustrate the overall seismic performance of the dam for a service life of 100 years in terms of i) horizontal deformations and excess pore pressure ratios , ii) ϕ-c reduction based estimated factor of safeties. As the concluding remark, comparisons between the deterministic and probabilistic seismic hazard and risk assessments were presented.

Chapter 6 summarized the research findings and the concluding remarks.

Finally in the appendix software codes and earthquake records are given.

CHAPTER 2

LITERATURE SURVEY

2.1 Definition of Embankment Dams

ICOLD (1985) (International Commission of Large Dams) defined an embankment dam as, "any dam constructed of excavated materials placed without addition of binding materials other than those inherent in the natural material. The materials are usually obtained at or near the dam site".

Embankment dams are constructed primarily of compacted earth, either homogeneous or zoned, and containing more than 50% of earth. They are classified into two main categories by types of construction materials used, namely earthfill and rockfill dams.

Many small embankment dams are built entirely of a single type of material such as stream alluvium, weathered bedrock, or glacial till. These are homogeneous earthfill dams, constructed more or less of uniform natural material. Larger embankment dams are zoned and constructed of a variety of materials. An important element in a zoned rockfill dam is an impermeable blanket or core which usually consists of clayey materials obtained locally. Typical cross sections of embankment dams are shown in Figure 2.1.

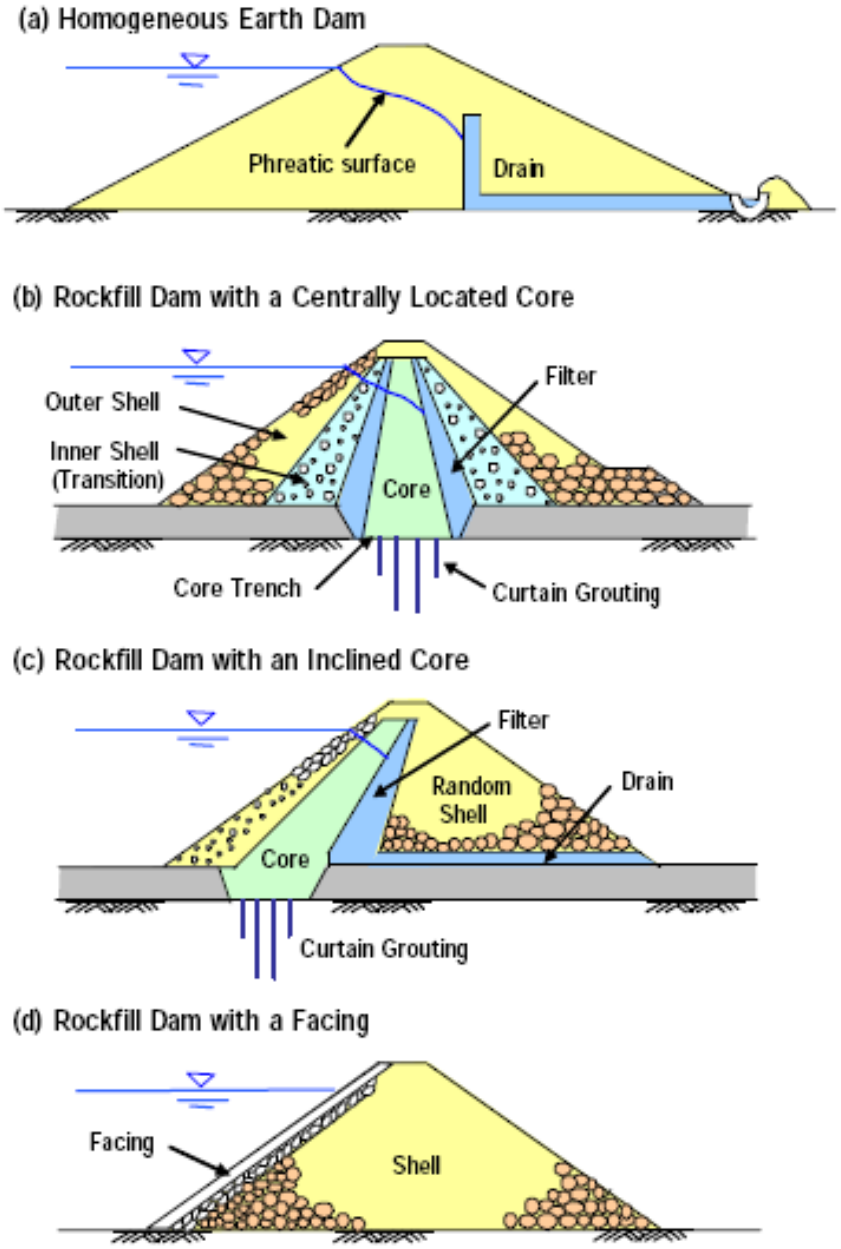

(Thomas, Henry H.1976, The Engineering of Large Dams)

Figure 2.1: Types of Embankment Dams

Embankment dams are built on a variety of foundations, ranging from weak glacial deposits to durable rock. The damage on embankments have been particularly destructive during various earthquakes when the underlying

saturated granular soils liquefied, resulting in cracking, settlement, lateral displacement, and slumping of the embankment.

2.2 Seismic Response of Embankment Dams

Seismic response of embankment dams has been conventionally assessed by pseudo-static analyses incorporating a 'seismic coefficient', k. This approach of seismic stability of the embankment is based on utilizing a horizontal force which represents the earthquake effect as a product of a 'seismic coefficient' and the weight of the potential sliding mass and determining the static factor of safety of the potential sliding mass under the horizontal loading (earthquake). An important shortcoming with the pseudo-static approach is that, it does not give much of an idea if and how permanent deformations are expected to occur during and after the earthquake.

2.2.1 Permanent Deformation Analysis

Earthquake-induced permanent deformations of an earth dam can be estimated by a number of approaches, varying in their degree of sophistication. Newmark (1965) sliding block analysis is widely used for the estimation of permanent displacements of slopes during earthquakes. Newmark made an analogy between the soil in a potentially unstable slope and a rigid block resting on an inclined plane. In this analysis, the mass of soil located above the critical failure surface is represented by a rigid block. As the rigid block is subjected to dynamic motion, it will slide down the inclined slope, if the block is not in equilibrium. The Newmark analysis, as introduced in 1965, has been modified over the years to improve its accuracy since the soil does not behave as a rigid mass and the slip along the failure plane does not follow elastic-perfectly plastic response.

2.2.2 Seismic Deformation Analysis by Makdisi and Seed Method

The method proposed by Makdisi and Seed (1978) for calculating permanent slope deformation of earth dams produced by earthquake shaking is based on the sliding block method but uses average accelerations computed with the procedure of Chopra (1966) and the shear beam method (Figure 2.2). The findings are summarized on figures that relate the average maximum acceleration with the depth of the potential failure surface (Figure 2.3) and the permanent displacement with yield acceleration for different earthquake magnitudes (Figure 2.4). The latter was produced by numeriacally subjecting real and hypothetical dam cross-sections to several ground motions, scaled to represent different earthquake magnitudes. The following procedure is used in order to evaluate the permanent slope deformations of a potential failure surface.

(i) The maximum acceleration (at crest level) is calculated with an iterative method. With this method the values of the shear modulus, G, damping ratio, d, and shear wave velocity, V_s, are selected and the three dominant modal periods calculated. The spectral accelerations S_{a1}, S_{a2} and S_{a3} are then estimated from tabulated spectral data and thus the maximum acceleration $\ddot{u}_{max}$ at crest level is calculated.

(ii) The critical yield acceleration for the particular failure surface is calculated using the dynamic yield strength (on the failure surface).

(iii) Using the average value read from Figure 2.3, the value of y/h is calculated, and the value $k_y/\ddot{u}_{max}$ of the potential sliding mass is determined.

(iv) By calculating the ratio k_y/k_{max}, the value of the normalized permanent displacement can be estimated from Figure 2.4.

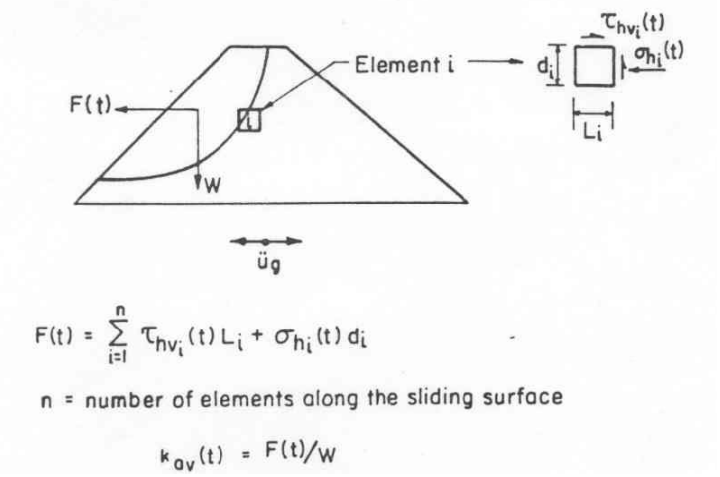

Figure 2.2: Calculation of average acceleration from finite element response analysis (after Makdisi & Seed, 1978)

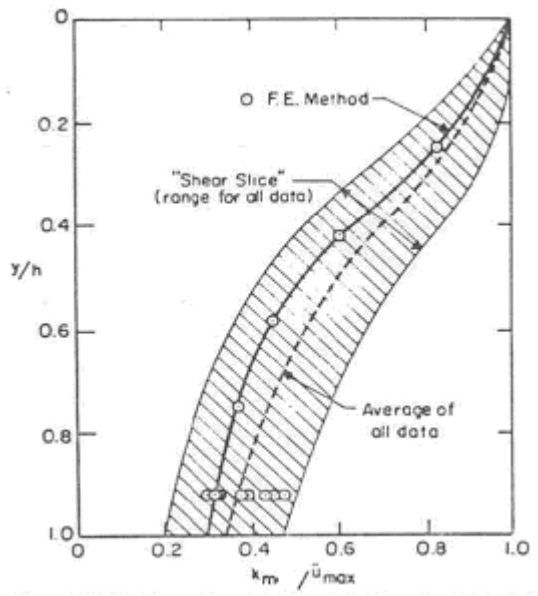

Figure 2.3: Variation of "maximum acceleration ratio" with depth of sliding mass (after Makdisi and Seed, 1978)

Curves given in Figure 2.3, estimate the critical acceleration for rockfill dams with clay core, using limit equilibrium principles, assuming a two-wedge failure plane and that undrained conditions prevail the clay core. The empirical solutions by i) Makdisi and Seed (1978) ii) Sarma and Barbosa (1975) and iii)

Ambraseys (1988) present the permanent deformations on the embankments shown in Figure 2.4.

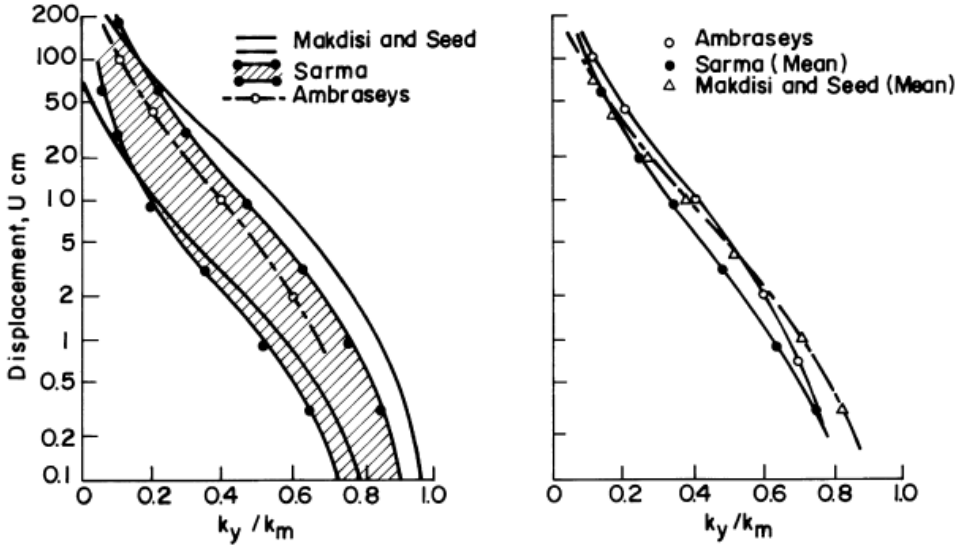

Figure 2.4: Computed displacements of embankment dams subjected to magnitude 6.5 earthquakes having little or no loss of strength due to earthquake induced deformations (After Seed, 1979)

2.3 Seismic Soil Liquefaction Engineering

Liquefaction of soils continues to be a major cause of damage and loss of life after earthquakes (e.g.; the 1964 Alaska, 1964 Niigata, 1983 Nihonkai-Chubu, 1989 Loma Prieta, 1993 Kushiro-Oki, 1994 Northridge, 1995 Hyogoken-Nambu (Kobe), 1999 Kocaeli and 1999 Ji-Ji earthquakes). The "almost failure" of the upstream slope of the Lower San Fernando Dam, downstream of which 80,000 Californian's reside initiated the improvement of seismic design and safety procedures for dams. In the last 40 years, liquefaction engineering assessment of earthfill dams has evolved from one step simple mostly deterministic assessment to more rigorous multi step evaluations of i) the risk of "triggering" (initiation) of liquefaction. ii) post-liquefaction strength and overall post-liquefaction stability, iii) expected liquefaction induced deformations and displacements, iv) the consequences of these deformations and displacements, v) engineered

mitigation, if necessary. Liquefaction engineering assessment is also shown schematically in Figure 2.5.

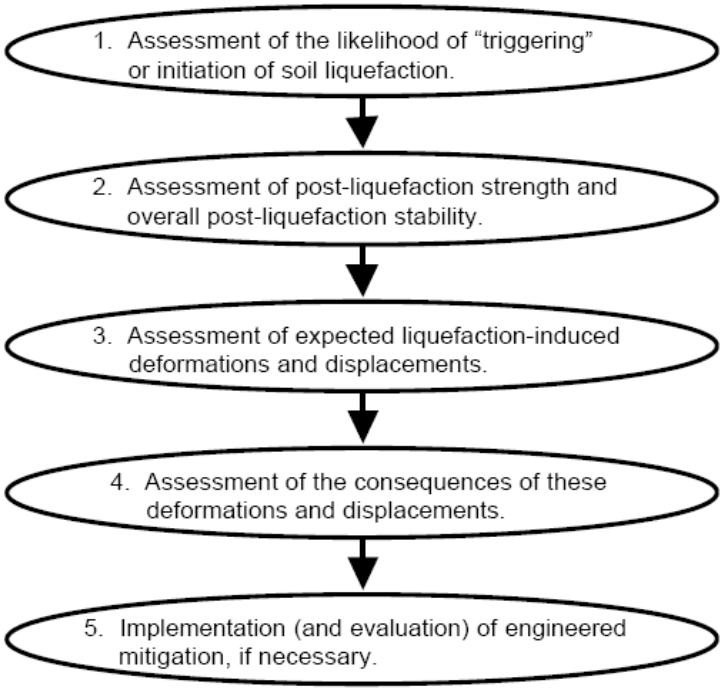

Figure 2.5: Key Elements of Soil Liquefaction Engineering (Seed et. al. 2001)

2.3.1 Liquefaction Definition and Mechanism

Liquefaction is defined as the transformation of a granular material from a solid to a liquefied state as a consequence of increased pore-water pressure and reduced effective stress (Marcuson 1978).

As a consequence of liquefaction, soft, young, water-saturated, well sorted, fine grain sands and silts behave as viscous fluids rather than solids. Liquefaction takes place when seismic shear waves pass through a saturated granular soil

layer, distort its granular structure, and cause some of its pore spaces to collapse. The collapse of the granular structure increases pore space water pressure, and decreases the soil's shear strength. If pore space water pressure increases to the point where the soil's shear strength can no longer support the weight of the overlying soil, buildings, roads, houses, etc., then the soil will flow like a liquid and cause extensive surface damage. Increased water pressure can also trigger landslides and cause the collapse of dams.

As an example case of this phenomenon, Lower San Fernando dam (Figure 2.6), suffered an underwater slide during the San Fernando earthquake, 1971. Fortunately, the dam barely avoided collapse, thereby preventing a potential disaster of flooding of the heavily populated areas below the dam.

Figure 2.6: Lower San Fernando Dam Damage during San Fernando Earthquake, 1971

The term liquefaction has actually been used to describe a number of related phenomena. Because the phenomena can have similar effects, it can be difficult to distinguish between them. The mechanisms causing them, however, are

different. These phenomena can be divided into two main categories: flow liquefaction and cyclic mobility.

2.3.1.1 Flow Liquefaction

Flow liquefaction is a phenomenon in which the static equilibrium is destroyed by static or dynamic loads in a soil deposit with low residual strength. Residual strength is the strength of a liquefied soil. Static loading, for example, can be applied by new buildings on a slope that exert additional forces on the soil beneath the foundations. Earthquakes, blasting, and pile driving are all example of dynamic loads that could trigger flow liquefaction. Once triggered, the strength of a soil susceptible to flow liquefaction is no longer sufficient to withstand the static stresses that were acting on the soil before the disturbance. Sheffield Dam suffered a flow failure triggered by the Santa Barbara Earthquake in 1925 (Figure 2.7). A 90 meter section (of the 220 meter long dam) moved as much as 30 meter downstream. The dam consisted mainly of silty sands and sandy silts excavated from the reservoir and compacted by routing construction equipment over the fill (Seed, 1968).

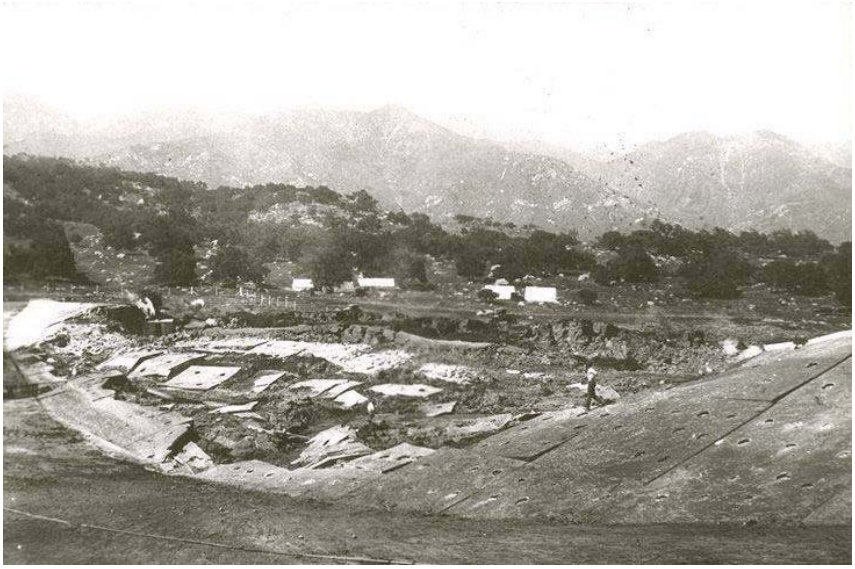

Figure 2.7: Sheffield Dam damage during Santa Barbara Earthquake, 1925

Cyclic softening is another phenomenon that can also produce unacceptably large permanent deformations during earthquake shaking. In contrast to flow liquefaction, cyclic softening occurs when static shear stress is less than the shear strength of the soil. The deformations produced by cyclic softening are driven by both cyclic and static shear stresses. Cyclic softening applies to both strain softening and strain hardening soils.

2.3.1.2 Cyclic Mobility

Cyclic mobility is a liquefaction phenomenon, triggered by cyclic loading, occurring in soil deposits with static shear stresses lower than the soil strength. Deformations due to cyclic mobility develop incrementally because of static and dynamic stresses that exist during an earthquake. Lateral spreading, a common result of cyclic mobility, can occur on gently sloping and on flat ground close to rivers and lakes.

2.3.2 Seismic Soil Liquefaction Triggering

Seed et al. (2001) define the term liquefaction as “significant loss of strength and stiffness due to cyclic pore pressure generation, in contrast to “sensitivity” or loss of strength due to monotonic shearing and/or remolding”. To better understanding of the liquefaction phenomena various investigations are implemented.

Liquefaction triggering assessments were first developed following the 1964 Niigata and Anchorage earthquakes. Laboratory experimentation was used in discerning trends of the phenomena of liquefaction but failed to capture important in situ characteristics such as soil fabric and the effects of aging. Moreover laboratory testing is difficult regarding sample disturbance during both sampling and reconsolidation. It is also expensive to perform high-quality laboratory testing for most seismic problems. Therefore, the use of in-situ testing is common in engineering practice.

Researchers in Japan and the U.S. began characterizing the susceptibility of liquefiable material in relation to the standard penetration test (SPT). The development of the simplified procedure for evaluation of seismically induced shear stresses (Seed & Idriss, 1971) allowed for a concise assessment of stresses within a particular soil layer. Based on SPT data from past events of seismic liquefaction/non-liquefaction, correlations were developed. This part presents the assessment of seismic soil liquefaction triggering potential based on the most common test; Standard Penetration Test (SPT) (Cetin et al., 2000, 2004).

2.3.2.1 SPT-Based Correlations

The standard penetration test (SPT) is an in-situ dynamic penetration test designed to provide information about properties of soil. Criteria for evaluation of liquefaction resistance based on the SPT have been rather robust over the

years and it is widely used for empirical determination of a sand layer's susceptibility to earthquake liquefaction. Those criteria are largely embodied in the CSR versus $N_{1,60}$ plot produced by the most widely accepted and used SPT-based correlations of Seed, et al. (1984) deterministic relationship. $N_{1,60}$ is the normalized SPT value.

The NCEER Working Group reproduce SPT- based correlation proposed by Seed, et al. (1984) as with minor modification at low CSR (NCEER 1997; Youd et al. 2001) shown in Figure 2.8. This familiar relationship is based on comparison between SPT N-values, corrected for both effective overburden stress and energy, equipment and procedural factors affecting SPT testing (to $N_{1,60}$ -values) vs. intensity of cyclic loading, expressed as magnitude-weighted equivalent uniform cyclic stress ratio (CSR_{eq}).or τ_{av}/τ'_{o}. The relationship between corrected $N_{1,60}$-values and the intensity of cyclic loading required to trigger liquefaction is also a function of fines content in this relationship, as shown in Figure 2.8.

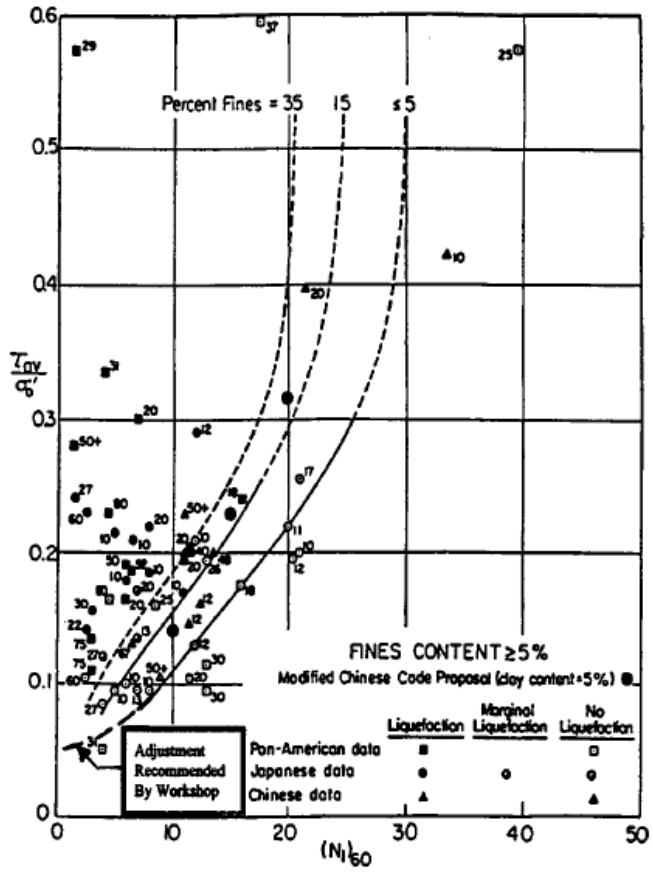

Figure 2.8: Correlation between equivalent uniform cyclic stress ratio and standard penetration test $N_{1,60}$ value for events of magnitude M<7.5 and for varying fines contents, with adjustment at low cyclic stress ratio as recommended by National Center for Earthquake Engineering Research working group (Seed et al. 1984)

Calculation, or estimation, of two variables is required for evaluation of liquefaction resistance of soils: (i) the seismic demand on a soil layer, expressed in terms of CSR; and (ii) the capacity of the soil to resist liquefaction, expressed in terms of cyclic resistance ratio (CRR). Figure 2.8 is a graph of calculated CSR and corresponding $N_{1,60}$ data from sites where liquefaction effects were or were not observed following past earthquakes with magnitudes of approximately 7.5. CRR curves on this graph were conservatively positioned to separate regions with data indicative of liquefaction from regions with data indicative of

nonliquefaction. Curves were developed for granular soils with the fines contents of 5 % or less, 15 %, and 35 % as shown on the plot. The CRR curve for fines contents <5 % is the basic penetration criterion for the simplified procedure and is referred to hereafter as the ‘‘SPT clean sand base curve.’’ The CRR curves in Figure. 2.8 are valid only for magnitude 7.5 earthquakes (Youd et.al.,2001).

Evaluation of the potential for liquefaction to occur is accomplished by comparing equivalent measures of earthquake loading and liquefaction resistance. The most common approach to characterization of earthquake loading is through the use of cyclic shear stresses. As used in the original development of simplified procedure the term cyclic stress ratio refers to both the cyclic stress ratio generated by the earthquake and the cyclic stress ratio required to generate a change of state in the soil to a liquefied condition. Seed and Idriss (1971) formulated the following equation for calculation of the equivalent cyclic stress ratio.

$$CSR_{eq} = \frac{a_{\max}}{g} \cdot \frac{\sigma_v}{\sigma_v'} \cdot r_d \qquad (2.1)$$

where a_{max}=peak horizontal ground surface acceleration; g=acceleration of gravity; σ_v=total vertical stress; σ_v'=effective vertical stress; and r_d=nonlinear shear mass participation factor.

The original values of the nonlinear shear mass participation factor (r_d) proposed by Seed and Idriss (1971) are shown by the heavy lines in Figure. 2.9(a). This is the same “simplified” r_d-based assessment of in-situ cyclic stress ratio (CSR).As a result, all suffer from moderately biased estimates of in-situ CSR, especially at shallow depths. It is accepted that r_d is nonlinearly dependent upon a suite of factors led to studies by Cetin and Seed (2001) to develop improved correlations for estimation of r_d, as shown by the heavy lines in Figure 2.9(b).

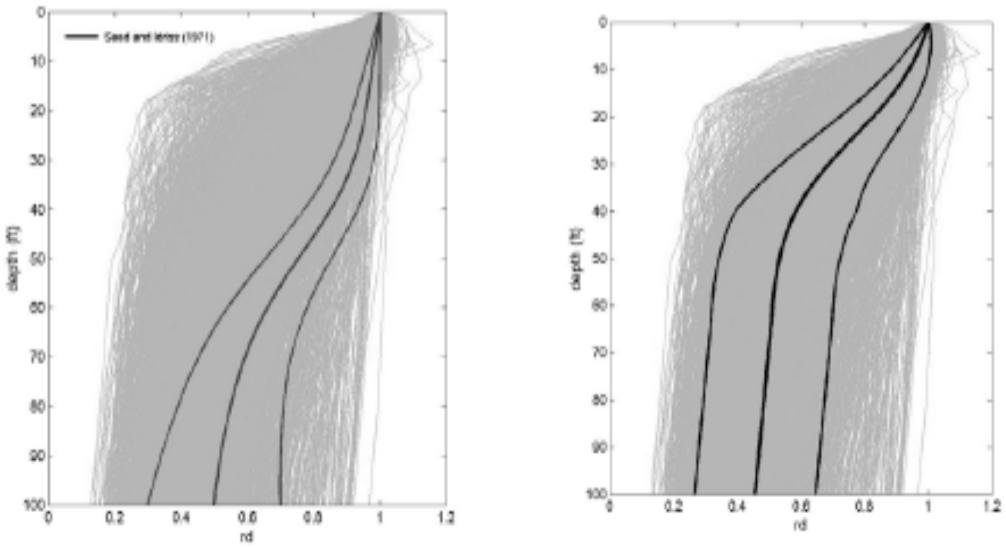

(a) Seed and Idriss (1971) **(b)** After Çetin and Seed (2001)

Figure. 2.9: R_d Results from Response Analyses Superimposed with Heavier Lines Showing (a) the Earlier Recommendations of Seed and Idriss (1971), and (b) the Mean and + 1 Standard Deviation Values (Cetin and Seed, 2001)

By normalizing the cyclic shear stress amplitude by the initial effective vertical stress, a cyclic stress ratio (CSR) can represent the level of loading induced at different depths in a soil profile by an earthquake. There are different procedures for evaluating the cyclic shear stresses - site response analyses may be performed or a "simplified" approach may be used to estimate CSR as a function of peak ground surface acceleration amplitude.

Liquefaction resistance is most commonly characterized on the basis of observed field performance. Detailed investigation of actual earthquake case histories has allowed determination of the combinations of in-situ properties (usually SPT or CPT resistance) and CSR for each case history. By plotting the $CSR_{(N_1)_{60}}$ (or CSR_{qc}) pairs for cases in which liquefaction was and was not observed, a curve

that bounds the conditions at which liquefaction was historically observed can be drawn. This curve, when interpreted as the maximum CSR for which a soil with a given penetration resistance can resist liquefaction, can be thought of as a curve of cyclic resistance ratio (CRR). Then, the potential for liquefaction can be evaluated by comparing the earthquake loading (CSR) with the liquefaction resistance (CRR) - this is usually expressed as a factor of safety against liquefaction in Equation 2.2.

$$FS = \frac{CRR}{CSR} \tag{2.2}$$

A factor of safety greater than one indicates that the liquefaction resistance exceeds the earthquake loading, and therefore that liquefaction is unlikely to occur. As mentioned in Cetin et al.(2001); the deterministic relationship by Seed et al. (1984) has been widely accepted and used in practice, but i) it is rather dated, namely field case histories are not included after 1984, ii) it has no formal probabilistic assessment iii) the recent new data, procedure and corrections of Standard Penetration Test (SPT) are not employed in interpreting case histories, and iv) it has shortage in field data wherein high cyclic stress ratios (CSR>0.3). This higher range of CSR >0.3 is increasingly important in practice, as higher levels of seismic excitation are increasingly employed as a design basis.

Formally, probabilistically- based correlations have been published by a number of researchers, including i) Liao, et al. (1988), ii) Youd and Noble (1997), iii) Toprak et al. (1999) and more recently iv) Cetin et. al. (2004).

Cetin et al.(2000, 2004)'s, probabilistic seismic soil liquefaction models, deal explicitly with the issues of fines content (FC), magnitude-correlated duration weighting factors (DWF_M), and effective overburden stress (K_σ effects), and they provide both an unbiased basis for evaluation of liquefaction initiation hazard,

and significantly reduced overall model uncertainty. The following equation can be used concisely as a single, composite relationship:

$$P_L(N_{1,60}, CSR_{eq}, M_w, \sigma_v', FC) = \Phi\left[-\frac{(N_{1,60}\cdot(1+0.004\cdot FC) - 13.32\cdot\ln(CSR_{eq}) - 29.53\cdot\ln(M_w) - 3.70\cdot\ln\left(\frac{\sigma_v'}{P_a}\right) + 0.05\cdot FC + 16.85)}{2.70} \right] \quad (2.3)$$

where

P_L = the probability of liquefaction in decimals (i.e. 0.3, 0.4, etc.)

FC= percent fines content (by dry weight) expressed as an integer (e.g., 12% fines is expressed as FC=12) with the limit of 5<FC<35.

P_a= atmospheric pressure (=1atm=101.3 kPa)

Φ= the standard cumulative normal distribution.

Also the cyclic resistance ratio for a given probability of liquefaction can be expressed as;

$$CRR(N_{1,60}, M_w, \sigma_v', FC, P_L) = \exp\left[\frac{(N_{1,60}\cdot(1+0.004\cdot FC) - 29.53\cdot\ln(M_w) - 3.70\cdot\ln\left(\frac{\sigma_v'}{P_a}\right) + 0.05\cdot FC + 16.85 + 2.70\cdot\Phi^{-1}(P_L))}{13.32} \right] \quad (2.4)$$

Note that $\Phi^{-1}(P_L)$ = the inverse of the standard cumulative normal distribution.

Figure 2.10 also shows the boundary curves calculated by this relationship. The contours shown (solid lines) are for probabilities of liquefaction of P_L=5 %, 20 %, 50 %, 80 %, and 95 %. All "data points" shown represent median values, also

corrected for duration and fines. These are superposed (dashed lines) with the relationship proposed by Seed et al. (1984) for reference (Cetin et al.2004).

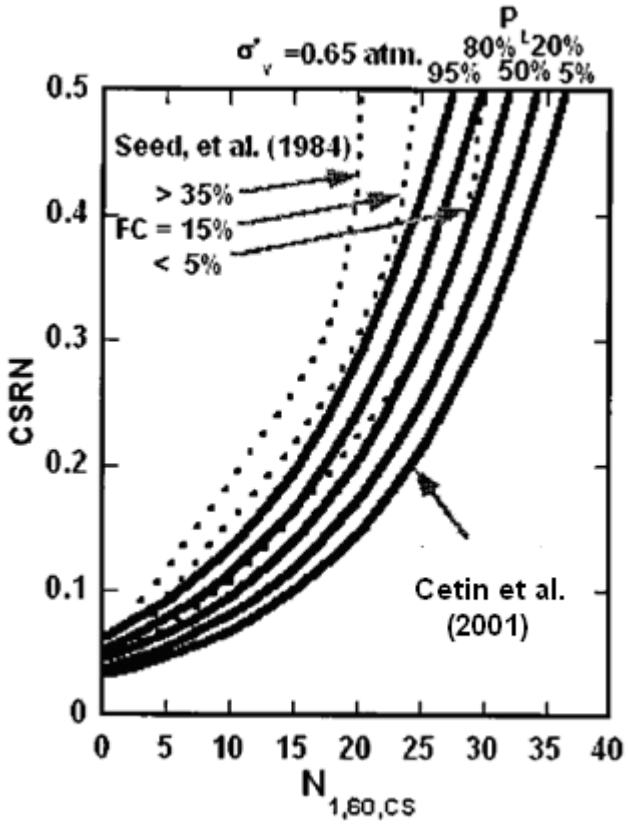

Figure 2.10: Probabilistic assessment of liquefaction initiation likelihood for M_w=7.5, σ'_v=0.65 atm (Cetin et al.,2004)

Seed et al. (2001) recommended that Seed et al. (1984) deterministic boundary curves for clean sands (5 % fines) does correspond to approximately P_L<10–40 %, except at very high CSR (CSR〉>0.3). Figure 2.11 shows the deterministic SPT- based Liquefaction Triggering Correlation for M_w=5.5 and σ'_v =0.65 atm with adjustments for fines content.

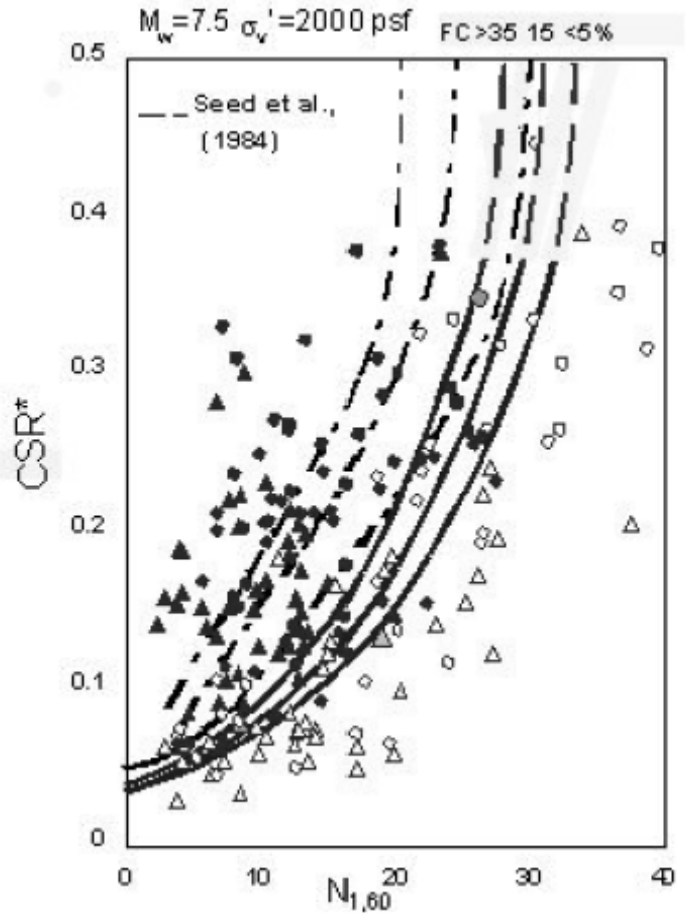

Figure 2.11: Recommended "Deterministic" SPT-Based Liquefaction Triggering Correlation (for Mw=7.5 and σ'_v=0.65atm), with Adjustments for Fines Content (Seed et al.,2001)

CHAPTER 3

SEISMIC HAZARD ASSESSMENT

Every once in a while something bad happens as a result of an earthquake and probabilistic seismic hazard analysis gives the basis on which engineers assess how often bad happens at some place of interest. The deterministic approach to seismic hazard analysis (DSHA) seems to be very different from probabilistic seismic hazard analysis (PSHA). DSHA deals with things like “maximum credible earthquake” or MCE, “safe-shut down earthquake” or SSE, “operating basis earthquake” or OBE in terminology piled in the large dams. (Krinitsky 1995). The goal of probabilistic seismic hazard analysis (PSHA) is to quantify the rate (or probability) of exceeding various ground-motion levels at a site (or a map of sites) given all possible earthquakes.

Generally, earthquakes of different magnitude levels are assumed to occur at different seismically active locations, determined by using the length of each fault and a rupture length vs. magnitude relationship (for example, Wells Coppersmith, 1994). Then the most critical seismic threat is determined as the seismic source zone generating the maximum ground motion at the corresponding site of interest. For this reason, deterministic approach is a simulation of a single scenario. On the other hand, probabilistic seismic hazard analysis aims to estimate the likelihood of occurrence of a hazardous magnitude earthquake, whose recurrence rate is low, during the relatively very short useful life of a structure (Gupta, 2002).

In the deterministic approach for seismic hazard analysis, initially the maximum possible earthquake magnitude for each of the seismic sources (important faults or seismic provinces) within certain vicinity, say 250 kilometer radius, around the selected site are determined. Then the ground motion at that site is predicted by using empirical attenuation relations for the maximum magnitude earthquakes occurring at the minimum possible distances of each source to the site. The deterministic approach requires rather less effort but more experience. The advocates of this approach claim that there are unnecessarily heavy amount of calculations in the probabilistic approach, while determining seismic hazard based on already highly uncertain input data (Gupta, 2002).

Given that probabilistic seismic hazard methodology is a convenient tool for managing the uncertainties present in seismic source characterization, as well as ground motion parameters of interest such as acceleration or velocity; it also provides the flexibility to adapt new components to the core system. The detailed explanation of the conventional seismic hazard assessment methodology can be found in Cornell (1968), and is not discussed herein.

The three basic steps in a regional seismic hazard analysis procedure particularly include: (1) identification of earthquake sources and regional seismicity, (2) estimating the attenuation of earthquake motions between the sources and the region, and (3) evaluating the local site effect on ground motion.

3.1 Seismic Source Characterization

Seismic source model provides a description of potential future earthquakes in terms of their spatial distribution the rate of seismic activity and the relative frequency of various size events. Stated most simply, the seismic-hazard source model is a description of the magnitude, location, and timing of all earthquakes.

First step of source characterization is determining the potential sources (such as point source, line source or area source) of regions with in the crust of future earthquakes. Secondly, description of source geometry of a seismic source is necessary in order to evaluate the distance from the site at which future earthquakes could occur. In addition, source geometry can place physical constrains on the maximum size earthquake that can occur on the source. Activity rate of a maximum size future earthquake is defined by investigating geological, historical and geodetic information of the site. Seismic energy release is balanced by the building of seismic moment. The built up of seismic moment is computed from the long term slip rate as:

$$M_0 = \mu.A.D \tag{3.1}$$

where μ_o is seismic moment, μ is rigidity of the crust, A is area of the fault and D is average slip on the fault.

Seismic moment released during on earthquake is computed as expressed in Equation 3.2.

$$Log_{10}(M_0) = 1.5\ M_w + 16.05 \tag{3.2}$$

where M_w is moment magnitude

To balance the moment built up and the moment release, the annual moment rate from the slip rate is set equal to the sum of the moment released in all of the earthquakes that are expected to occur each year. Recurrence rates are estimated by using historical and digital records within a seismic moment balancing concept (Abrahamson 2000). Seismic moment balancing equation is expressed in (Equation 3.3).

$$\mu.A.S = N(M_{\min}) \cdot \int_{m=M_{\min}}^{M_{\max}} f_m(m) \cdot 10^{M_0}\, dm \tag{3.3}$$

where μ is the shear modulus given in dyne/cm^2, A is the fault area, S is the slip rate and $f_m(m)$ is the magnitude density function. The second term within the integral defines the seismic moment released during an earthquake in terms of moment magnitude $N(M_{min})$, namely the activity rate defines the number of annual events greater than the minimum magnitude earthquake M_{min}. Given the slip rate, S, fault area A, and magnitude density function, the activity rate $N(M_{min})$ can be calculated.

3.2 Attenuation Relationships

After identification of the earthquake sources and the regional, the next step in the regional seismic hazard and risk analysis is to determine the bedrock motion in the region regarding the modeling of the earthquake occurrence on each seismic source.

It should be noted that seismic hazard analysis requires an appropriate strong-motion attenuation relationship, which describes the propagation and modification of ground motions as a function of earthquake size (magnitude, M) and the distance (R) between the source and the site of interest. In general, there are two basic approaches in developing design ground motions that are commonly used in practice: deterministic and probabilistic.

In the deterministic approach that is utilized in this dissertation, individual earthquake scenarios (earthquake magnitude and location) are developed for each relevant seismic source and a specified ground motion probability level is selected (by tradition, it either possesses 0 or 1 standard deviation above the median). Based on the seismic source location, the distance to the site is computed. Given the magnitude, distance, and number of standard deviations for

the ground motion, the ground motion is then computed for each earthquake scenario, using a ground motion attenuation relation or a numerical simulation method. The largest ground motion from any of the considered scenarios is used for the design ground motion. The approach is “deterministic” in that single values are selected for the scenario parameters (magnitude, distance, and number of standard deviations for the ground motion) for each scenario (Abrahamson, 2003).

The relationships express a given ground motion parameter in a region as a function of the size and location of an earthquake event. Numerous relationships have been developed since then, typically by applying statistical regression analyses to recorded data. Often these relationships are developed with different functional forms and with different definitions of ground motion, magnitude, distance, and site conditions (Campbell, 1985).

Within the confines of the study, Boore et al. (1997) attenuation model was adopted. Boore et. al. (1997) proposed attenuation relationships for random horizontal peak ground acceleration and pseudo-acceleration response spectra for shallow earthquakes in western North America of earthquake magnitude (M) greater than or equal to 5.3. The equations predict ground motion characteristics in terms of moment magnitude, distance, and site conditions for strike-slip, reverse-slip, or unspecified faulting mechanisms. Boore et al. (1997) use moment magnitude as a measure of earthquake size and a distance term defined as the closest horizontal distance from the station to a point on the earth’s surface that lies directly above the rupture (r_{jb}), widely referred to as the “Joyner-Boore distance”. Site conditions are represented by the shear wave velocity averaged over the upper 30 m. Recommended values of average shear wave velocity are given for typical rock and soil sites as well as site categories used in the National Earthquake Hazard Reduction Program’s (NEHRP) recommended seismic code provisions.

The ground-motion estimation equation is:

$$\ln Y = b_1 + b_2(M-6) + b_3(M-6)^2 + b_5 \ln r + b_v \ln \frac{V_S}{V_A} \tag{3.4}$$

where

$$r = \sqrt{r_{jb}{}^2 + h^2} \tag{3.5}$$

and

$$b_1 = \begin{cases} b_{1SS} & for\ strike-slip\ earthquakes \\ b_{1RS} & for\ reverse-slip\ earthquakes \\ b_{1ALL} & if\ mechanisim\ not specified \end{cases} \tag{3.6}$$

In Eq. (3.4), Y is the ground-motion parameter (peak horizontal acceleration in g); where, the predictor variables are moment magnitude (M), distance (r_{jb}, in km), and average shear-wave velocity to 30 m (V_S, in m/s). b_{1SS}, b_{1RS}, b_{1ALL}, b_2, b_3, b_5 h, b_v, and V_A, are coefficients or entries for zero period (Boore et al., 1997). Note that h is a fictitious depth that is determined by the regression.

In the Boore et al. (1997) method, the coefficients in the equations for predicting ground motion were determined using a weighted, two-stage regression procedure. In the first stage, the distance and site condition dependence were determined along with a set of amplitude factors, one for each earthquake. In the second stage, the amplitude factors were regressed against magnitude to determine the magnitude dependence.

The mean plus one standard deviation of sigma value of the natural logarithm of the ground-motion value from Equation (3.4) is lnY + σlnY, where σlnY is the square root of the overall variance of the regression, given by

$$\sigma^2_{lnY} = \sigma^2_r + \sigma^2_e \tag{3.7}$$

where, σ^2_e represents the earthquake-to-earthquake component of the variability and is determined in the second stage of the regression, and σ^2_r represents all other components of variability.

$$\sigma^2_r = \sigma^2_1 + \sigma^2_c \tag{3.8}$$

where σ^2_1 is the variance from the first stage of the regression and σ^2_c represents the correction needed to give the variance corresponding to the randomly-oriented horizontal component.

3.3 Summary of Seismic Hazard Framework

The self-explanatory details about the seismic hazard approach are shown in Figure 3.1.

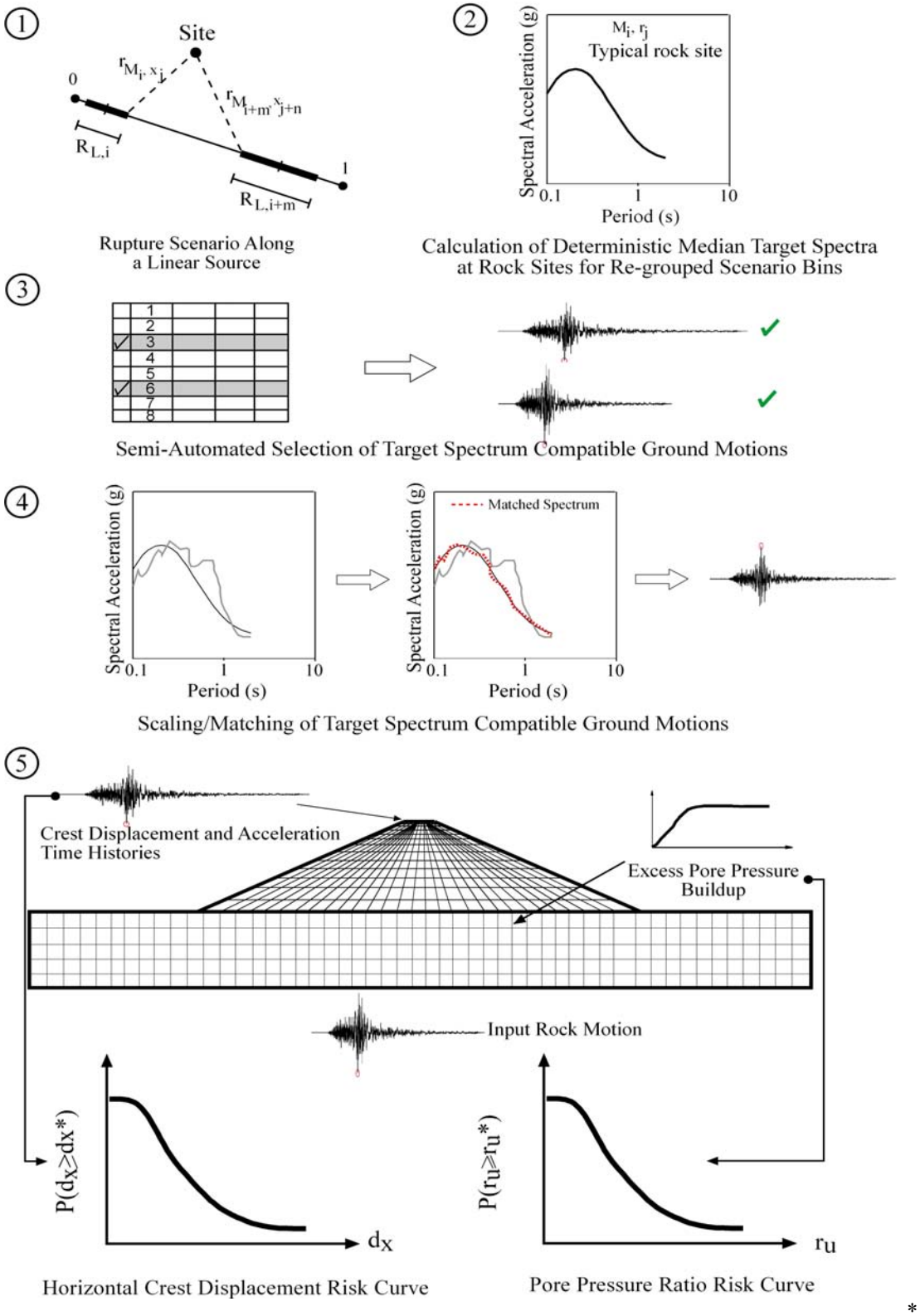

Figure 3.1: Integrated workflow for assessing the liquefaction triggering of dam foundations (Modified from Yunatci et al., 2007)

In the preliminary stage of the proposed workflow, geometric characterization of the defined seismic source is performed parallel to the conventional methodology. The rupture locations and source to site distances for every contributing stage of the probabilistic scenario are calculated in compliance with the distance term that is planned to be used in the attenuation relationship. Next step includes the deterministic calculation of median acceleration response spectra for a suite of magnitude distance bins which are systematically re-grouped after discretization of the whole rupture scenario. Optimized subsets that enable robust execution of spectrum compatible ground motion record generation are formed by applying a systematic regrouping of source to site distances for every magnitude bin. A simple approach for the present case is defined as 5 distance sets that contain equal number of distance values for each magnitude bin. Median distance values of each bin are selected as the representative source to site distances for the magnitude bin of interest, while forming the median rock acceleration response spectra. It then becomes possible to carry on further re-grouping of bins for cases which the differences between the median distance values are minimal.

Third stage is dominantly composed of selecting and matching the appropriate ground motions representing typical rock sites with the response spectra for every bin. Two different approaches are followed to produce the spectrum compatible ground motions. One of the methods is non-stationary response spectrum matching technique proposed by Abrahamson (1993), while the other is simple PGA scaling. Processed earthquake records from ground motion catalogs are scanned and filtered to obtain the suitable set of acceleration time histories to be used in the dam response analyses. The proposed method is a substitute to using the maximum design earthquake or any other single scenario earthquake derived using either deterministic or de-aggregated probabilistic seismic hazard assessment; that in turn enables the development of a performance based evaluation of dam response.

Development environment of the custom code required to run the analyses was selected as MATLAB. Response spectrum matching was carried out using RSPMATCH software developed by Abrahamson (1993). The sample problem to be solved was modeled as a linear fault. The closest distance of the selected site to the fault trace was chosen as 15 km., with complete geometry sketched in Figure 3.2. Fault was modeled to be strike-slip in mechanism, with a dip angle of 90 degrees. Magnitude recurrence relation was chosen as truncated exponential where M_{min}=5 and M_{max} =7.4. Activity rate was calculated using the moment balancing equation.

Figure 3.2: The closest distance of the site to the fault trace

Within the confines of the study, Boore et al. (1997) attenuation model was adopted as discussed earlier. As the next step, 600 discretized magnitude distance bins for the single linear rupture scenario belonging to the probabilistic model were re-grouped into 16 new subsets according to the principles defined previously. The reduction is dependent on the conditions of the specific problem. Equal element principle for every bin was taken into consideration, and the median distance of every bin was selected as the representative distance. After determination of the suite of representative moment magnitude values and Boore- Joyner distances, deterministic target spectra for typical rock sites ($V_{s,30}$= 550 m/s) were derived using Boore et al. (1997) attenuation relationship. For 16 re-grouped magnitude-distance bins, shown in Table 3.1, 24 earthquake records were selected from the PEER (2007) NGA online catalog based on mechanism, site class, distance, PGA and spectral accelerations at T=0.2 s and T=1.0 s. The

original earthquake records filtered for grid and baseline size was corrected. These selected 24 earthquake records' acceleration, velocity and displacement time responses are given at the Appendix.

For dams, the probability of liquefaction vs. time relation can be corresponding to return periods. USGS suggest that dams have 10 percent, 5 percent, and 2 percent probabilities of exceedance in 50 years. These probabilities of exceedance correspond to return periods of approximately 500, 1000, and 2500 years, respectively. For the seismic design of dams, abutments and safety relevant components (spillway gates, bottom outlets, etc.) the following types of design earthquakes are used (ICOLD, 1989).

Operating Basis Earthquake (OBE) design is used to limit the earthquake damage to a dam project and, therefore, is mainly a concern of the dam owner. Accordingly, there are no fixed criteria for the OBE although ICOLD has proposed an average return period of 145 years (50 % probability of exceedance in 100 years). Sometimes return periods of 200 or 500 years are used. The dam shall remain operable after the OBE and only minor damage easily.

According to ICOLD Bulletin 72 (1989), large dams have to be able to withstand the effects of the ***Maximum Credible Earthquake MCE***. This is the strongest earthquake that could occur in the region of a dam, and is considered to have a return period of several thousand years (typically 10.000 years in regions of low to moderate seismicity). The stability of the dam must be ensured under the worst possible ground motions at the dam site and no uncontrolled release of water from the reservoir shall take place, although significant structural damage is accepted. In the case of significant earthquake damage, the reservoir may have to be lowered. Probabilistic seismic hazard assessment is achieved for a specific case of earthfill dam alluvium foundation through this study. In order to make a sense of this approach, the results are compared to the most acceptable probabilistic and deterministic assessments of liquefaction triggering.

Table 3.1: Magnitude- Distance Bins

Earthquake Scenario Bins	Bin Number	Moment Magnitude	Representative Moment Magnitude (M_w)	Boore Joyner Distance (km)	Representative Boore Joyner Distance (r) (km)	$P(M_w)$*	P(r)**	Number of Records	Record Numbers	Matched Peak Accelerations (g)	$N(M_{min})$ (events/yr)
1	1-1	5.0-5.4	5.2	15-23	18	0.567	0.384	2	1-2	0.069	0.299
2	1-2	5.0-5.4	5.2	23-34	27	0.567	0.192	1	3	0.051	
3	1-3	5.0-5.4	5.2	34-52	43	0.567	0.192	1	4	0.036	
4	1-4	5.0-5.4	5.2	52-74	63	0.567	0.232	1	5	0.027	
5	2-1	5.4-5.8	5.6	15-35	20	0.247	0.588	1	6	0.079	
6	2-2	5.4-5.8	5.6	35-52	43	0.247	0.196	1	7	0.045	
7	2-3	5.4-5.8	5.6	52-73	62	0.247	0.216	1	8	0.034	
8	3-1	5.8-6.2	6.0	15-32	19	0.108	0.581	2	9-10	0.101	
9	3-2	5.8-6.2	6.0	32-49	40	0.108	0.193	1	11	0.058	
10	3-3	5.8-6.2	6.0	49-69	59	0.108	0.226	1	12	0.044	
11	4-1	6.2-6.6	6.4	15-29	18	0.047	0.600	2	13-14	0.135	
12	4-2	6.2-6.6	6.4	29-45	37	0.047	0.200	2	15-16	0.076	
13	4-3	6.2-6.6	6.4	45-61	53	0.047	0.200	2	17-18	0.058	
14	5-1	6.6-7.0	6.8	15-31	18	0.021	0.754	2	19-20	0.160	
15	5-2	6.6-7.0	6.8	31-46	38	0.021	0.246	1	21	0.092	
16	6-1	7.0-7.4	7.2	15-21	16	0.009	1.000	3	22-23-24	0.215	

* Probability of occurrence of representative magnitudes
** Probability of occurrence of representative distances

CHAPTER 4

NUMERICAL ASSESSMENT OF THE STUDY

4.1 Modeling Basics

Seismic response analysis of a 56 m high central clay core earthfill dam, founded on 24 m thick "loose" ($N_{1,60,cs}$ ~ 20 blows/30 cm) alluvial deposits, lying on the bedrock is performed by two-dimensional, explicit, finite difference software FLAC v4.0 (Fast Lagrangian Analysis of Continua) software. Mesh generation, constitutive models and modeling parameters are explained in detail in the following sections.

4.1.1 Mesh Generation and Boundary Conditions

The modeling grid is composed of dam body, alluvial soil and bedrock. Unlike many modeling programs based on the finite element method, *FLAC* organizes its zones (or "elements") in a row-and-column fashion, like a crossword puzzle. Although the numbering scheme resembles that of a crossword puzzle, the physical shape of a *FLAC* grid need not be rectangular: the rows and columns can be distorted so that the boundary fits the sloped regions. Moreover, dam body and alluvium have finer meshes (more zones per unit length) compared to bedrock lead to more-accurate results.

For the purpose of realistically modeling construction stages, 12 stages are defined, as shown in Table 4.1. The adopted mesh and three of these construction and modeling stages are illustrated in Figures 4.1 to 4.4.

Table 4.1: Construction stages

Stage	Explanation
1	Alluvial soil and bedrock
2	Dam elevation +8 m
3	Dam elevation +16 m
4	Dam elevation +24 m
5	Dam elevation +32 m
6	Dam elevation +40 m
7	Dam elevation +48 m
8	Dam elevation +56 m
9	Impoundment (No flow)
10	Phreatic Surface (Flow)
11	Dynamic (No flow)
12	Excess pore pressure dissipation (Flow)

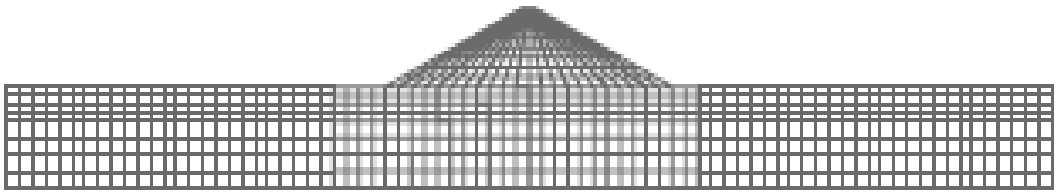

Figure 4.1: Finite element mesh of the dam with foundation used in static and dynamic analyses

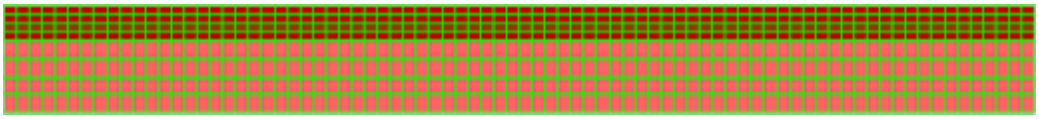

Figure 4.2: Model mesh of foundation, alluvium upon bedrock (Stage 1)

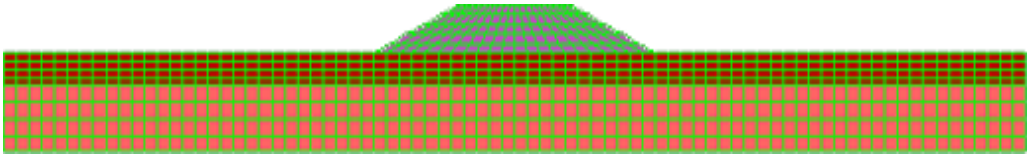

Figure 4.3: Model mesh, dam body with foundation (Stage 5)

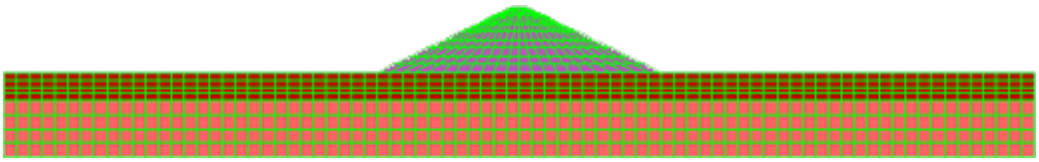

Figure 4.4: Model mesh of entire dam (Stage 8)

After the grid is generated, boundary and initial conditions are applied. In the static analysis, 'standard fixities' are applied to the dam foundation as the grid has the left- and right-hand sides fixed from movement in the *x*-direction, and the bottom fixed in the *y*-direction.

In the dynamic analysis, 'free-field' boundaries are applied to the foundation as fixed grid point conditions are removed, except for the *y*-fixed conditions at the bottom grid points. Free-field boundary provides that plane waves propagating upward suffer no distortion at the boundary. Moreover, mechanical (plain strain), groundwater flow and dynamic conditions are applied to the model boundary in the related parts of analyses.

FLAC models a region of material subjected to external or internal dynamic loading by applying a dynamic input boundary condition at either the model boundary or at internal grid points. Wave reflections at model boundaries are minimized by specifying either quiet (viscous), free-field or three-dimensional radiation-damping boundary conditions. Numerical analyses of the seismic response of surface structures require the discretization of a region of the material adjacent to the foundation. The seismic input is normally represented by plane waves propagating upward through the underlying material. The boundary conditions at the sides of the model must account for the free-field motion which would exist in the absence of the structure. In some cases, elementary lateral boundaries may be sufficient. These boundaries should be placed at sufficient distances to minimize wave reflections and achieve free-field conditions. For soils with high material damping, this condition can be obtained with a relatively small distance (Seed et al. 1975). However, when the material damping is low, the required distance may lead to an impractical model. An alternative procedure is to "enforce" the free-field motion in such a way that boundaries retain their non-reflecting properties i.e., outward waves originating from the structure are properly absorbed. A technique of this type was developed for FLAC, involving the execution of a one-dimensional free-field calculation in parallel to the main-grid analyses.

4.1.2 Constitutive Models

For materials like soil, rock etc. frictional and dilatational effects need to be incorporated in the constitutive modeling. This section presents i) equivalent linear model, ii) elastic-perfectly plastic model, iii) effective-stress based models of: UBCSAND and iv) modified UBCSAND.

4.1.2.1 Equivalent Linear Model

The linear elastic behavior, which is used to describe the material properties of an element, assumes that strain is proportional to the stress on the element. This assumption explains how deformations appear when stress is applied and how they disappear when stress is removed. The loading modulus and unloading modulus are the same for this model. The linear elastic model is based on Hooke's law, which mathematically expresses this linear relationship, allows us to express the strains in terms of the stresses

In the elastic isotropic model, the relation of stress to strain in incremental form is expressed by Hooke's law in plane strain as:

$$\Delta\sigma_{11} = \alpha_1 \Delta e_{11} + \alpha_2 \Delta e_{22}$$
$$\Delta\sigma_{22} = \alpha_2 \Delta e_{11} + \alpha_1 \Delta e_{22}$$
$$\Delta\sigma_{12} = 2G\, e_{12} \quad (\Delta\sigma_{21} = \Delta\sigma_{12})$$
$$\Delta\sigma_{33} = \alpha_2 (\Delta e_{11} + \Delta e_{22}) \qquad (4.1)$$

where $\alpha_1 = K + (4/3)G;$ (4.2)

$\alpha_2 = K - (2/3)G;$ (4.3)

K = bulk modulus;
G = shear modulus.

$$\Delta e_{ij} = 1/2[\partial u_i / \partial x_j + \partial u_j / \partial x_i] \Delta t \qquad (4.4)$$

where Δe_{ij} = the incremental strain tensor;
u_i = the displacement rate; and
Δt = time step.

In plane stress, these equations become

$$\Delta\sigma_{11} = \beta_1 e_{11} + \beta_2 e_{22}$$
$$\Delta\sigma 22 = \beta_2 e_{11} + \beta_1 e_{22} \quad (2.3)$$
$$\Delta\sigma_{12} = 2G e_{12} \quad (\sigma_{21} = \sigma_{12})$$
$$\Delta\sigma_{33} = 0 \quad (4.5)$$

where

$$\beta_1 = \alpha_1 - (\alpha^2_2/\alpha_1); \quad (4.6)$$
$$\beta_2 = \alpha_2 - (\alpha^2_2/\alpha_1). \quad (4.7)$$

For axisymmetric geometry:

$$\Delta\sigma_{11} = \alpha_1 \Delta e_{11} + \alpha_2 (\Delta e_{22} + e_{33})$$
$$\Delta\sigma_{22} = \alpha_1 \Delta e_{22} + \alpha_2 (\Delta e_{11} + \Delta e_{33})$$
$$\Delta\sigma_{12} = 2G\Delta e_{12} \quad (\Delta\sigma_{21} = \Delta\sigma_{12})$$
$$\Delta\sigma_{33} = \alpha_1 \Delta e_{33} + \alpha_2 (\Delta e_{11} + \Delta e_{22}) \quad (4.8)$$

There are four material parameters for an elastic model the elastic modulus E, Poisson's ratio ν, bulk modulus K and shear modulus G as expressed in Equations 4.9 to 4.12. Only two are required to fully specify the material response.

$$\varepsilon_{xx} = \frac{1}{E} (\sigma_{xx} - \nu\sigma_{yy}) \quad (4.9)$$

$$\gamma_{xy} = \frac{\tau_{xy}}{G} \quad (4.10)$$

$$G = \frac{E}{2(1+\nu)} \tag{4.11}$$

$$K = \frac{E}{3(1-2\nu)} \tag{4.12}$$

where ε is axial strain, γ is shear strain, σ is normal stress, τ is shear stress and E is young's modulus, K is bulk modulus, G is modulus of rigidity. Due to the poisson effect, an expanding normal strain in the x-direction will cause a proportional compressive normal strain in the y-direction, and the constant of proportionality is poisson's ratio, ν. The equations above are merely different expressions of Hooke's law for plane stress, with the strains being added together by means of the principle of superposition. It should be noted that the expressions are valid only if the material behaves in a linear-elastic manner.

4.1.2.2 Elastic Perfectly Plastic Model

Plasticity is associated with the development of irreversible strains. In order to evaluate whether or not plasticity occurs in a calculation, a yield function, f, is introduced, usually as a function of stress and strain. A yield function can often be presented as a surface in principal stress space. A perfectly-plastic model is a constitutive model with a fixed yield surface i.e. a yield surface that is fully defined by model parameters and not affected by (plastic) straining. For stress states represented by points within the yield surface, the behavior is purely elastic and all strains are reversible.The basic principle of elasto-plasticity is that strains and strain rates are decomposed into an elastic part and a plastic part as $\varepsilon=\varepsilon^{e}+\varepsilon^{p}$.

The Mohr-Coulomb criterion is the most common failure criterion encountered in geotechnical engineering. The Mohr-Coulomb failure criterion describes a

linear relationship between normal and shear stresses (or maximum and minimum principal stresses) at failure. Values of normal stress and shear stress must relate to a particular plane of failure within an element of soil. In general, the stresses on another plane will be different.

An elastic perfectly plastic constitutive model with Mohr-Coulomb failure criterion needs five input parameters, i.e. E and ν for soil elasticity; friction angle, ϕ, and cohesion, c, for soil plasticity and ψ as an angle of dilatancy. This model represents a 'first-order' approximation of soil or rock behavior. Mohr-Coulomb failure envelope is schematically shown in Figure 4.5.

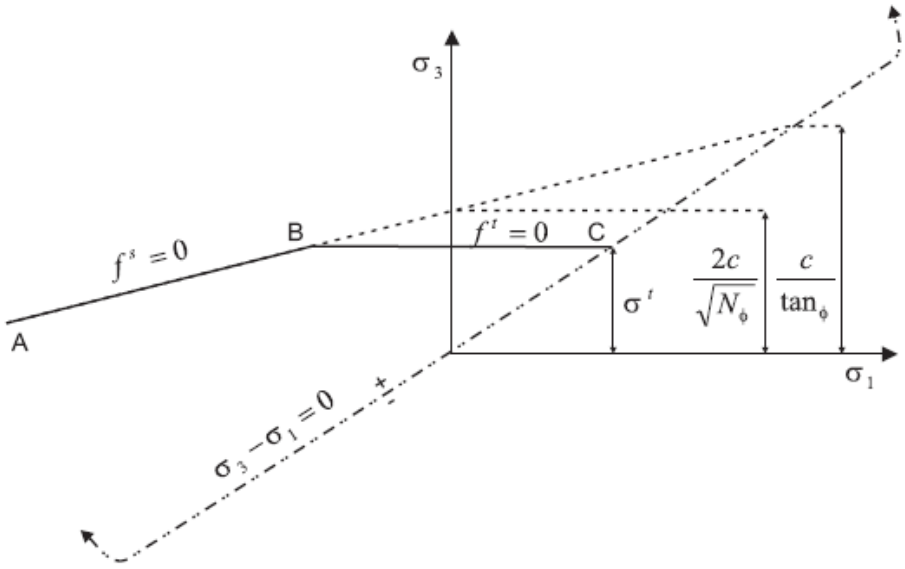

Figure 4.5: Mohr-Coulomb failure envelope
(source: FLAC v4.0 manual)

The failure envelope is defined from point A to point B by the Mohr-Coulomb yield function

$$f_s = (\sigma_1 - \sigma_3)N_\phi + 2c\sqrt{(N_\phi)} \qquad (4.13)$$

and from B to C by a tension yield function of the form

$$f_t = \sigma_t - \sigma_3 \tag{4.14}$$

where ϕ is the friction angle, c, the cohesion, σ_t , the tensile strength and;

$$N_\phi = (1 + \sin \phi) / (1 - \sin \phi) \tag{4.15}$$

Note that only the major and minor principal stresses are active in the shear yield formulation; the intermediate principal stress has no effect. For a material with friction, $\phi \neq 0$ and the tensile strength of the material cannot exceed the value σ_{tmax} given by;

$$\sigma_{tmax} = c.\tan \phi \tag{4.16}$$

The shear potential function g_s corresponds to a non-associated flow rule and has the form;

$$g_s = \sigma_1 - \sigma_3 N_\psi \tag{4.17}$$

where ψ is the dilation angle and;

$$N_\psi = (1 + \sin \psi) / (1 - \sin \psi) \tag{4.18}$$

The basic parameters used in Mohr Coulomb failure criteria are discussed in details as;

i) Young's modulus (E): Young's modulus is the basic stiffness modulus in the elastic model and the Mohr-Coulomb model, but some alternative stiffness moduli are displayed as well. A stiffness modulus has the dimension of stress. In

soil mechanics the initial slope is usually indicated as E_0 and the secant modulus at 50 % strength is denoted as E_{50} (shown in Figure 4.6). For materials with a large linear elastic range it is realistic to use E_0, but for loading of soil one generally uses E_{50}.

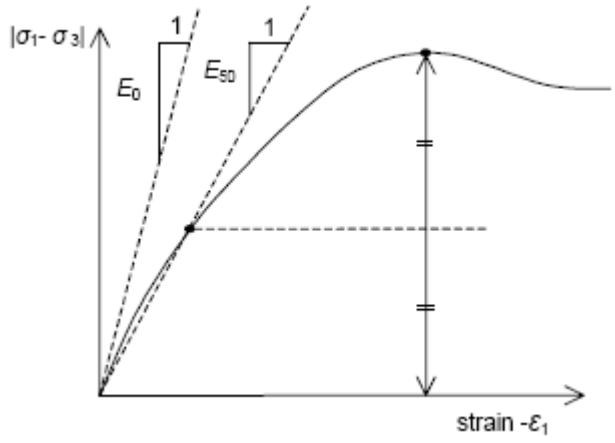

Figure.4.6: Definition of E_0 and E_{50} for standard drained triaxial test results (source: Plaxis V8. Material Models Manual)

ii) Poisson's ratio (ν): Standard drained triaxial tests may yield a significant rate of volume decrease at the very beginning of axial loading and, consequently, a low initial value of Poisson's ratio (ν). The selection of a Poisson's ratio is particularly simple when the elastic model or Mohr-Coulomb model is used for gravity loading. Both models will give the well-known ratio σ_h/σ_v, shown in Equation 4.13. For one-dimensional compression it is easy to select a Poisson's ratio that gives a realistic value of $K_{0.}$ Hence, μ is evaluated by matching $K_{0.}$

$$\frac{\sigma_h}{\sigma_v} = K_o = \frac{\nu}{(1-\nu)} \tag{4.13}$$

iii) Cohesion (c) & Friction angle (ϕ): Structural strength of soil is primarily a function of its shear strength, where shear strength refers to the soils ability to resist sliding along internal, 3-dimensional surfaces within a mass of soil. Soil strength comes from internal friction and cohesion. It follows the formula;

$$\tau = c + \sigma' \cdot \tan(\phi) \tag{4.14}$$

where τ = shear strength, c = cohesion, σ′ = effective intergranular normal (to the shear plane) pressure, and ϕ = angle of internal friction. The quantities τ, c, and σ have units of pressure.

4.1.2.3 Effective Stress Model: UBCSAND

In the mid-1990's, Peter Byrne and his graduate students at the University of British Columbia (UBC) developed a constitutive model known as UBCSAND for simulating soil liquefaction events (Park and Byrne, 2004).

UBCSAND is an effective stress model with mechanical loading and pore pressure generation and flow fully coupled. A fully coupled effective stress dynamic analysis procedure for modeling seismic liquefaction is presented. An elastoplastic formulation is used for the constitutive model UBCSAND in which the yield loci are radial lines of constant stress ratio and the flow rule is non-associated. The flow rule specifies the direction of the plastic strain increment vector as that normal to the potential surface; it is called associated if the potential and yield functions coincide, and non-associated otherwise. This is incorporated into the 2D version of FLAC by modifying the existing Mohr-Coulomb model. This numerical procedure is used to simulate centrifuge test data from the Rensselaer Polytechnic Institute (RPI). UBCSAND is first calibrated to cyclic simple shear tests performed on Nevada sand. Both pre- and post-liquefaction behaviour is captured. The centrifuge tests are then modeled

and the predicted accelerations, excess porewater pressures, and displacements are compared with the measurements. The results are shown to be in general agreement when stress densification and saturation effects are taken into account. The procedure is currently being used in the design of liquefaction remediation measures for a number of dam, bridge, tunnel, and pipeline projects in Western Canada (Byrne et al., 2004)

As Byrne et al., (2004) mentioned; Mohr-Coulomb elastic-plastic model is the simplest model for soils as schematically shown in Figure 4.7(a). Soils are modeled as elastic below the strength envelope and plastic on the strength envelope with increments of plastic shear and volumetric strains being described by the dilation angle, ψ. The UBCSAND stress-strain models modified from Mohr-Coulomb model that the plastic strains that occur at all stages of loading. Yield loci are assumed to be on a line of constant stress ratio as shown in Figure 4.7(b). Unloading is assumed to be elastic. Reloading induces plastic response but with a stiffened plastic shear modulus. ϕ_d describes the current yield locus. The differences of Mohr Coulomb model and UBCSAND model is clearly seen in Figure 4.7.

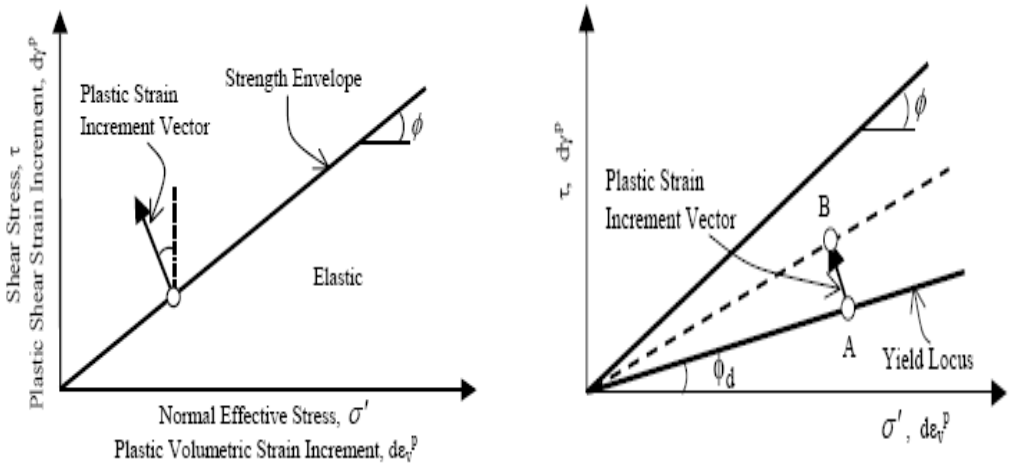

a) Mohr Coulomb model b) UBCSAND model

Figure 4.7: Mohr Coulomb model and UBCSAND model (Byrne et al., 2004)

As the elastic response of UBCSAND model, shear modulus and bulk modulus is assumed to be isotropic and mentioned in Equations 4.15 and 4.16 respectively.

$$G^e = K_e^G P_a \left(\frac{\sigma'}{P_a}\right)^{n_e} \tag{4.15a}$$

where

$$500 \le K_e^G \le 2000 \tag{4.15b}$$

$$0.4 \le n_e \le 0.6 \tag{4.15c}$$

and

$$B^e = \alpha\, G^e \tag{4.16a}$$

where

$$\frac{2}{3} \le \alpha \le \frac{4}{3} \text{ or } \quad \alpha \approx 1 \tag{4.16b}$$

B^e =The elastic bulk modulus

K_e^G = A shear modulus number (depends on the density of the sand).

P_a = Atmospheric pressure in the chosen units.

σ' = The mean stress in the plane of loading.

n_e = An elastic exponent (approximately 0.5)

α =A constant depends on the elastic Poisson's ratio.

As the plastic response of the UBCSAND model, plastic strains are both shear and volumetric. As shown in Figure 4.8, initial shear loading case, the yield locus is controlled by the current stress state, point A. As the shear stress increases, the stress ratio $n = \tau / \sigma'$ increases and causes the stress point to move to point B, where τ and σ' are the shear and normal effective stresses, respectively, on the plane of maximum shear stress. The plastic shear modulus relates the shear stress and the plastic shear strain ($d\gamma^P$) and is assumed to be hyperbolic with stress ratio as shown in Figure 4.8 and can be expressed as in equation 4.17.

$$d\gamma^P = \frac{1}{G^P / \sigma'} d\eta \tag{4.17}$$

G^P = Plastic shear modulus

The associated plastic volumetric strain increment, $d\varepsilon_v^P$, is obtained from the dilation angle ψ which is based on laboratory data and energy considerations;

$$\Delta\varepsilon_v^P = \Delta\gamma^P \sin\psi \tag{4.21}$$

The plastic properties used by the model are the peak friction angle ϕ_P, the constant volume friction angle ϕ_{cv}, and plastic shear modulus G^P;

$$G^P = G_i^P \left(1 - \frac{\eta}{\eta_f} R_f \right)^2 \tag{4.18a}$$

where

$$\eta_f = \sin \phi_f \tag{4.18b}$$

$$0.70 \le R_f \le 0.98 \tag{4.18c}$$

G^P_i = Plastic modulus at a low stress ratio level (η=0)

η_f = the stress ratio at failure

ϕ_f = the peak friction angle;

R_f = the failure ratio, decreases with increasing relative density.

Note that R_f is used for truncating the best fit hyperbolic relationship and prevent the overprediction of strength at failure.

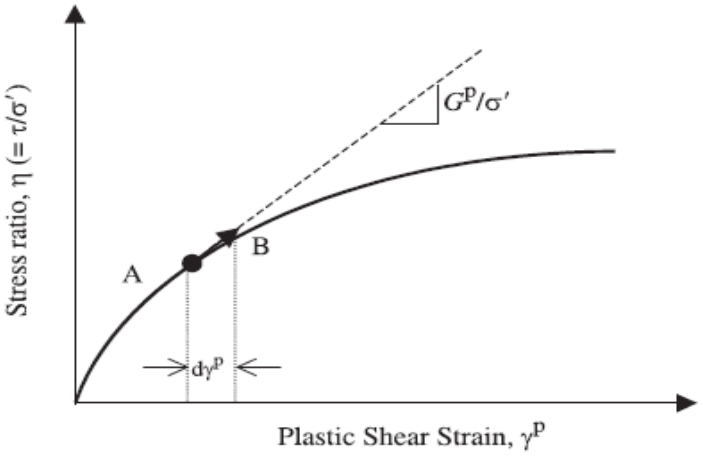

Figure 4.8: Hyperbolic stress-strain relationship

It has been useful to relate G^P_i to G_e and relative density D_r through the approximate relationship;

$$G_i^P = 3.7\,(D_r)^4\,G_e + P_a \tag{4.19}$$

The yield loci and direction of the plastic strains resulting from the flow rule are shown in Figure 4.9. Figure 4.9 shows that at low stress ratios, significant shear-induced plastic compaction is occurring, whereas no compaction is predicted at stress ratios corresponding to ϕ_{cv}. For stress ratios greater than ϕ_{cv}, shear-induced plastic expansion or dilation is predicted. This simple flow rule is in close agreement with the characteristic behavior of sand observed in laboratory element testing. Upon unloading (reducing stress ratio), the sand is assumed to behave elastically. Upon reloading, the sand is assumed to behave plastically but with a plastic modulus that is several times stiffer than that for first-time loading until the prior maximum value is reached, at which point it reverts to first-time loading.

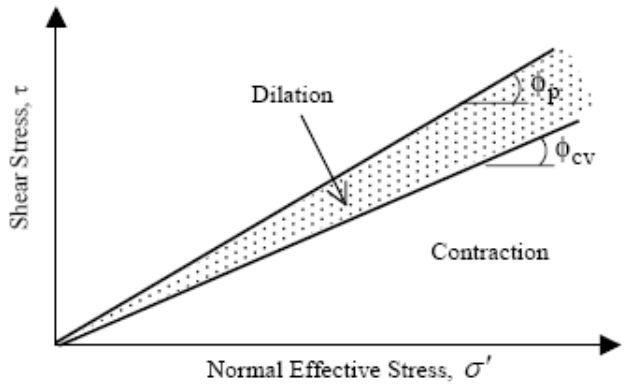

Figure 4.9: Direction of the plastic strains (Flow Rule)

The elastic and plastic parameters are highly dependent on relative density, which must be considered in any model calibration. These parameters can be selected by calibration to laboratory test data. The response of the model can also be compared to a considerable database for triggering of liquefaction under earthquake loading in the field. This database exists in terms of penetration resistance, typically from standard penetration (SPT) tests. A common relationship between $(N_1)_{60}$ values from the SPT and the cyclic stress ratio that triggers liquefaction for a magnitude 7.5 earthquake (Byrne et al., 2003). A simulation using UBCSAND was made of 2 centrifuge tests carried out at RPI and the procedure does not discussed in detailed.

The model has also been calibrated to predict liquefaction triggering response in terms of normalized standard penetration resistance $(N_1)_{60}$ in agreement with the National Center for Earthquake Engineering Research (NCEER) chart (Youd and Idriss 1997). The predicted CSR to cause liquefaction in 15 cycles versus $(N_1)_{60}$ is shown in Figure 4.10 along with the NCEER chart relationship based on field experience. The model is shown to be in close agreement with the field data (Byrne e al., 2004).

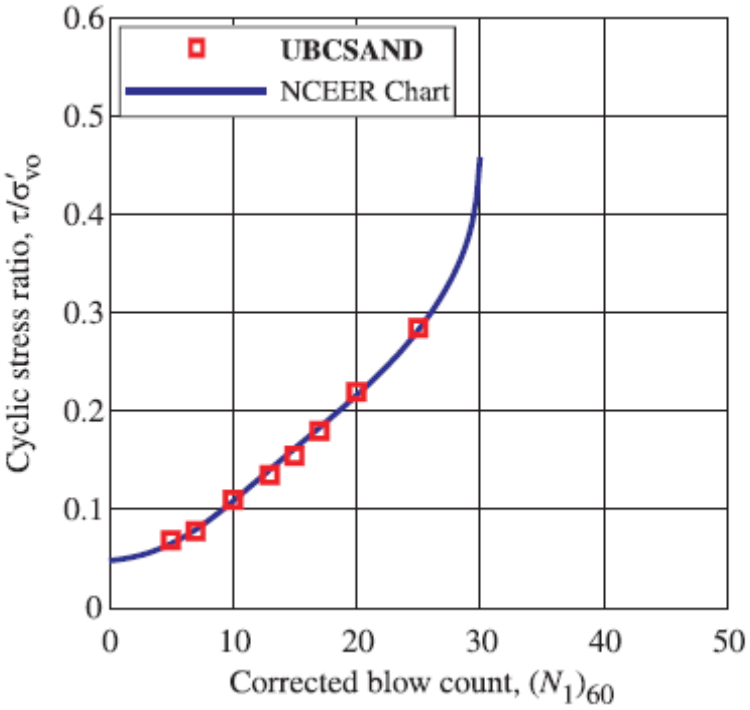

Figure 4.10: Comparison of predicted (UBCSAND) and field-observed(NCEER Chart) liquefaction resistance (Byrne e al., 2004)

4.1.2.4 Modified UBCSAND Model

The UBCSAND modifies the Mohr-Coulomb model incorporated in FLAC (Fast Lagrangian Analysis of Continua) Version 4.0 (Itasca 2000) to incorporate the plastic strains that occur at all stages of loading. This model has been substantially improved to better model observed sand behavior and include the effects of effective overburden stress (σ_v') to the cyclic resistance of the dams.

In the original model, changes in cyclic pore pressure response of saturated cohesionless soils due to changes in effective confining stresses, and presence of static shear stresses, were not fully captured. Thus a modification incorporating widely known K_σ and K_α issues was needed.

An application of the K_α correction factor is needed because the undrained cyclic loading behavior of saturated sand is affected by the presence of an initial static shear stress, which has been shown through numerous laboratory and physical modeling studies. Seed (1983) developed the K_α correction factor to represent the effects of an initial static shear stress ratio (α) on liquefaction resistance, and used it to extend the semiempirical standard penetration test (SPT)-based liquefaction correlations from levelground conditions to sloping-ground conditions. Afterwards; numerous researchers have since studied this phenomena and these studies have shown that K_α is dependent on relative density (D_R), confining stress, failure criteria (or definition of ‘‘liquefaction’’ for determining cyclic resistance), and somewhat on the laboratory test device (Boulanger,2003).

The dependency of K_α on relative density and confining stress is well explained by simple state parameter index (ξ_R). The state parameter index (Konrad 1988) provides better correlations to the shear behavior of sand shown in equation 4.20.

$$\xi_R = \frac{1}{Q - In\left(\frac{100\,p'}{P_a}\right)} - D_R \tag{4.20}$$

ξ_R is an empirical index that has a functional form consistent with critical stress concepts. Obtaining the relative state parameter index for an in situ soil requires estimates of relative density, D_R, and empirical constant, Q. p′ is mean effective normal stress and P_a is atmospheric pressure. K_α values are also dependent on the choice of failure criterion, particularly for more dilatant sands with K_α values greater than unity. The relation between K_α and ξ_R can be approximated by the following equation (Idriss and Boulanger 2003);

$$K_\alpha = a + b\,\exp\left(\frac{\xi_R}{c}\right) \tag{4.21a}$$

$$a = 1267 + 636\,\alpha^2 - 634\exp(\alpha) - 632\exp(-\alpha) \quad (4.21b)$$

$$b = \exp\left[-1.11 + 12.3\alpha^2 + 1.31\ln(\alpha + 0.0001)\right] \quad (4.21c)$$

$$c = 0.138 + 0.126\alpha + 2.52\alpha^3 \quad (4.21d)$$

K_σ overburden correction factor is the adjustment factor for the effects of σ'_v on cyclic resistance ratio. K_σ relations can be critical for liquefaction evaluations at high overburden stresses, such as what can be encountered beneath large earth dams or embankments.

The effect of overburden stress on a liquefaction analysis is illustrated by tracking its effects on both penetration resistance and CRR. Relative state parameter index (ξ_R) based approach of simplified implementation with the $CRR_{\sigma=1}$ is proposed by Harder and Boulanger (1997) as approximated in equation 4.22.

$$K_\sigma = 1 - C_\sigma \ln\left(\frac{\sigma'_v}{P_a}\right) \quad (4.22)$$

with C_σ =0.185

As a result cyclic resistance ratio, CRR should be corrected for these effects using the following expression:

$$CRR = K_\sigma \cdot K_\alpha \cdot CRR_{\sigma=1,\alpha=0} \quad (4.23a)$$

where

$$\alpha = \frac{\tau_s}{\sigma'_{v0}} \quad (4.23b)$$

$CRR_{\sigma=1,\alpha=0}$= cyclic resistance ratio for $\sigma'_{v0}/P_a=1$ and $\alpha=0$ as obtained through a semiempirical correlation for the earthquake magnitude and other conditions under consideration.

P_a=atmospheric pressure

α=static horizontal shear stress ratio

σ'_{vo}=vertical effective consolidation stress

τ_s =static horizontal shear stress

The application of K_α and K_σ corrections on $N_{1,60}$ is different than the conventional applications of them on CRR. However one can easily prove that, applying corrections on CRR or $N_{1,60}$ (in the form given in Equation 4.24) produce identical liquefaction triggering probabilities, based on Cetin et al. (2004) probabilistic liquefaction triggering methodology (Equation 2.3). It should be noted however that these modified $N_{1,60}$ values are only used in the excess pore pressure generation loops, but not in the estimation of modulus or failure envelope parameters. The application of K_α and K_σ corrections on $N_{1,60}$ is presented in Figures 4.11 and 4.13.

Different than the original UBCSAND model, input parameter, $N_{1,60}$ is modified through series of K_α and K_σ corrections as shown in Equation 4.24.

$$N_{1,60_{(eqv.)}} = N_{1,60} + 13.32\ln(K_\alpha) + 13.32\ln(K_\sigma) \qquad (4.24)$$

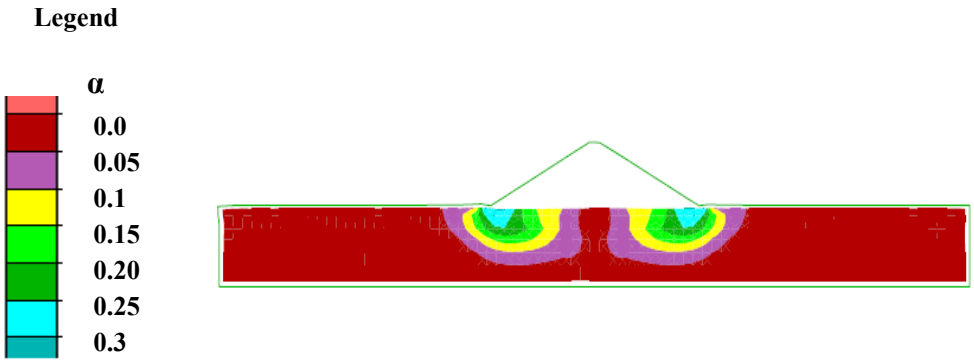

Figure 4.11: Static shear stress ratio, α values on the dam foundation

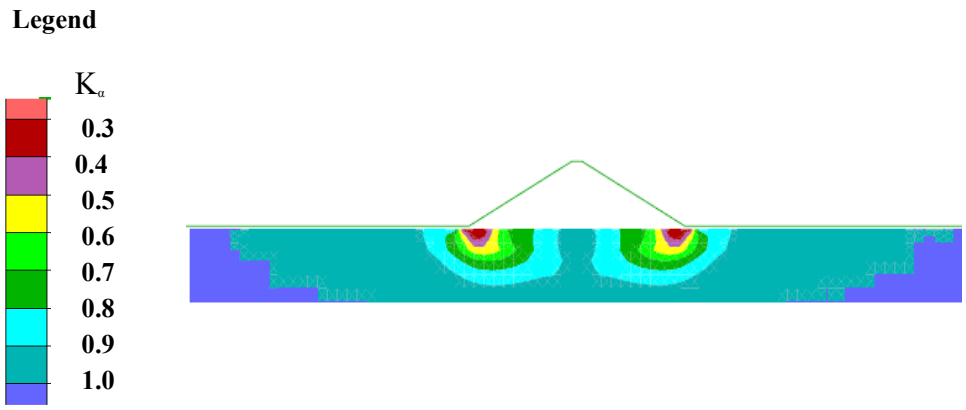

Figure 4.12: K_{α} adjustment values on the dam foundation

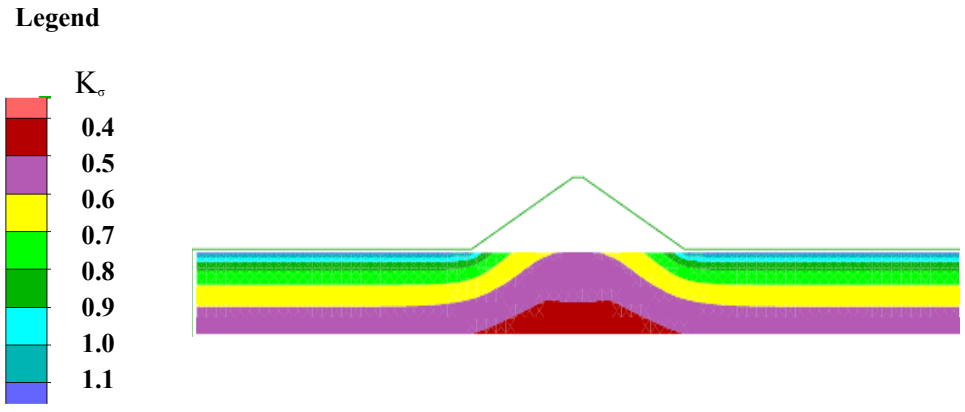

Figure 4.13: K_{σ} overburden correction values on the dam foundation

K_α is confining stress dependent (Figure 4.11). It is unity beneath the center of the dam and decreasing through beneath the toes. In contrast to K_α effects, overburden correction factor, K_σ is decreasing with increasing confining pressure. It is unity beneath the toes and increasing through the centerline of the dam. The SPT-N values with and without K_α and K_σ corrections are shown in Figure 4.14 $(N_1)_{60}$ values significantly decreases around the toe of the dam body with the applications of K_α and K_σ corrections.

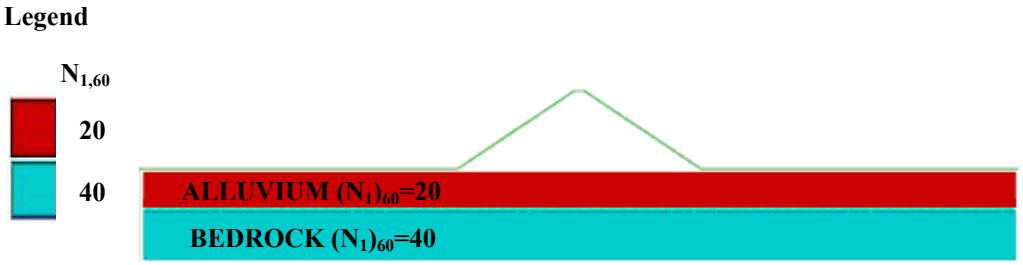

a): UBCSAND model

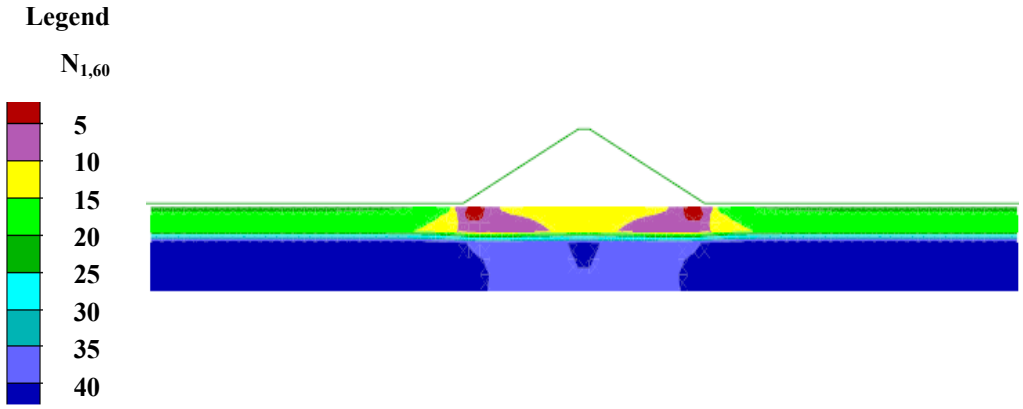

b) Modified UBCSAND model

Figure 4.14: $(N_1)_{60}$ values on the dam foundation
a) UBCSAND model b) Modified UBCSAND model

4.1.3 Modeling Parameters

For the finite element analysis, a suitable material model is needed in order to model stress-strain behavior of the materials. Material model parameters are selected mainly referring to the previous studies on the dams consisting of similar materials. Modelling parameter using in the numerical analysis is presented in Table 4.2.and the cross section properties of the dam body are shown in Table 4.3. The modeled cross section of the embankment can be seen in Figure 4.15.

Table 4.2: Material propertiesof the dam

	Material Behaviour	Failure Criteria		Unit Weight (kN/m^3)	Shear Modulus (MPa)	Poisson's Ratio		Cohesion (kPa)		Internal Friction Angle°		Permeability (m/s)
		Static	Dynamic									
Clay Core	Elastic-Perfectly Plastic	Mohr-Coulomb	Mohr-Coulomb	19	76	Undrained	Drained	Undrained	Drained	Undrained	Drained	10^{-8}
						0.5	0.33	75	15	0	26	
Earthfill			Mohr-Coulomb	19	190	0.44		0		35		10^{-4}
Alluvium			UBCSAND	18	80	0.41		0		38		10^{-4}
Bedrock			UBCSAND	22	850	0.25		150		43		10^{-7}

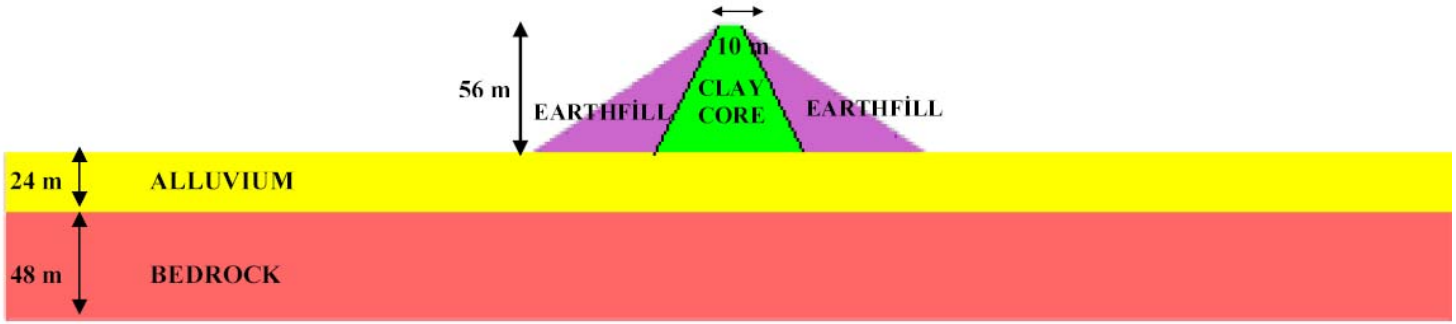

Figure 4.15: Cross section model of the earthfill dam

Table 4.3: Cross section properties of the dam

	Dam Body
Dam Height (from foundation)	56 m
Crest Widlth	10 m
Upstream Slope (Vertical/Horizontal)	1/3
Downstream Slope (Vertical/Horizontal)	1/3

4.2 Static Analysis of the Earthfill Dam

In order to determine the stresses and displacements in earth dams under static conditions, finite element or finite difference method can be used by performing the analysis in a number of steps. Use of incremental analyses procedures provides a convenient means of representing changes in geometry during construction of the embankment, changes in loading during filling of the reservoir and nonlinear stress-strain behavior of the embankment materials. As mentioned earlier, FLAC explicit finite difference program is used to perform these analyses.

Embankment is an earthfill dam having a clay core, with sand and gravel filter zones. Static analysis is performed to obtain the mean effective stresses for the assessment of the dynamic material properties which represent the nonlinear behavior of the embankment dam. The Mohr-Coulomb model is the conventional model used to represent shear failure in soils and rock.

Numerical analysis results for static condition of the dam are represented in the case of i) horizontal displacements, ii) vertical displacements, iii) total vertical stress, iv) total horizontal stress and v) maximum shear strains; respectively shown in Figures 4.16-4.21 for after construction stage.

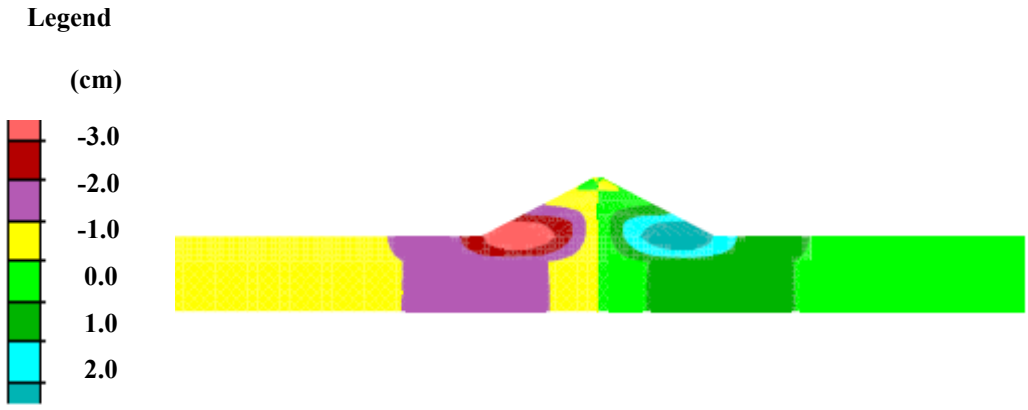

Figure 4.16: Horizontal displacements after end of construction stage

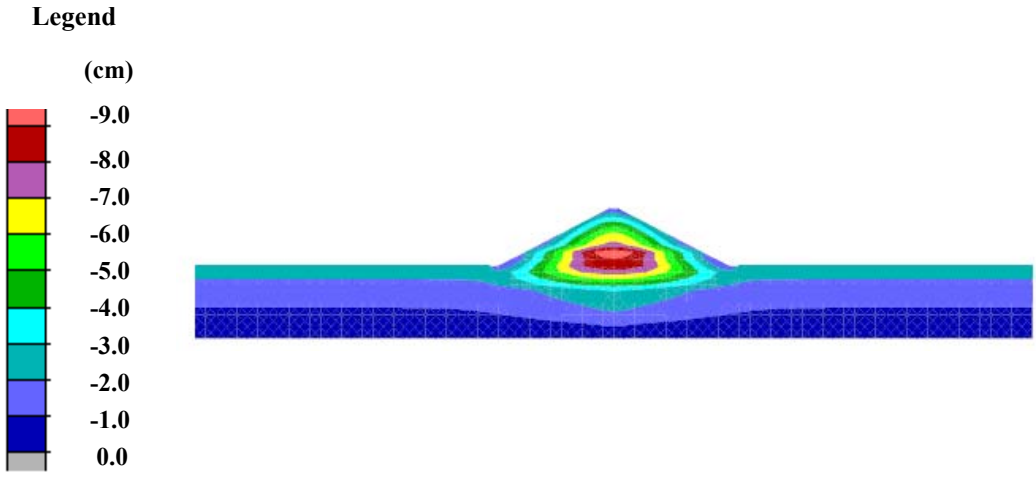

Figure 4.17: Vertical displacements after end of construction stage

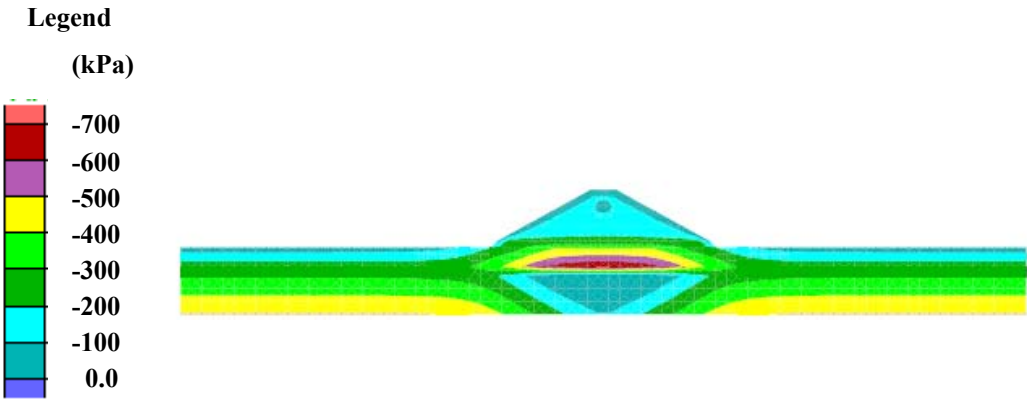

Figure 4.18: Total horizontal stress after end of construction stage

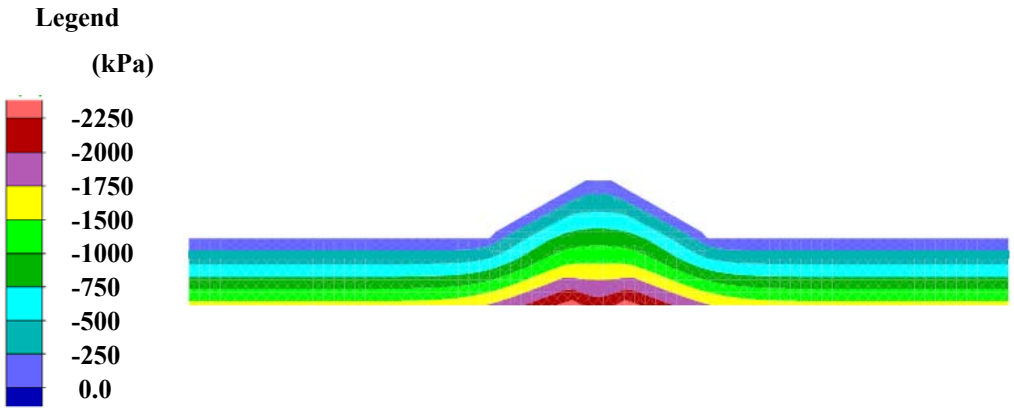

Figure 4.19: Total vertical stress after end of construction stage

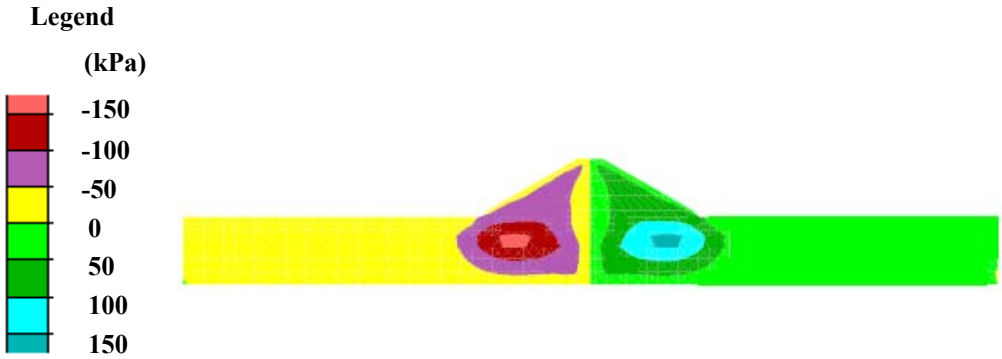

Figure 4.20: Total shear stresses after end of construction stage

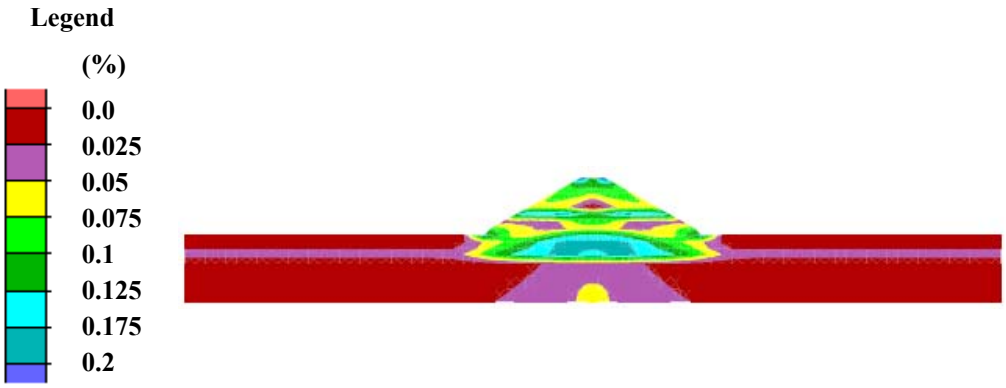

Figure 4.21: Maximum shear strain increment after end of construction stage

As a result of the numerical analyses, horizontal and vertical total stresses on the dam body are compatible with the weight of the materials. For instance, as shown in Figure 4.13, maximum vertical stress on the center of the dam body is approximately 1000 kPa and this value is compatible with the multiplication of unit weight and height of the dam.(=19*56=1064 kPa). Furthermore, maximum horizontal and vertical displacements are 3 and 9 cm, respectively, at the end of the construction stage.

After construction stage, by applying a mechanical pressure to the upstream face of the dam, the dam responds mechanically. Next, phreatic surface develops and fluid flow is allowed. Numerical analysis results for reservoir fill of the dam are represented for the cases of i) horizontal displacements, ii) vertical displacements, iii) total vertical stress, iv) total horizontal stress and v) maximum shear strains; respectively, as shown in Figures 4.22-4.27 for the phreatic surface stage.

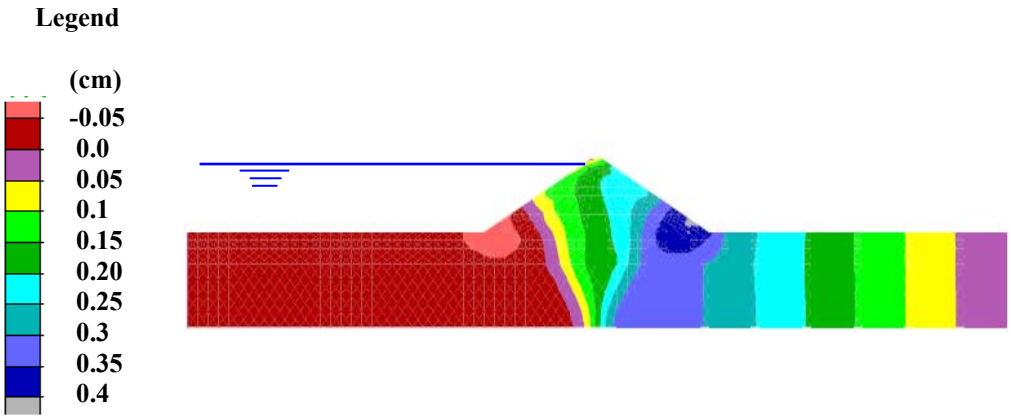

Figure 4.22: Horizontal displacements corresponding to phreatic surface stage

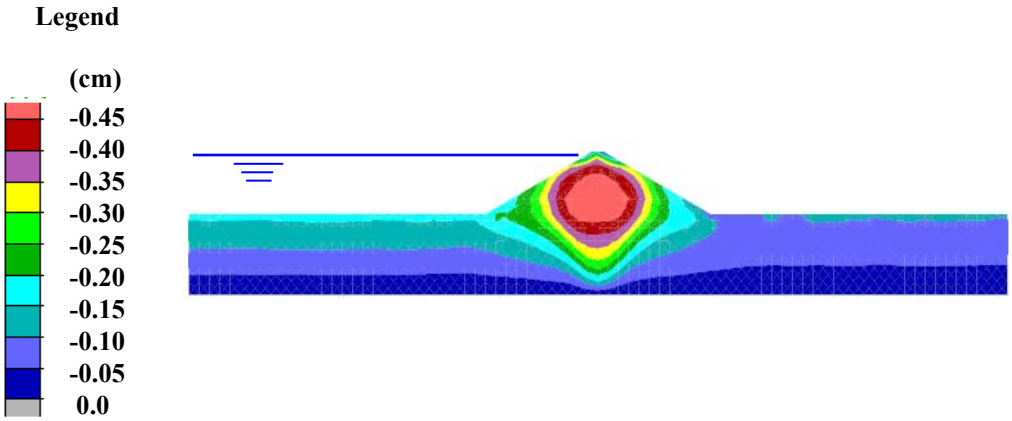

Figure 4.23: Vertical displacements corresponding to phreatic surface stage

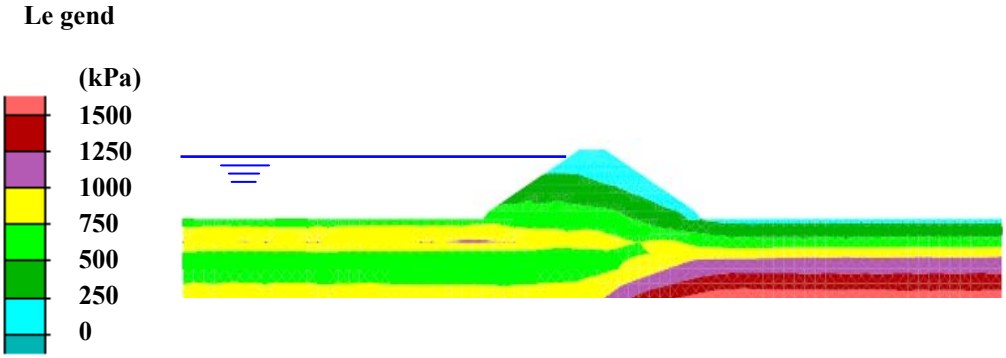

Figure 4.24: Total horizontal stress corresponding to phreatic surface stage

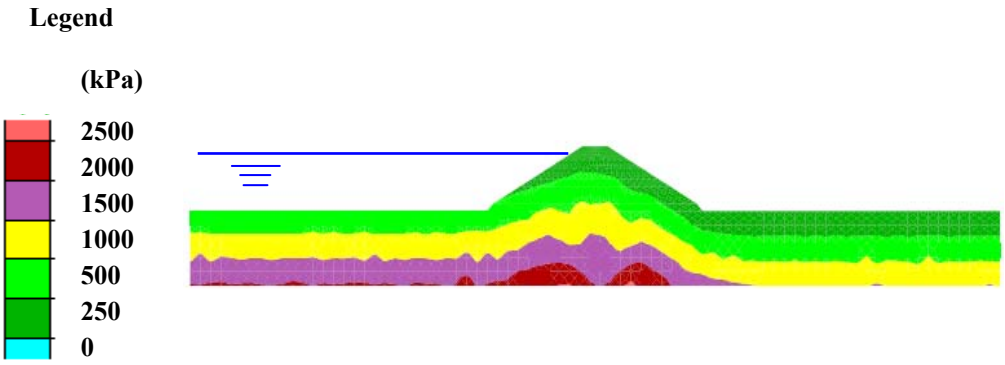

Figure 4.25: Total vertical stresses corresponding to phreatic surface stage

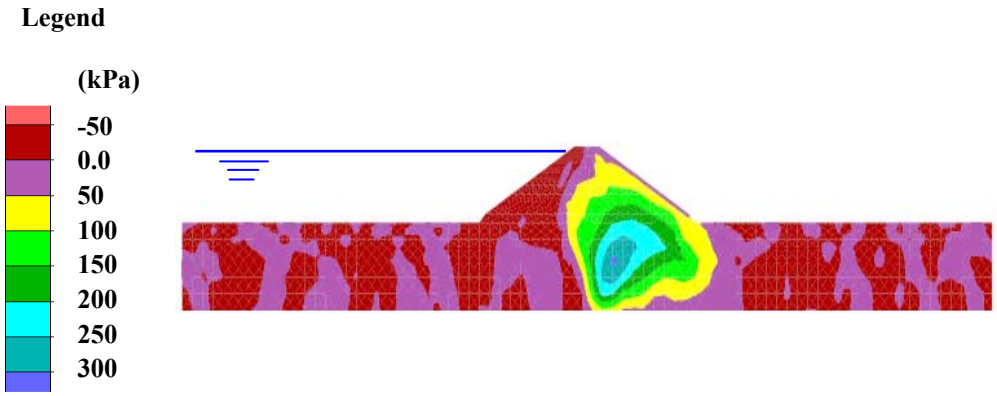

Figure 4.26: Total shear stresses corresponding to phreatic surface stage

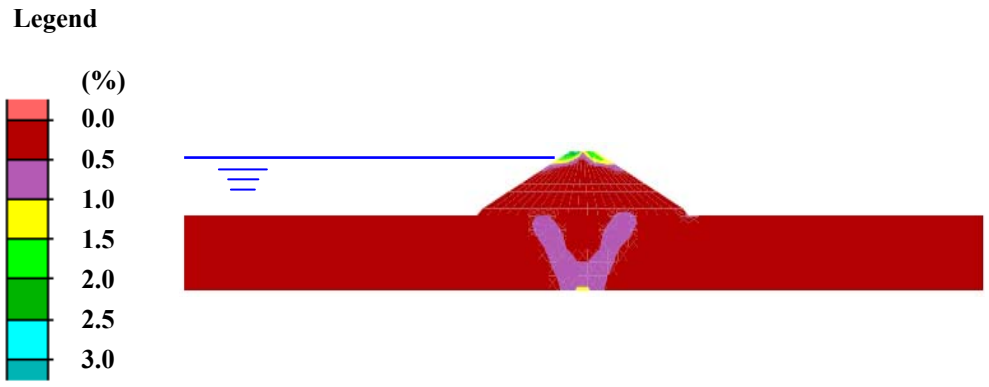

Figure 4.27: Maximum shear strains corresponding to phreatic surface stage

4.3 Dynamic Analysis of the Earthfill Dam

Dynamic analyses of the dam were performed by using UBCSAND effective stress model on the dam foundation. No doubt that the finite element method has been one of the most powerful tools for evaluation the dynamic response of fill dams under earthquake loading. As part of the site conditions scenario, $N_{1,60}$=20 is selected for the alluvium and $N_{1,60}$=40 for bedrock. As discussed earlier, SPT based K_α and K_σ corrections are applied to the UBCSAND model and liquefaction triggering potential of the alluvium type dam foundation is analyzed.

The procedure of the analyses was as follows:

i) Mean effective stresses needed for the dynamic analyses were determined by performing static analyses with Mohr-Coulomb failure criteria. Before starting the dynamic analysis, displacements were reset to zero to estimate only seismically-induced deformations.

ii) For 16 re-grouped magnitude-distance bins, 24 earthquake records were selected by probabilistic seismic hazard assessment.

iii) Material properties and strong ground motions are given as input data to the program in order to obtain the acceleration time histories of the required points at the slip surface.

iv) Post earthquake stresses, excess pore pressures and displacements are evaluated.

For illustration purposes, seismic response analysis results are presented in the form of i) horizontal displacements, ii) vertical displacements, iii) total horizontal stress and iv) maximum shear strains; as shown in Figures 4.28-4.33. Similarly, a) acceleration, b)velocity, c) displacement time histories occurred at

bedrock, dam foundation, and crest elevations are shown in Figures 4.34 to 4.36 for the earthquake scenario no 13 (i.e.: M_w = 6.4, and r_{jb}=53 km).

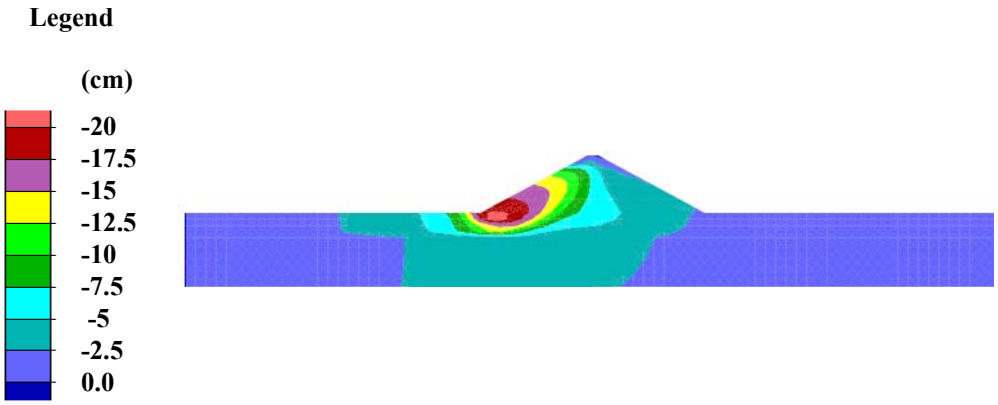

Figure 4.28: Seismically-induced maximum horizontal displacements

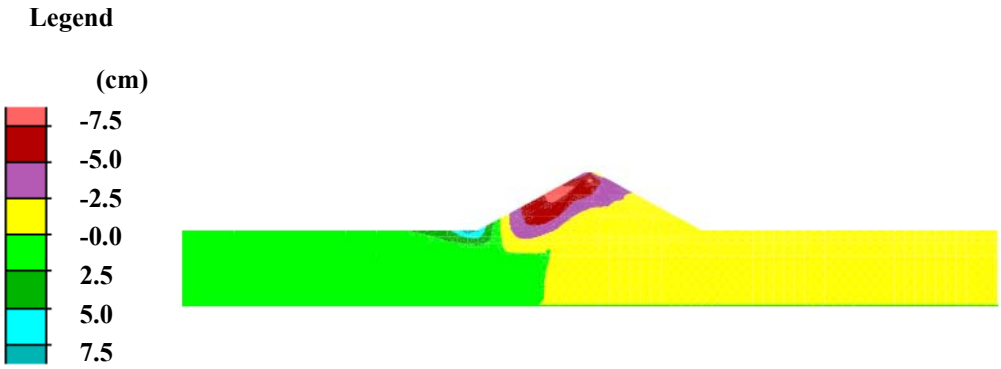

Figure 4.29: Seismically-induced maximum vertical displacements

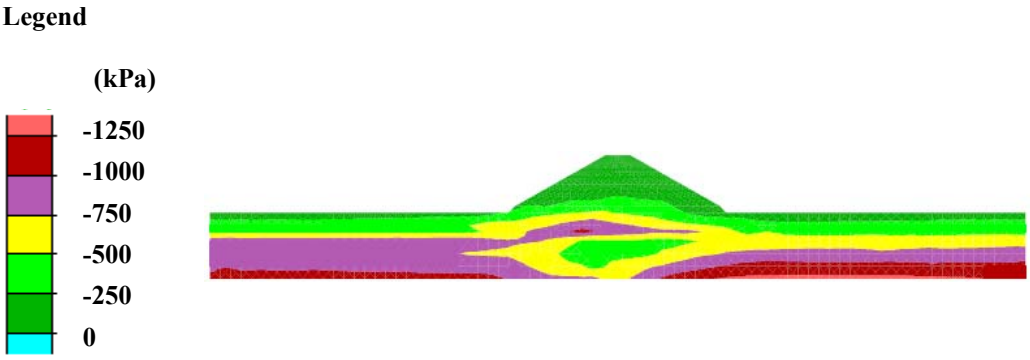

Figure 4.30: Seismically-induced maximum total horizontal stresses

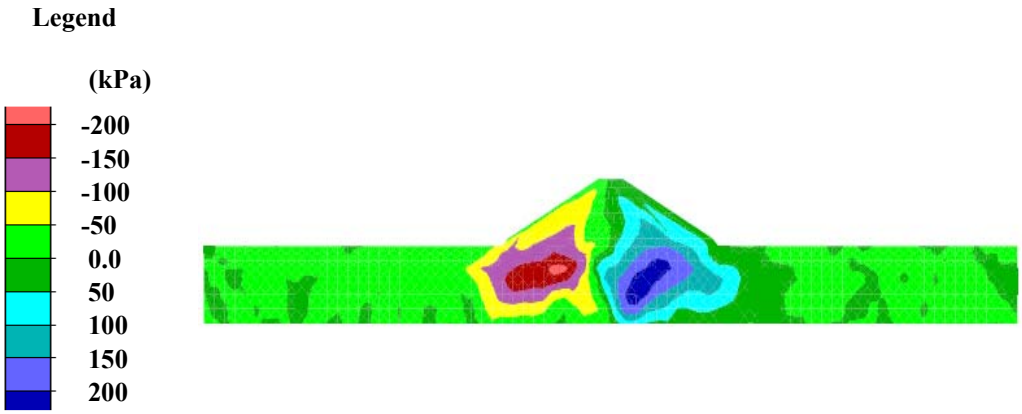

Figure 4.31: Seismically-induced maximum total shear stresses

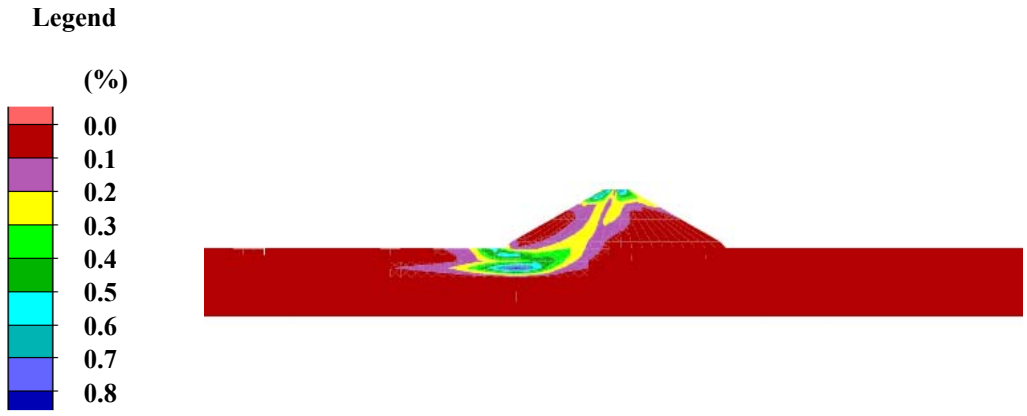

Figure 4.32: Seismically-induced maximum shear strain increments

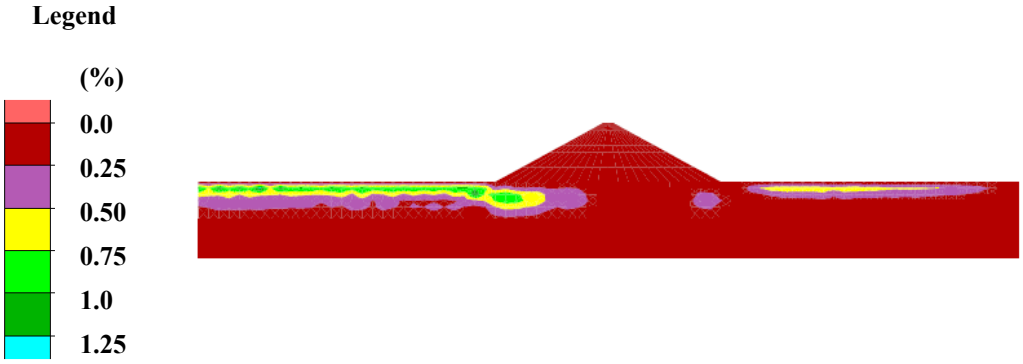

Figure 4.33: Seismically-induced excess pore pressure ratio, r_u

As can be seen from the Figure 4.32, the critical failure mode is slope stability failure on the upstream side of the dam. This was the case of all earthquake bins.

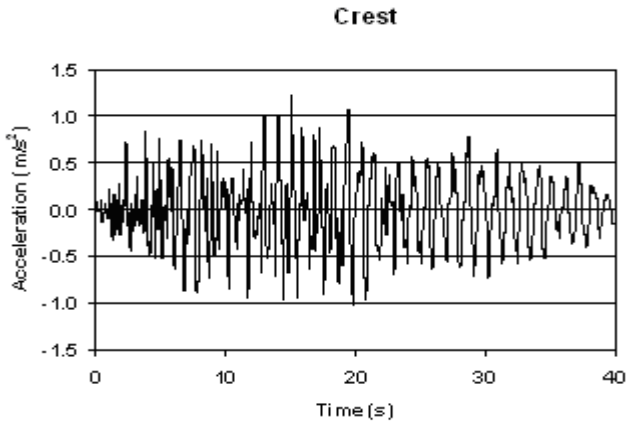

(a)

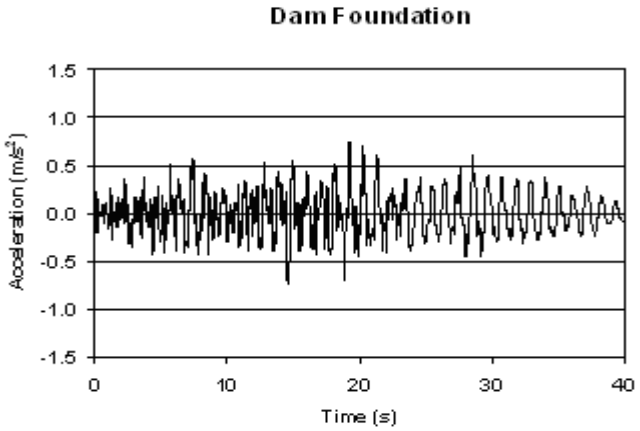

(b)

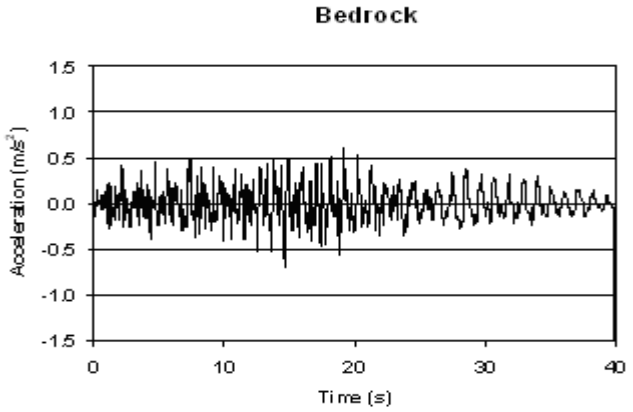

(c)

Figure 4.34: Acceleration time histories of a) Crest, b) Dam Foundation c) Bedrock

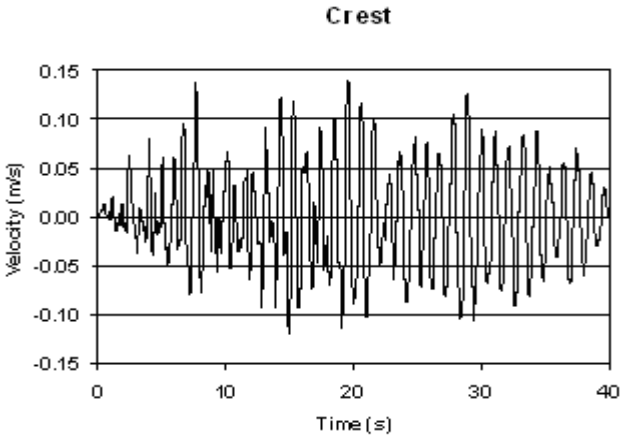

(a)

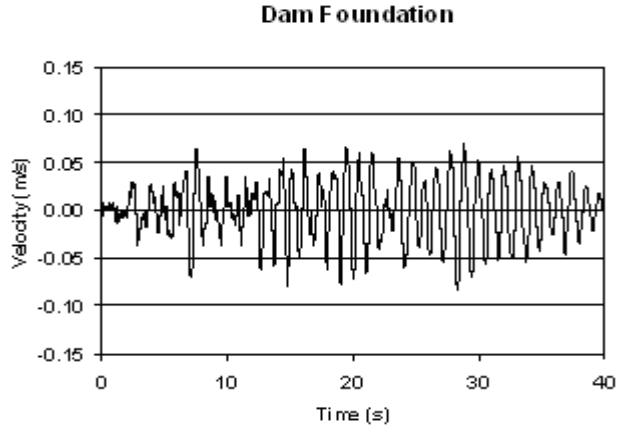

(b)

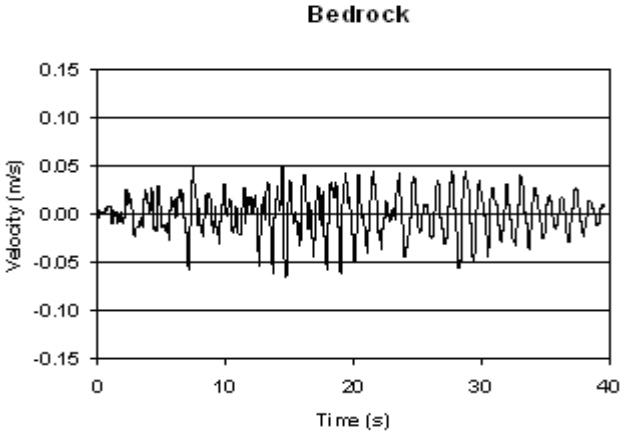

(c)

Figure 4.35: Velocity-time histories of a) Crest, b) Dam Foundation c) Bedrock

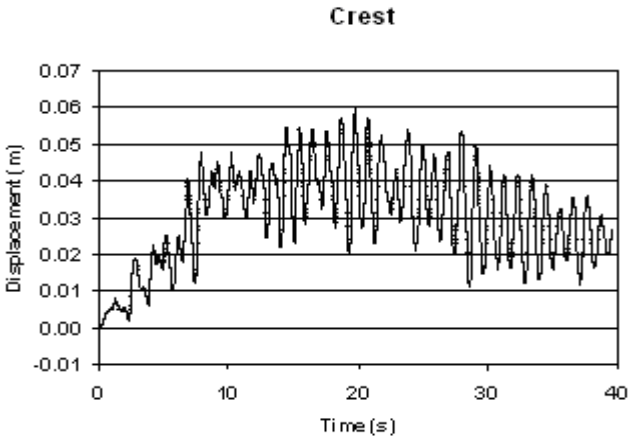

(a)

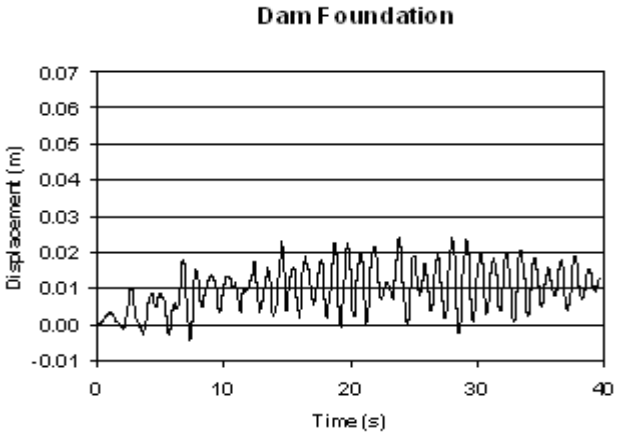

(b)

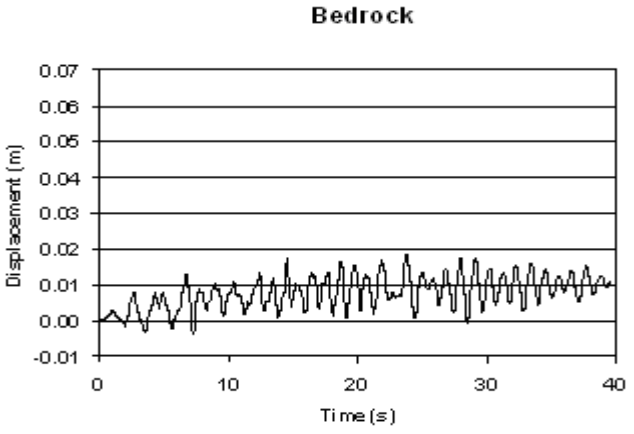

(c)

Figure 4.36: Displacement-time histories of a) Crest, b) Dam Foundation c) Bedrock

CHAPTER 5

POST PROCESSING OF NUMERICAL ASSESSMENT RESULTS

Seismic response analyses are presented for five points located in the alluvium layer as shown in Figure 5.1. Point C is just beneath the center of the dam body. Point B and D are located 3 meter below the ground surface at the toes. Point A and E are located 3 meters below the ground surface at a distance of 40 m away from the toes.

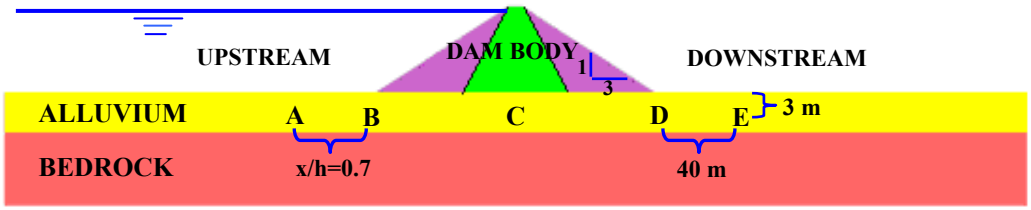

Figure 5.1: The location of five points selected on the alluvium

5.1 Post-Earthquake Horizontal Deformations and Excess Pore Pressure Ratio

The results are summarized in Table 5.1 in the form of maximum i) excess pore pressure ratio, r_u, (= the ratio of excess pore pressure to initial vertical effective stress) and ii) horizontal displacements, d_x, for the five points, A through E corresponding to 16 earthquake scenarios.

Table 5.1. Summary of seismic response analysis for points A,B,C,D and E

EQ Scenario Bin	M_w	Fault Distance, r_{jb}	Maximum Matched Accelerations	Point A		Point B		Point C		Point D		Point E	
		km	g	r_u	d_x cm	r_u	d_x cm	r_u	d_x cm	r_u	d_x cm	r_u	d_x cm
1	5.2	18	0.069	0.23	0.64	0.29	2.0	0.04	0.85	0.25	2.60	0.35	0.75
2	5.2	27	0.051	0.32	0.50	0.19	2.0	0.05	1.0	0.15	2.50	0.33	0.70
3	5.2	43	0.036	0.30	0.20	0.15	1.0	0.05	0.60	0.13	1.80	0.31	0.50
4	5.2	63	0.027	0.35	0.30	0.10	0.80	0.10	0.40	0.10	1.20	0.25	0.25
5	5.6	20	0.079	0.83	1.10	0.65	6.70	0.05	1.80	0.35	5.0	0.49	1.50
6	5.6	43	0.045	0.40	0.60	0.33	2.20	0.03	1.50	0.22	3.10	0.39	0.65
7	5.6	62	0.034	0.90	0.50	0.87	5.0	0.10	2.50	0.30	4.0	0.55	0.45
8	6	19	0.101	0.73	1.15	0.42	5.50	0.38	1.90	0.45	4.45	0.65	1.40
9	6	40	0.058	0.80	1.00	0.60	5.50	0.0	1.20	0.25	4.10	0.45	1.50
10	6	59	0.044	0.60	0.50	0.65	3.80	0.0	1.80	0.25	4.20	0.42	0.90
11	6.4	18	0.135	1.0	50.0	0.80	210.0	0.02	4.0	0.80	130.0	0.85	5.0
12	6.4	37	0.076	0.83	10.50	0.68	70.50	0.08	2.50	0.51	14.0	0.65	2.0
13	6.4	53	0.058	0.91	1.10	0.86	23.50	0.07	2.10	0.40	6.25	0.55	1.60
14	6.8	18	0.16	0.95	40.0	0.75	250.0	0.30	4.50	0.81	220.0	0.9	90.0
15	6.8	38	0.092	1.0	15.0	0.75	120.0	0.10	3.50	0.80	20.0	0.9	4.0
16	7.2	16	0.215	1.0	80.0	0.75	140.0	0.30	32.0	0.8	166.0	0.9	123.

For illustration purposes, excess pore pressure ratio, r_u vs. time response is also shown for the earthquake scenario no 13 (i.e.: M_w = 6.4, and r_{jb}=53 km) in Figure 5.2. As this figure implies, r_u reaches to a maximum value of 0.1 at point C (at a location right beneath the centerline of the dam body) which can be interpreted as "no-liquefaction". However, for the same seismic scenario, liquefaction of the upstream region (Point A) and upstream toe region (Point B) is expected based on estimated large r_u values (> 0.8). The distribution of the r_u values throughout the foundation, as shown in Figure 5.3, also clarifies that upstream toe region of the alluvium is expected to liquefy.

For the purpose of illustrating the importance of K_α and K_σ corrections, the predictions of UBCSAND effective stress model is compared with the modified UBCSAND model. Dynamic response analysis of earthquake scenario bin 13 was performed without including K_α and K_σ corrections. As Figures 5.3 and 5.4 imply, if K_α and K_σ corrections were not applied, overconservatively biased estimates of r_u values are calculated, leading to dangerous conclusions.

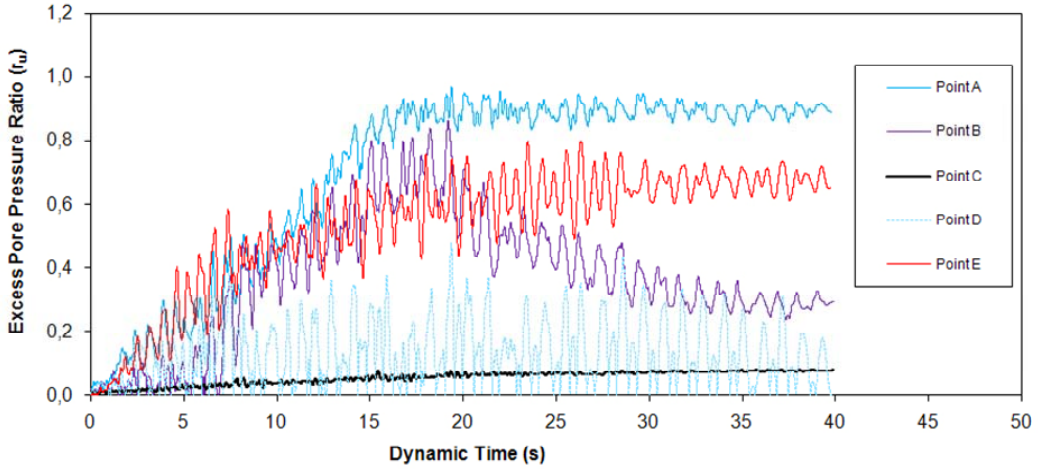

Figure 5.2: Excess pore pressure ratio, r_u vs. time response for earthquake scenario bin 13, M_w = 6.4, and r_{jb}=53 km

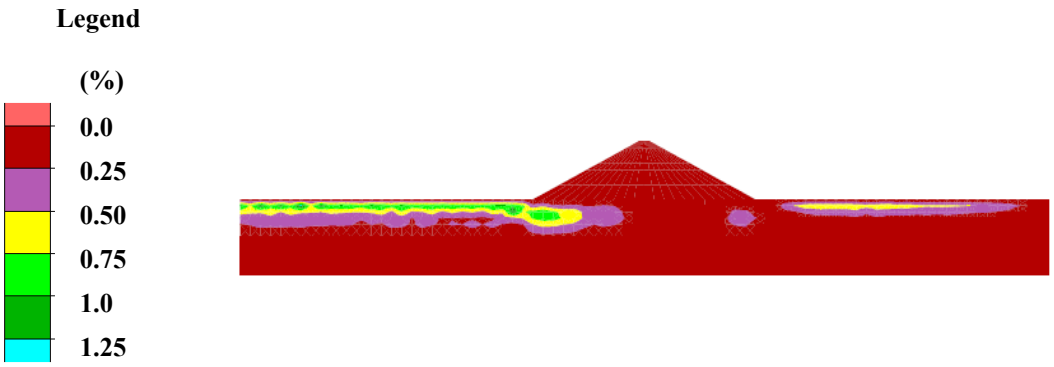

Figure 5.3: Excess pore pressure ratio, r_u for earthquake scenario bin 13, M_w = 6.4, and r_{jb}=53 km (Modified UBCSAND Model)

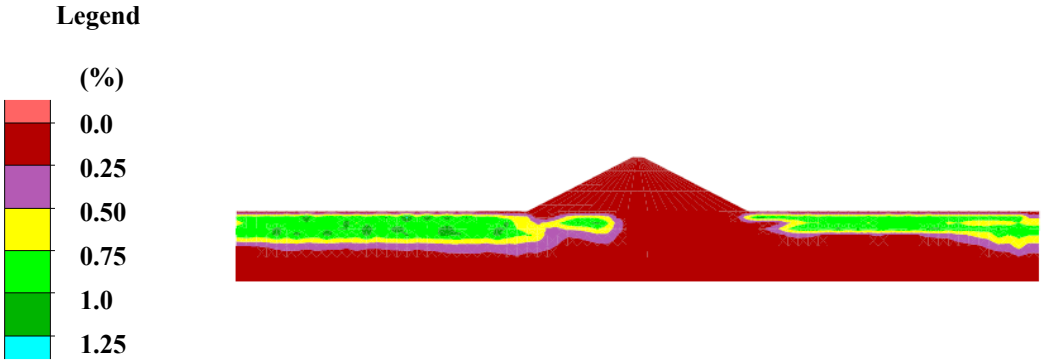

Figure 5.4: Excess pore pressure ratio, r_u for earthquake scenario bin 13 (UBCSAND Model)

After having explained the numerical assessment results for a specific earthquake case, (no 13) the probability-based liquefaction triggering assessment is now presented for all the earthquake scenario cases. As discussed earlier, seismic response analyses are performed for 16 earthquake scenarios, grouped into magnitude-distance bins (summarized in Table 3.1). 24 earthquake records were selected from the PEER (2007) NGA online catalog, consistent with the earthquake scenarios. The probability of occurrence of representative magnitude and distance bins are multiplied with the exceedence probabilities of excess pore pressure ratios for every bin. Figure 5.5 and Figure 5.6 show the annual probability of excess pore pressure ratio and annual probability of horizontal displacement respectively incorporating the activity rate of 0.299.

Following conclusions were reached based on analyses results provided in Figures 5.5 and 5.6:

From pore pressure generation point of view;

- Different locations of the dam have significantly different liquefaction triggering vulnerability and risk. Thus, mitigation methods should consider this variability in the associated risks.
- There is no risk of liquefaction at the central region of the dam (point C) due to the fact that annual probability of r_u*=0.8 is infinitely small.
- The most liquefaction vulnerable zone is estimated as the upstream toe of the dam (Point A), followed by the downstream toe region.
- Annual probability of liquefaction triggering is estimated as 0.06, 0.02, 0.0001, 0.01, and 0.01 for points A through E, respectively.

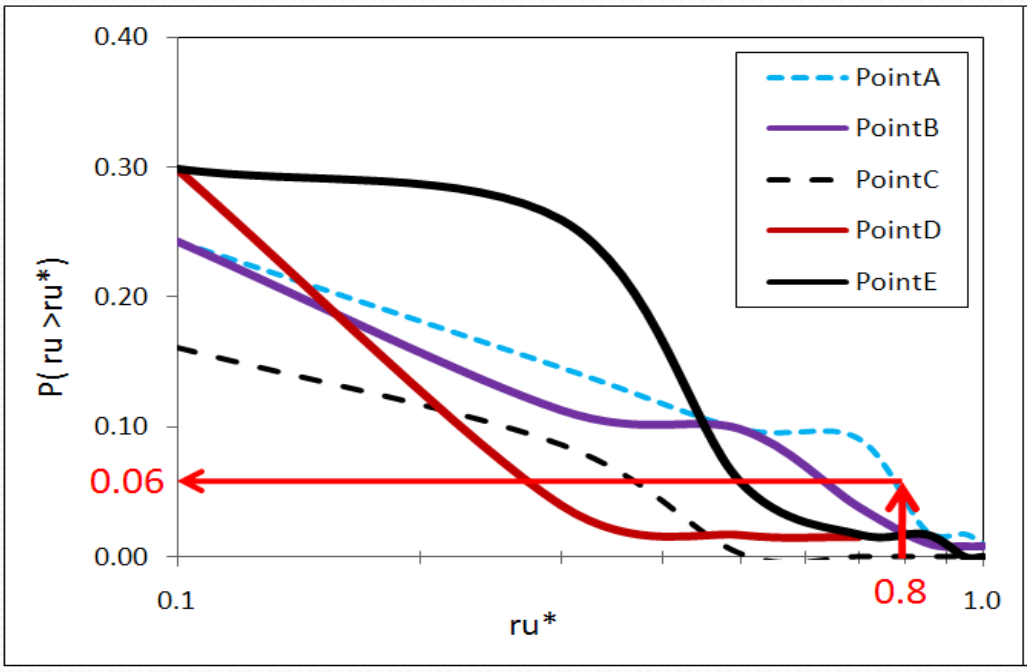

Figure 5.5: Annual probability of excess pore pressure ratio, r_u.

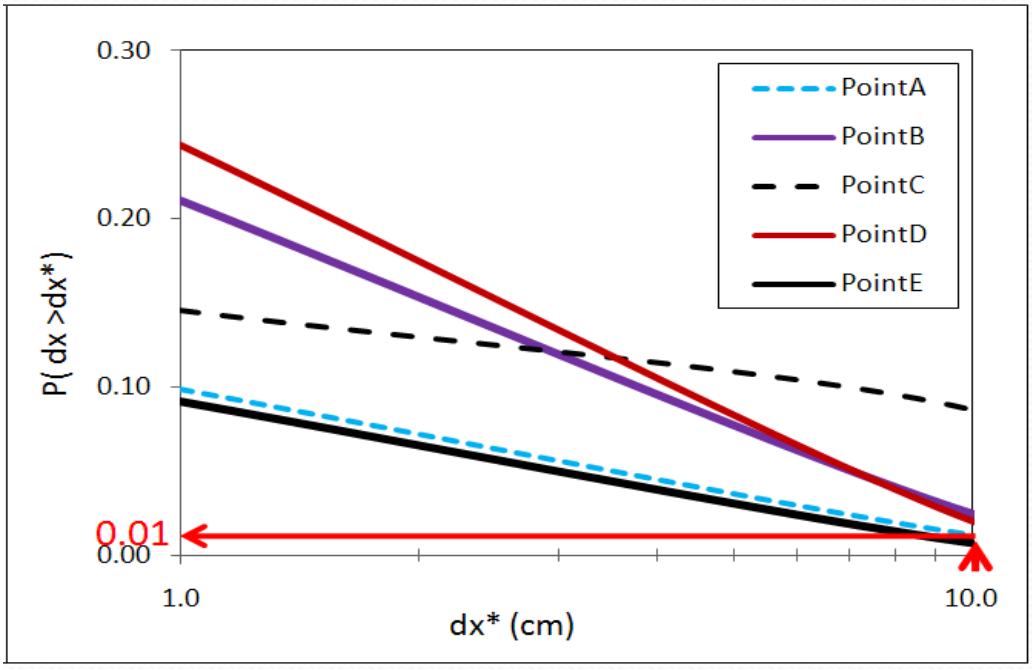

Figure 5.6: Annual probability of horizontal displacements

From seismically-induced lateral deformations point of view,

- Central region of the dam (point C) is the most critical region where significant seismically-induced lateral deformations (dx ≥10 cm) are concentrated.
- At upstream and downstream toe regions (points B and D) annual probability of lateral displacements exceeding the value of 10 cm is estimated as 0.05.

It should be noted that these results just present the seismic response of individual points but not the overall performance of the dam body.

Probability of liquefaction triggering in t years can be calculated as follows:

$$\lambda_{t\ years} = 1 - e^{-\lambda t} \tag{5.1}$$

where λ is annual probability of exceedence .

As an illustration, probability of liquefaction triggering defined by r_u>0.8 is estimated as 0.9 for point A, during the service life of 100 years as shown in Figure 5.7. In simpler terms, point A is expected to liquefy with a probability of 90 % during the economic life of the dam.

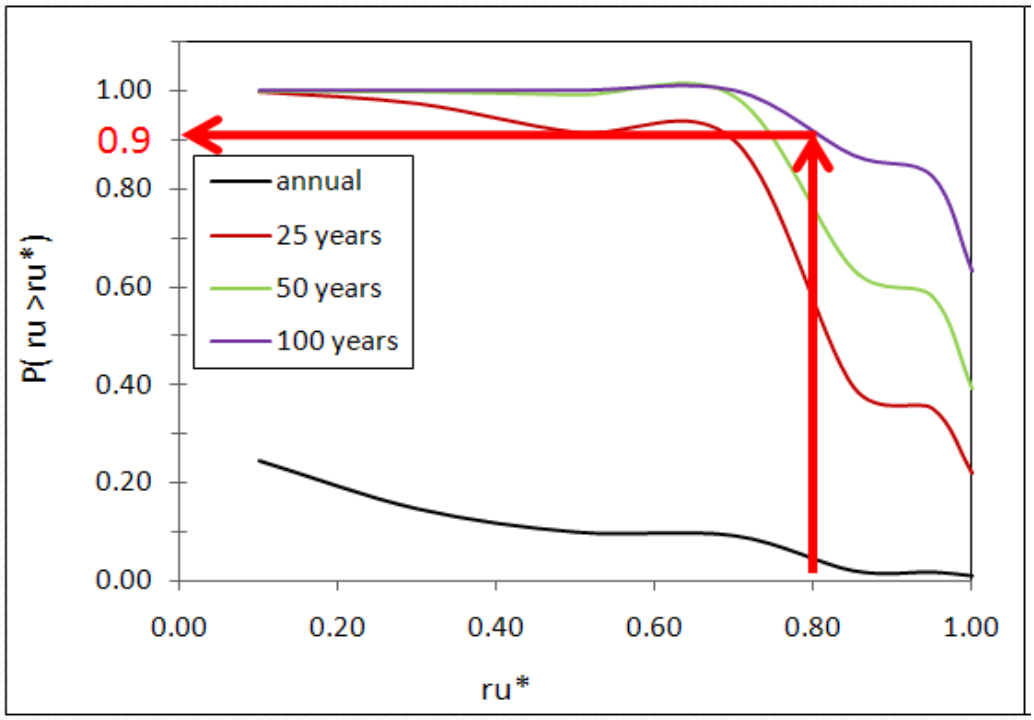

Figure 5.7: Probability of exceedance of r_u* at Point A

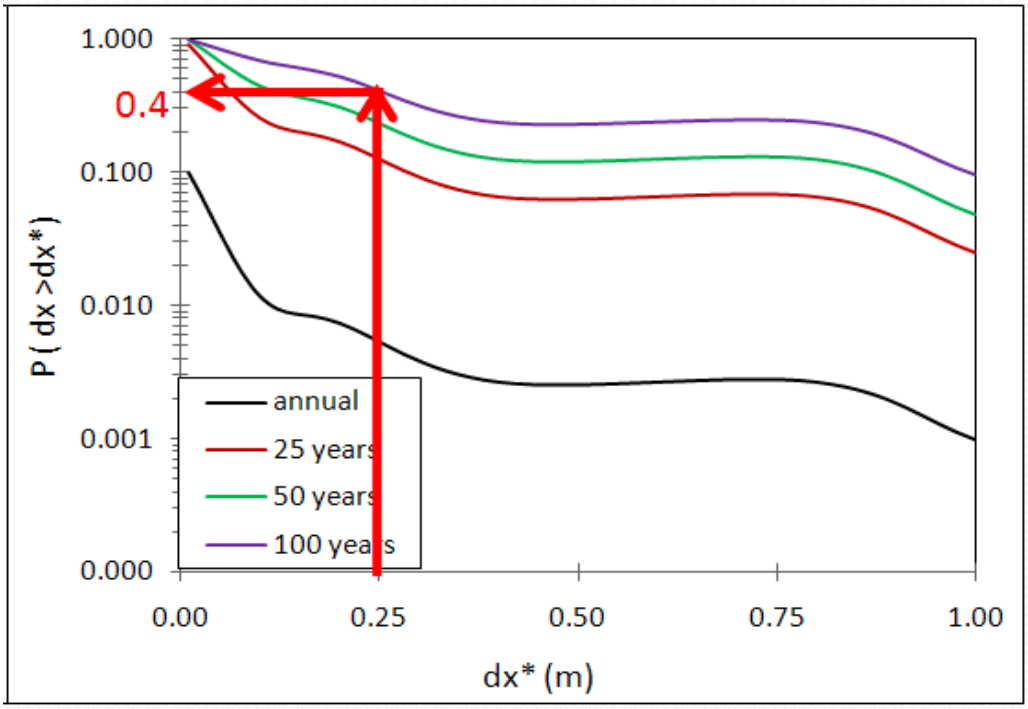

Figure 5.8: Probability of exceedance of displacement at Point A

Similarly, for different service life periods, probabilities of liquefaction triggering at different excess pore pressure ratios were estimated for the Point A as presented in Figure 5.9. Probability of $r_u > r_u^*$ for the threshold values of $r_u^*=0.8$, $r_u^*=0.9$ and $r_u^*=1.0$ are 0.9, 0.55 and 0.15 respectively.

Similarly, seismically-induced lateral deformations for Point A are expressed probabilistically, as shown in Figures 5.8. Figure 5.8 summarizes the induced deformation exceeding various threshold values during different service lives. For illustration purposes, the probability of seismically-induced lateral deformations exceeding 25 cm during a service life of 100 years is estimated as 0.4.

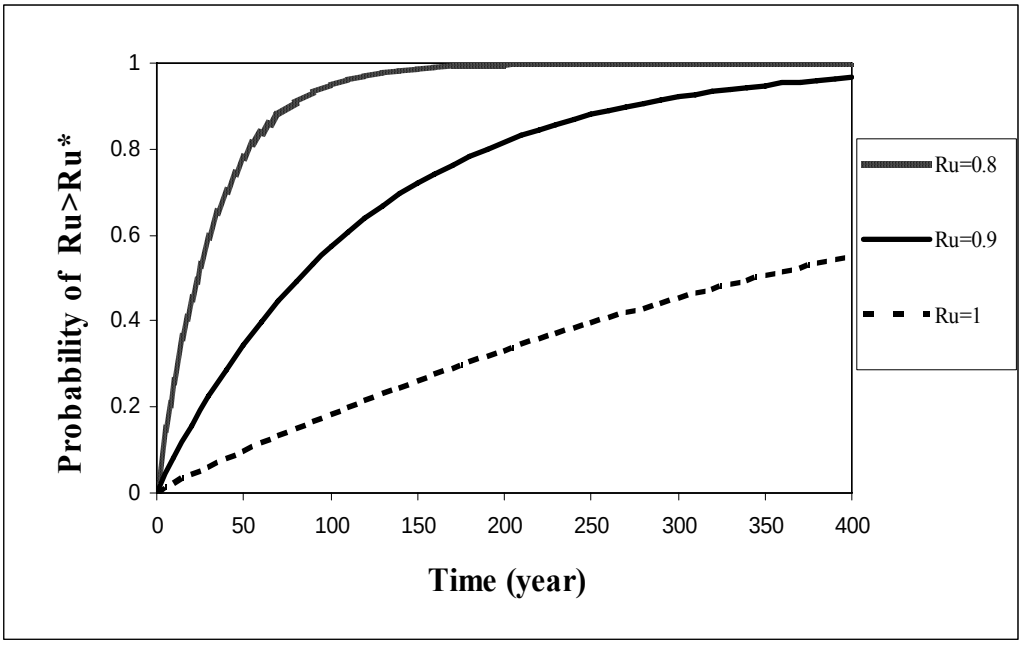

Figure 5.9: Probability of liquefaction triggering for different service lives.

As the results imply, if acceptable risk levels are defined, then seismic performance of the Point A can be identified in order to form a basis for decisions as to whether any mitigation is necessary. For illustration purposes, probability of liquefaction triggering can be estimated as 90 % in 100 years, if liquefaction is defined by $r_u > 0.8$ (Fig. 5.7). Similarly, if acceptable performance

is defined as maximum horizontal displacements to be less than - let's say – 25 cm, then probability of dam performance within acceptable limits is estimated as 40 % in 100 years (Fig. 5.8). Probability of $r_u > r_u^*$ is 90%, 55% and 15% for the threshold values of $r_u^*=0.8$, $r_u^*=0.9$ and $r_u^*=1.0$ respectively.

5.2 Probabilistic Slope Stability Assessments

In slope stability analyses, factor of safeties are used to determine whether a failure is expected or not. This section adopts ϕ-c reduction type slope stability assessment to estimate the factor of safety of slopes. A detailed description of the methodology is discussed in the PLAXIS manual and will not be repeated herein. The slope stability analysis are also performed by FLAC 4.0 software

ϕ-c reduction assessments were performed to evaluate the lateral deformations on the critical slip surface of the dam body for i) initial (static) state, ii) post earthquake liquefaction state, iii) steady state conditions. Initial state slope stability is obtained from "after construction stage" of the static analysis. Post-liquefaction slope stability assessments are based on the estimated excess pore pressures throughout the dam foundation. The shear strength changes with the excess pore pressure and factor of safety is calculated during the earthquake by using updated pore pressure values along with steady state friction angle values used for liquefied regions.

Poulos (1981) states that the steady state condition is defined as "the state in which the mass is continuously deforming at constant volume, constant normal effective stress, constant shear stress, and constant velocity". The steady state strength is defined as the shear strength of the soil when it is at the steady state condition. The steady state applies to both the drained and undrained conditions and this strength value is used for seismic design. The ϕ-c reduction based factor

of safety is analyzed in the steady state condition with friction angle of the dam and foundation is 28°.

By using slope stability assessment results within a probabilistic seismic hazard framework, annual probabilities of factor of safety of slopes exceeding various threshold values were estimated as shown in Figure 5.10. Figure 5.10 is plotted by simply reducing both cohesion and tan ϕ of the shear strength by reduction factor and estimating the induced lateral deformations. As the figure implies, beyond a reduction of 2.2, stability can not be achieved; thus factor of safety is estimated as 2.2.

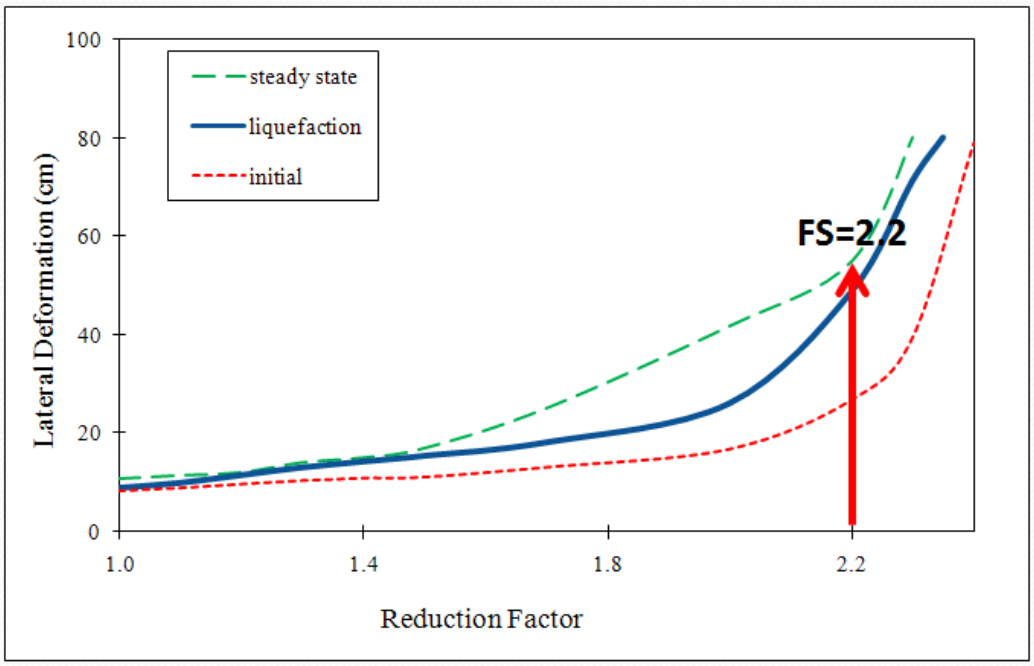

Figure 5.10: ϕ-c reduction based factor of safety

Moreover, if acceptable performance is defined as maximum horizontal displacements to be less than - let's say 25 cm - then the corresponding FS can

be estimated as 2.0. Figure 5.10 reveals that, lateral deformations should be evaluated as part of liquefaction triggering assessments.

5.3 Comparisons with Conventional Liquefaction Triggering Assessments

For evaluation of liquefaction resistance, three approaches are employed (for Point A shown in Figure 5.1); i) NCEER (1997) (Seed et al., 1984), deterministic assessment, ii) Cetin et al.(2004) probabilistic liquefaction triggering assessment and, iii) Cetin et al.(2004) deterministic correlations.

Deterministic approaches are used within the probabilistic seismic hazard framework. However, decisions are made in a simple "yes" or "no" manner (Table 5.2 and 5.3). DWF_M is magnitude-correlated duration weighting factor and $\mathbf{K_\sigma}$ correction factor used as recommended by NCEER Workshop (1997). $\mathbf{K_\alpha}$ correction factor is estimated from Equation 4.21.

Table 5.2: Hybrid framework of NCEER, 1994 (Seed et. al., 1984)

(M_w=7.5 →CRR=0.22*)							
M_w	**DWF_M**	**K_σ**	**K_α**	**$CRR_{corrected}$**	**CSR_{eq}****	**FS (CRR/CSR)**	**P(L)*****
5.2	2.08	1	0.8	0.37	0.31	1.18	0
5.6	2.00	1	0.8	0.35	0.31	1.13	0
6.0	1.75	1	0.8	0.31	0.31	0.99	1
6.4	1.50	1	0.8	0.26	0.31	0.85	1
6.8	1.29	1	0.8	0.23	0.31	0.73	1
7.2	1.13	1	0.8	0.20	0.31	0.63	1

* CRR is obtained for $(N_1)_{60}$=20 from Figure 2.8
** CSR is obtained from Equation 2.1
***P(L) is probability of liquefaction.

Table 5.3: Hybrid framework of Cetin et. al., 2004

M_w	CRR*	K_α	$CRR_{corrected}$	CSR_{eq}	FS (CRR/CSR)	P(L)
5.2	0.500	0.8	0.40	0.31	1.28	0
5.6	0.480	0.8	0.38	0.31	1.23	0
6.0	0.440	0.8	0.35	0.31	1.13	0
6.4	0.360	0.8	0.29	0.31	0.92	1
6.8	0.310	0.8	0.25	0.31	0.79	1
7.2	0.270	0.8	0.22	0.31	0.69	1

* CRR is obtained from Equation 2.4

The different approaches for assessing liquefaction triggering vulnerabilities until 600 years of a service life are presented in Figure 5.11. For a service life of 100 years, NCEER (1997) methodology estimates 100% liquefaction triggering probability. Similarly Cetin et al.(2004) deterministic methodology predicts 88% probability of liquefaction. Modified Byrne model (for r_u=1) and probabilistic Cetin et al (2004) predict very close probability of liquefaction which are in the order of 20 %. .

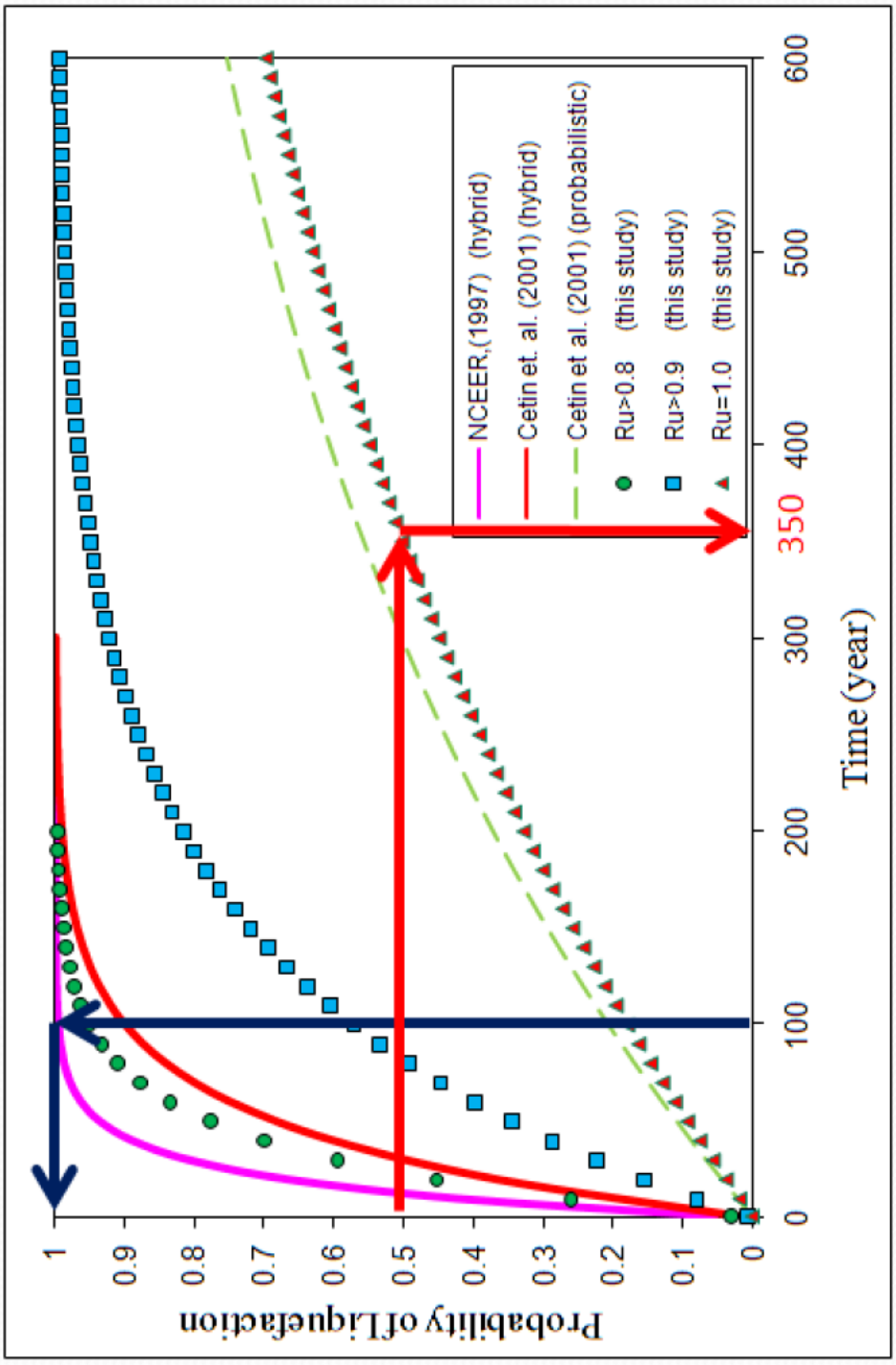

Figure 5.11: Probability of liquefaction using different approaches

CHAPTER 6

SUMMARY AND CONCLUSIONS

Seismic soil liquefaction triggering potential of a dam foundation is assessed within an integrated probabilistic seismic hazard assessment framework. The proposed methodology successively, i) processes the discrete stages of probabilistic seismic hazard workflow upon seismic source characterization, ii) forms the target elastic acceleration response spectra for typical rock sites, covering all the scenario bins that are re-grouped with respect to earthquake magnitude and distance, iii) matches the strong ground motion records selected from a database with the target response spectra for every defined bin, and iv) performs 2-D equivalent linear seismic response analyses of a 56 m high earth fill dam founded on 24 m thick alluvial deposits. The motivation behind this study is founded on the controversial issues and difficult decisions regarding if removal of potentially liquefiable loose alluvial soils or costly mitigation of these soils against liquefaction triggering hazard and induced risks is necessary.

Results of seismic response analyses are presented in the form of annual probability of excess pore pressure ratios and lateral deformations exceeding certain threshold values. For the purpose of assessing the safety of the dam slopes, ϕ-c reduction-based slope stability analyses were also performed for post liquefaction conditions. By using these results within a probabilistic framework, annual probabilities of factor of safety of slopes exceeding various threshold values were estimated. As the concluding remark, probability of liquefaction triggering, induced deformations and factor of safeties are presented for a service life of 100 years. It is believed that the proposed probabilistic seismic

performance assessment methodology ,which incorporates both factor of safety-based failure probabilities and seismic soil liquefaction-induced deformation potentials, provides dam engineers to rationally quantify the level of confidence with their decisions regarding if costly mitigation of dam foundation soils against seismic soil liquefaction triggering hazard and induced risks is necessary.

Followings are more specific conclusions of this study:

- Integrated seismic hazard and risk assessments provide a robust methodology regarding the decisions involving catastrophic but rare events.
- Within a dam body, including its foundation soils, there exist several regions with significantly different seismic soil liquefaction triggering vulnerabilities. Thus, an optimum mitigation scheme requires an assessment methodology which can quantify these vulnerabilities and develop and produce equi-risk solutions.
- Upstream and downstream toe regions are more vulnerable to liquefaction triggering than the central region.
- Liquefaction triggering assessments are not adequate to assess the overall seismic liquefaction performance of the dam. An assessment scheme which can address induced-pore pressures and deformations is needed for unbiased decisions regarding the overall seismic risk of a dam. In simpler terms, certain regions of a dam or its foundation soils can liquefy but may not lead to an overall instability or excessive deformation.
- Compared to probabilistic Cetin et al.(2004) and modified Byrne et al methodologies, NCEER deterministic assessment overpredicts liquefaction triggering vulnerability.
- In the original Byrne model, changes in cyclic pore pressure response of saturated cohesionless soils due to changes in effective confining stresses, and presence of static shear stresses, were not fully

addressed. Thus, a modification incorporating widely known K_σ and K_α issues was needed.

- Without these corrections, Byrne model produces uncorservative estimates of cyclic pore pressure response for loose alluvial deposits.

Specific to the illustrative example studied:

From pore pressure generation point of view,

- Different locations of the dam have significantly different liquefaction triggering vulnerability and risk. Thus mitigation methods should consider this variability in the associated risks.
- There is no risk of liquefaction at the central region of the dam (point C) due to the fact that annual probability of r_u>0.1 is very small.
- The most liquefaction vulnerable zone is estimated as the upstream toe of the dam (Point A), followed by the downstream toe region.
- Annual probability of liquefaction triggering is estimated as 0.06, 0.02, 0.0001, 0.01, 0.01 for points A through E, respectively.

From seismically-induced lateral deformations point of view,

- central region of the dam (point C) is the most critical region where significant seismically-induced lateral deformations are concentrated.
- at upstream and downstream toe regions (points B and D) annual probability of lateral displacements exceeding the value of 10 cm is estimated as 0.2.

For comparison of different metedologies,

- For point A, probability of liquefaction triggering corresponding to a service life of 100 years were estimated as 100 %, 88%, 20% by using the triggering assessment methodologies of NCEER, deterministic Cetin et al., and probabilistic Cetin et. al. Similarly, the probabilities of seismically-induced lateral deformations exceeding threshold values of

25, 50 and 100 cm were estimated as 0.4, 0.22 and 0.1, again for a service life of 100 years. For point A, return period of liquefaction triggering was estimated as 350 years. In simpler terms within a period of 350 years, point A is expected to liquefy.

It should be noted that these results just present the seismic response of individual points but not the overall performance of the dam body.

As a summary, the modified version of the Byrne model powerfully captures effective stress based seismic response of saturated cohesionless soils. Close agreement with the predictions of field performance based methodology (e.g.: Cetin et al., 2004) and numerical simulations by FLAC software was found to be mutually supportive. Probabilistically based seismic hazard and risk framework is a robust and rational tool in helping decisions which involves catastrophic, costly but rare events such as liquefaction-induced dam failures.

As part of future research studies, it is recommended to study the following issues in a more detailed framework:

i) 3-D effects on numerical simulations,
ii) a comparison of seismic response of mitigated vs. nonmitigated dam foundation responses.
iii) integration of the cost of mitigation vs failure cost into decision making scheme.

REFERENCES

Abrahamson N.A. 1993, "RSPMATCH": *A Program for Non-Stationary Response Spectrum Matching*.

Ambresseys, N.N. 1988, "Engineering Seismology, Earthquake Engrg. and Structural Dynamics", 17, 1–105.

Bray, J. D, Sancio, R. B., Reimer, M. Durgunoglu, H. T. 2003, "Liquefaction Susceptibility of Fine-Grained Soils", *Proceedings, 11th International Conference on Soil Dynamics and Earthquake Engineering – 3rd International Conference on Earthquake Geotechnical Earthquake Engineering (11th ICSDEE)*, University of California Berkeley, 7-9 January, 2003, Vol. 1, pp. 655-662.

Boore, D. M., Joyner, W. B., Fumal, T. E. 1997, "Equations for Estimating Horizontal Response Spectra and Peak Acceleration from Western North American Earthquakes", *A summary of Recent Work*, *Seismological Research Letters*,68(1),128-153.

Byrne, P.M., Park, S.S., Beaty, M., Sharp, M., Gonzalez, L. & Abdoun, T. 2004, "Numerical modeling of liquefaction and comparison with centrifuge tests", *Can. Geotech. Journal*, vol. 41, no. 2: 193-211.

Cornell C. A. 1968, "Engineering Seismic Risk Analysis", *Bulletin of the Seismological Society of America,* 58,1583-1606.

Cetin, K. O. 2000, "Reliability-based Assessment of Seismic Soil Liquefaction Initiation Hazard", *Dissertation Submitted in Partial Satisfaction of the Requirements for the Degree of Doctor of Philosophy*, University of California at Berkeley.

Cetin, K. O., Der Kiureghian, A., and Seed, R. B. 2002, "Probabilistic Models for the Initiation of Seismic Soil Liquefaction", *Structural Safety*, 24(2002), pp.67-82.

Cetin K. O., Seed R. B., Kiureghian A. D., Tokimatsu K., Harder L. F., Jr., & Kayen R. E., Moss R. E. S. 2004, "SPT based probabilistic and deterministic assessment of seismic soil liquefaction potential", A*SCE Journal of Geotechnical and Geoenvironmental Engineering*, 130(12), 1314-1340.

FLAC (Fast Lagrangian Analysis of Continua) version 4.0, "ReferanceManual".

Gupta, I.D. 2002, "The Sate of the Art in Seismic Hazard Analysis", *ISET Journal of Earthquake Technology,* Paper No. 428, Vol. 39, No. 4, pp. 311-346.

Harder, L. F., Jr., and Boulanger, R. W. 1997, Application of K_σ and K_α correction factors. *Proc., NCEER Workshop on Evaluation of Liquefaction Resistance of Soils,* National Center for Earthquake Engineering Research, SUNY Buffalo, N.Y., 97(22), 167–190.

ICOLD 1985, "Selecting Parameters for Large Dams-Guidelines and Recommendations". *ICOLD Committee on Seismic Aspects Of Large Dams, Bulletin* 72.

Idriss, I. M., and Boulanger, R. W. 2003, "Estimating K_σ for use in evaluating cyclic resistance of sloping ground", *Proc., 8th U.S.–Japan Workshop on Earthquake Resistant Design of Lifeline Facilities and Countermeasures against liquefactions*, Multidisciplinary Center for Earthquake Engineering Research, SUNY Buffalo, Buffalo, N.Y.

Kramer, S. L. 1996, "Geotechnical Earthquake Engineering", *Upper Saddle River, N.J.*, Prentice Hall.

Kramer S. L. Mayfield R. T. 2007, "Return Period of Soil Liquefaction" *ASCE Journal of Geotechnical and Geoenvironmental Engineering.* 133(7), 802-813.

Liao, S. S. C., Whitman, R. V. 1986, "Overburden Correction Factor for SPT in Sand", *Journal of Geotechnical Engineering, ASCE*, Vol. 112, No. 3, pp. 373-377.

Maksidi, F.I. and Seed, H.B. 1978, "Simplified procedure for estimating dam and embankment deformations", *J. Geotechnica Engrg. Div., ASCE*, 104(GT7), 849–867.

Marcuson III, W.F. and Franklin, A.G. 1983, "Seismic design, analysis, and remedial measures to improve stability of existing earth dams, in: Proc. of the Symposium on Seismic Design of Embankments and Caverns" sponsored by ASCE Geotechnical Division in conjunction with the ASCE National Convention, Philadelphia, PA, 16–20 , pp. 65–78.

NCEER 1997, "Proceedings of the NCEER Workshop on Evaluation of Liquefaction Resistance of Soils", Edited by Youd, T. L., Idriss, I. M., Technical Report No. NCEER-97-0022.

Ozkan M. Y. 1998, "A review of considerations on seismic safety of embankments and earth and rock-fill dams", *Soil Dynamics and Earthquake Engineering* 17 , 439–458.

Pacific Earthquake Engineering Center 2007, "Next Generation Attenuation Relationships", Project Database, viewed 5 August 2008, http://peer.berkeley.edu/nga/.

Plaxis (2D) version 8.0, "Referance Manual".

Sarma, S.K. 1975, "Seismic stability of earth dams and embankments" *Geotechnique*, 25(4), 743–761.

Schanbel P. B., Lysmer, J., Bolton, S. H., 1972, SHAKE: "A Computer Program for Earthquake Response Analysis of Horizontally Layered Sites". Report No. UCB/EERC-72/12, Earthquake *Engineering Research Center, University of California*, Berkeley, December, 102p.

Seed, H. B., Idriss, I. M. 1970, "Soil Moduli and Damping Factors for Dynamic Response Analyses", *Report No. EERC 70-10, Earthquake Engineering Research Center*, University of California, Berkeley, Berkeley, CA.

Seed, H. B., Idriss, I. M. 1971, "Simplified Procedure for Evaluating Soil Liquefaction Potential", *Journal of the Soil Mechanics and Foundations Division, ASCE*, Vol. 97, No SM9, Proc. Paper 8371, pp. 1249-1273.

Seed, H.B., Maksidi, Faiz, I. and De Alba 1978, "P. Performance of earth dams during earthquakes", *J. Geotechnical Division ASCE*, 104(GT), 967–995.

Seed, H.B. 1979, "Considerations in the earthquake-resistant design of earth and rockfill dams", *Geotechnique*, 29(3), 215– 263.

Seed, H. B. 1979, "Soil Liquefaction and Cyclic Mobility Evaluation for Level Ground During Earthquakes", *Journal of Geotechnical Engineering Division, ASCE*, 105 (GT2): 201-255.

Seed, H.B. and Idriss, I.M. 1982, "Ground Motions and Soil Liquefaction during Earthquakes", *EERI Monograph*, Berkeley, CA, 1982.

Seed, H. B., Idriss, I.M and Arango, I. 1983, "Evaluation of Liquefaction Potential Using Field Performance Data and Cyclic Mobility Evaluation for Level Ground During Earthquakes ", Journal *of Geotechnical Engineering, ASCE*, Vol.109, No.3, pp. 458-482.

Seed, R. B., Cetin, K. O., Der Kiureghian, A., Tokimatsu, K., Harder, L. F. Jr., and Kayen, R. E. 2001, "SPT-Based Probabilistic and Deterministic Assessment of Seismic Soil Liquefaction Potential", *Pacific Earthquake Engineering Research Center, PEER*.

Seed, R. B., Cetin, K. O., Moss, R. E. S., Kammerer, A. M., Wu, J., Pestana, J. M. and Reimer, M. F. 2001, "Recent Advances in Soil Liquefaction Engineering and Seismic Site Response Evaluation," *Proceedings, 4th International Conference on Recent Advances in Geotechnical Earthquake Engineering and Soil Dynamics*, San Diego, March 28-31.

Thomas, H.H. 1976, "The Engineering of Large Dams", *John Wiley and Sons Ltd*

University of Washington 2000 Soil Liquefaction web site, viewed 15 September 2008, http://www.ce.washington.edu/~liquefaction/html/main.html

Wells, D. L., and Coppersmith, K. J. 1994, "New Empirical Relationships Among Magnitude, Rupture Length, Rupture Width, Rupture Area, and Surface Displacement", *Bulletin of the Seismological Society of America*, 84(4): 974-1002.

Youd, T. L., and Noble, S. K. 1997, "Liquefaction criteria based on statistical and probabilistic analyses." *Proc., NCEER Workshop on Evaluation of Liquefaction Resistance of Soils*, *NCEER Technical Rep. No: NCEER-97-0022*, 201–205.

Youd, T. L., et al. 2001, "Liquefaction resistance of soils; summary report from the 1996 NCEER and 1998 NCEER/NSF workshops on evaluation of liquefaction resistance of soils." *J. Geotech. Geoenviron. Eng.*, 127(10), 817–833.

Yunatci, A., and Cetin, K. O. 2007, "Site specific response and soil liquefaction triggering assessment integrated within probabilistic seismic hazard framework". *6th National Conference on Earthquake Engineering*, Istanbul, Turkey.

APPENDIX A

UBCSAND CODE

FISH version of UBCSAND MODEL from Mohr-Coulomb model with strain hardening/softening. Effective stress stress approach primary and secondary plastic hardener.

Recent revisions:

NOV 14 2001 pmb Change to post trigger plastic modulus and crossover counter m_count4,m_ocr

DEC 27 2001 pmb m_triax = 1 to simulate comp ext tests

Feb 6 2002 pmb Modified plastic hardeners and basic relationship between plastic and elastic moduli.

Feb 13 2002 pmb Change to anisotropy (only for first time loading)

Sep 12 2002 mhb Change m_count4 to $gplim & $ratlim
modified $hard1 for m_n160 of 5 to 10
modified m_dt at low $sig
reset 2ary yield surface if dilation
introduced zart for averaging stress components
limited maximum m_knew2 to m_knewp
*****

Determining the appropriateness and accuracy of this routine for any purpose is sole responsibility of end user. Routine is provided to specific organizations by author and is not transferrable outside of this organization. Please new users and potential bugs to primary author at pmb@civil.ubc.ca.

```
set echo off
def m_mss
 constitutive_model  99
 f_prop  m_kge      m_ne     m_kb      m_me     m_ocr     m_triax
 f_prop  m_kgp      m_np     m_phicv   m_phif   m_rf      m_pa    m_n160
 f_prop  m_g        m_k      m_coh     m_ten    m_ind
 f_prop  m_csnp     m_nphi   m_npsi    m_e1     m_e2      m_x1    m_sh2
 f_prop  m_anisofac m_$fac   m_css     m_knew   m_knew1   m_knew2
 f_prop  m_ratio    m_ratcv  m_ratf    m_gpsum  m_ratcrs  m_knewp
 f_prop  m_dratmob  m_ratmob m_dt      m_flago  m_ratmobold
m_cross
 f_prop  m_hfac1    m_hfac2  m_hfac3   m_epsum  m_epsum1  m_rtymax
 f_prop  m_ratmax   m_ncyc   m_ncyc1   m_epsav  m_epsum4
m_epsum4old
 f_prop  m_ratmax0  m_ratmax1 m_sxyold  m_ratioy  m_rtmax
m_gpstar

 float  $sphi  $spsi  $s11i  $s22i $s12i  $s33i  $sdif  $s0   $rad
 float  $s1    $s2    $s3    $dc2  $dss
 float  $si    $sii   $psdif $fs   $alams $ft    $alamt $cs2  $si2
 float  $apex  $epsav $tpsav $de1ps $de3ps $depm  $eps   $ept
 float  $bisc  $pdiv  $anphi $tco  $sig   $hard1 $area
 float  $sd    $sxy   $dumsig $dumsd $dumsxy $epn   $epsum $cross
 float  $eps1  $epn1  $ratmax $hard $sy    $dumsy $ratlim $gplim

;-----------------------------------------
 Case_of  mode
; --------------------
; Initialisation section
; --------------------
```

```
  Case 1
; --- data check ---
    $m_err = 0
    if m_phif > 89.0 then
      $m_err = 1
    end_if
    if m_coh  < 0.0 then
      $m_err = 3
    end_if
    if m_ten < 0.0 then
      $m_err = 4
    end_if
    if $m_err # 0 then
       nerr = 126
       error = 1
    end_if
; ----FLAG TO SET UP INITIAL CONDITIONS THE FIRST TIME IT
GOES THROUGH
;-----AND EACH RESTART
   if  m_flago < 5.0  then      ;AVOIDS CHANGES ON RESTART
      m_ratf  = sin(m_phif * degrad)
      m_ratcv = sin(m_phicv * degrad)
      m_k     = m_kb  * m_pa
      m_g     = m_kge * m_pa
      m_e1    = m_k + 4.0 * m_g / 3.0
      m_e2    = m_k - 2.0 * m_g / 3.0
      m_sh2   = 2.0 * m_g
; --- set tension to prism apex if larger than apex ---
      $apex = m_ten
      if m_phif # 0.0 then
        $apex = m_coh / tan(m_phif * degrad)
```

```
      end_if
      m_ten = min($apex,m_ten)
    end_if
    if $ratlim = 0.0 then
      $ratlim = 0.01        ;used for crossovers
    end_if
    if $gplim  = 0.0 then
      $gplim  = 0.00005     ;used for crossovers
    end_if
    if m_n160  = 0.0 then
      m_n160  = 5.0
    end_if

    Case 2
; ---------------
; Running section
; ---------------
    m_flago = m_flago +1.0
    if m_flago < 5.0 then   ;FOR STARTUP
      if m_ratmob = 0.0 then
        m_ratmob =  0.01
      end_if
      m_ratmob= min(m_ratmob,m_ratf)
      m_dt    = m_ratcv - m_ratmob      ;Dt
      $sphi   = m_ratmob
      $spsi   = -m_dt
      m_npsi  = (1.0 + $spsi) / (1.0 - $spsi)
      m_nphi  = (1.0 + $sphi) / (1.0 - $sphi)
      m_x1    = m_e1 - m_e2*m_npsi + (m_e1*m_npsi - m_e2)*m_nphi
      m_csnp  = 2.0 * m_coh * sqrt(m_nphi)
      if abs(m_x1) < 1e-6 * (abs(m_e1) + abs(m_e2)) then
```

```
        $m_err = 5
        nerr = 126
        error = 1
      end_if
    end_if
    zvisc = 1.0
    if m_ind # 0.0 then
      m_ind = 2.0
    end_if
    $anphi = m_nphi
; --- get new trial stresses from old, assuming elastic increments ---
    $s11i = zs11 + (zde22 + zde33) * m_e2 + zde11 * m_e1
    $s22i = zs22 + (zde11 + zde33) * m_e2 + zde22 * m_e1
    $s12i = zs12 + zde12 * m_sh2
;    $s33i = zs33 + (zde11 + zde22) * m_e2 + zde33 * m_e1
;    $s33i = $s22i
    $s33i = .5*($s11i+$s22i)
    $sdif = $s11i - $s22i
    $s0   =  0.5 * ($s11i + $s22i)
    $rad  =  0.5 * sqrt ($sdif*$sdif + 4.0 * $s12i*$s12i)
; ----principal stresses ---
    $si    =  $s0 - $rad
    $sii   =  $s0 + $rad
    $psdif =  $si - $sii
; --- determine case ---
;   section
;     if $s33i > $sii then
; --- s33 is major p.s. ---
;       $icase = 3
;       $s1    = $si
;       $s2    = $sii
```

```
;         $s3    = $s33i
;         exit section
;       end_if
;       if $s33i < $si then
;; --- s33 is minor p.s. ---
;         $icase = 2
;         $s1    = $s33i
;         $s2    = $si
;         $s3    = $sii
;         exit section
;       end_if
; --- s33 is intermediate ---
        $icase = 1
        $s1    = $si
        $s2    = $s33i
        $s3    = $sii
;     end_section
      section
; --- shear yield criterion ---
        $fs    = $s1 - $s3 * $anphi + m_csnp
        $alams = 0.0
; --- tensile yield criterion ---
        $ft    = m_ten - $s3
        $alamt = 0.0
; --- tests for failure ---
        if $ft < 0.0 then
          $bisc = sqrt(1.0 + $anphi * $anphi) + $anphi
          $pdiv = -$ft + ($s1 - $anphi * m_ten + m_csnp) * $bisc
          if $pdiv < 0.0 then
; ---       shear failure ---
            $alams = $fs / m_x1
```

```
            $s1 = $s1 - $alams * (m_e1 - m_e2 * m_npsi)
            $s2 = $s2 - $alams * m_e2 * (1.0 - m_npsi)
            $s3 = $s3 - $alams * (m_e2 - m_e1 * m_npsi)
            m_ind = 1.0
          else
; ---      tension failure ---
            $alamt = $ft / m_e1
            $tco= $alamt * m_e2
            $s1 = $s1 + $tco
            $s2 = $s2 + $tco
            $s3 = m_ten
            m_ind = 3.0
          end_if
        else
          if $fs < 0.0 then
; ---      shear failure ---
            $alams = $fs / m_x1
            $s1 = $s1 - $alams * (m_e1 - m_e2 * m_npsi)
            $s2 = $s2 - $alams * m_e2 * (1.0 - m_npsi)
            $s3 = $s3 - $alams * (m_e2 - m_e1 * m_npsi)
            m_ind = 1.0
          else
; ---      no failure ---
            zs11 = $s11i
            zs22 = $s22i
            zs33 = $s33i
            zs12 = $s12i
            exit section
          end_if
        end_if
```

```
; --- direction cosines ---
      if $psdif = 0.0 then
        $cs2   = 1.0
        $si2   = 0.0
      else
        $cs2   = $sdif       / $psdif
        $si2   = 2.0 * $s12i / $psdif
      end_if
; --- resolve back to global axes ---
      case_of  $icase
        case 1
          $dc2  = ($s1 - $s3) * $cs2
          $dss  =  $s1 + $s3
          zs11  = 0.5 * ($dss + $dc2)
          zs22  = 0.5 * ($dss - $dc2)
          zs12  = 0.5 * ($s1  - $s3) * $si2
          zs33  = $s2
        case 2
          $dc2  = ($s2 - $s3) * $cs2
          $dss  =  $s2 + $s3
          zs11  = 0.5 * ($dss + $dc2)
          zs22  = 0.5 * ($dss - $dc2)
          zs12  = 0.5 * ($s2  - $s3) * $si2
          zs33  = $s1
        case 3
          $dc2  = ($s1 - $s2) *$cs2
          $dss  =  $s1 + $s2
          zs11  = 0.5 * ($dss + $dc2)
          zs22  = 0.5 * ($dss - $dc2)
          zs12  = 0.5 * ($s1  - $s2) * $si2
          zs33  = $s3
```

```
      end_case
   ; zvisc = 0.0
    end_section


;  ------------------------------------------------------------------
;  -----UBC add on to account for change of elastic and plastic parameters
;  ------------------------------------------------------------------
; --------  PLASTIC STRAINS ---
    if m_ind = 1.0 then
      $de1ps = $alams
      $de3ps = -$alams * m_npsi
      $eps1  = abs($de1ps-$de3ps)
      $epn1  = -($de1ps+$de3ps)
      $eps   = $eps + $eps1*zart
      $epn   = $epn + $epn1*zart
    end_if
;-------------- STRESSES
    $sig    = -0.5*(zs11+zs22)
    $sd     = -(zs11-zs22) / 2.0
    $sxy    = zs12
    $sy     = -zs22
    $dumsig = $dumsig + $sig*zart
    $dumsd  = $dumsd  + $sd *zart
    $dumsxy = $dumsxy + $sxy*zart
    $dumsy  = $dumsy  + $sy *zart
    $area   = $area   + zart
  SECTION
; ---GET AVERAGE VALUES OF STRESSES AND STRAINS
    if zsub > 0.0 then          ;zsub loop
;-----STRAINS
      $epsav = 0.0
```

```
      $epsum = 0.0
      $epsav = $eps / $area          ;PLASTIC SHEAR STRAIN
INCREMENT
      $epsum = $epn / $area          ;PLASTIC VOLUMETRIC STRAIN
INCREMENT
      $eps   = 0.0
      $epn   = 0.0
;---- STRESSES
      $sig   = $dumsig/$area
      $sig   = max($sig,0.005*m_pa)
      $sd    = $dumsd/$area/$sig
      $sxy   = $dumsxy/$area/$sig
      $sy    = $dumsy/$area
      $sy    = max($sy,0.005*m_pa)
      m_ratioy = $sxy/$sy * $sig
      if m_triax = 1.0  then
        m_ratioy = (1.0 - $sy/$sig)   ;When sxy = 0.0, control by sxx-syy
      end_if
      m_ratio  = sqrt($sd*$sd+$sxy*$sxy)
      $dumsd   = 0.0
      $dumsxy  = 0.0
      $dumsig  = 0.0
      $dumsy   = 0.0
      $area    = 0.0
;************************************
;     Resets yield loci  and other factors
      if m_ratmax = 0. then
        m_ratmax1  = 0.0
        m_ratmax0  = 0.0
        m_ratmax   = 1.0
        m_ratmob   = m_ratio
```

```
        m_epsum    = 0.0
        m_epsum1   = 0.0
        m_ncyc     = 0.0
        m_ncyc1    = 0.0
        m_ratcrs   = m_ratio
        m_cross    = 10.0
      end_if
;*************************************

      m_dratmob = 0.0
      if $epsav > 0.0 then           ; PLASTIC  LOOP
        m_epsum = m_epsum + $epsum
        m_epsav = m_epsav + $epsav
        if $epsum < 0.0 then         ; DILATION
          m_epsum1 = m_epsum1 + $epsum
        end_if
        m_ratmax0 = max(m_ratmax0,m_ratioy)
        m_ratmax1 = min(m_ratmax1,m_ratioy)

;----Evaluate anisotropy factor
        m_css=$cs2
        if m_css>=0.0 then
          m_$fac = m_anisofac
        else
          m_$fac = m_anisofac + (m_anisofac - 1.0) * m_css
        end_if


;----PLASTIC SHEAR MODULUS
        m_knew = m_kgp/$sig * m_pa*($sig/m_pa)^m_np*m_hfac1
```

```
;-------secondary yield:
        $hard1  = max(0.5, 0.1*m_n160)    ;correction at low N160
        $hard1  = min(1.0, $hard1)
        m_knew1 = m_knew*( 4. + m_ncyc1) *$hard1 * m_hfac2

;-------primary yield:
        if m_ocr <= 2.0 then
          if m_ratioy > 0.0 then
            $ratmax = m_ratmax0
          else
            $ratmax = abs(m_ratmax1)
          end_if
          if abs(m_ratioy) > 0.99*$ratmax then
            m_knew1 = m_knew *m_$fac
          end_if
        end_if
        m_knewp = m_knew *m_$fac

;-------dilation "softener" to control post-liq:
;-------m_epsum4 is the accumulated dilation during the previous stress
pulse
        if m_epsum4 < -1e-6 then
          $hard   = max(0.03, exp(m_epsum4 *m_hfac3*m_n160 *600.))
;$hard in range 1 to 0.03
          m_knew2 = m_knew * $hard
        end_if

;-------modify for stress ratio:
        m_gpstar  = m_knew1*(1.0-(m_ratio*m_rf/m_ratf))^2
        if m_epsum4 < -1e-6 then
          m_knewp  = m_knewp*(1.0-(m_ratio*m_rf/m_ratf))^2
```

```
        m_gpstar = min(m_knew2,m_knewp)
      end_if
      m_dratmob = m_gpstar*$epsav
      m_dratmob = max(m_dratmob,0.0)
      m_ratmob  = m_ratmob + m_dratmob
      m_ratmob  = min(m_ratmob,m_ratf)  ;current yield locus
    end_if                    ;END OF PLASTIC LOOP


;---CROSSING AXIS RESETS PLASTIC PARAMETERS
    if m_ratioy*m_sxyold < 0.0 then        ;crossover check

;------Crossover has occurred
      $cross   = max(m_rtymax,m_rtmax-m_ratcrs) / $ratlim
      $cross   = max($cross, m_gpsum/$gplim)
      m_ratcrs = m_ratio
      m_rtmax  = m_ratio
      m_gpsum  = 0.0
      m_rtymax = 0.0

;-------Previous half cycle is "large"
      if max(m_cross, $cross) > 1.0 then
        if m_cross # 99.0 then
          m_ncyc     = m_ncyc  + 0.5
          m_ncyc1    = m_ncyc1 + 0.5
          m_ratmobold = m_ratmob
        else
          m_ratmobold = max(m_ratmob,m_ratmobold)
        endif
        m_ratmob    = m_ratio
        m_epsum4old = m_epsum4
```

```
          m_epsum4    = m_epsum1              ;preserves the prior dilation
          if m_epsum4 < -1e-6 then            ;reset 2ary yield surface if dilation
           m_ratmax0 = 0.0
           m_ratmax1 = 0.0
           m_ncyc1   = 0.0
          endif
          m_epsum1    = 0.0
          m_cross     = 0.0

;-------Previous half cycle is "small"
         else
           m_ratmob    = m_ratio + 0.75*(max(m_ratmobold,m_ratio) -
m_ratio)
           m_epsum1    = m_epsum4
           m_epsum4    = m_epsum4old
           m_cross     = 99.                ;remember small half cycle
         endif
      else

;-------No crossover
         m_gpsum     = m_gpsum + $epsav        ;ignore initial crossover step
(uses old parameters)
         m_rtymax    = max(m_rtymax, abs(m_ratioy))
         m_rtmax     = max(m_rtmax, m_ratio)
       end_if
       m_sxyold = m_ratioy


;---COMPUTE NEW PARAMETERS ACCORDING TO THE CURRENT
MOB FRIC ANGLE
;---------- SET PLASTIC VALUES
```

```
      $sphi  = m_ratmob
      m_dt   = m_ratcv-m_ratmob
      m_dt   = min(m_dt,.5*m_ratcv)
      if m_epsum4 < 0.0 then
        if m_dt > 0.0 then
          m_dt=(m_ratcv-m_ratmob)
        end_if
      end_if
      if $sig < 0.02*m_pa then
        m_dt =  min(m_ratcv - m_ratf, -1.0*m_ratcv/5.)
      end_if

;*************************IMPOSE STEADY STATE STRENGTH
************************
;      if m_epsav > .05 then
;        if m_dt < 0.0 then
;          if $sy > 0.005*m_pa*m_n160^2/sin(m_phicv) then
;            m_dt = 0.0
;          end_if
;        end_if
;      end_if
;*****************************************************************
**************
;---------- PLASTIC PARAMETERS
      $spsi   = -m_dt
      m_npsi  = (1.0 + $spsi) / (1.0 - $spsi)
      m_nphi  = (1.0 + $sphi) / (1.0 - $sphi)

; ---STRESS DEPENDENT ELASTIC MODULI

      m_k     = m_kb  * m_pa * ($sig/m_pa)^m_me
```

```
      m_g     = m_kge * m_pa * ($sig/m_pa)^m_ne
      m_e1    = m_k + 4.0 * m_g / 3.0
      m_e2    = m_k - 2.0 * m_g / 3.0
      m_sh2   = 2.0 * m_g
      m_x1    = m_e1 - m_e2*m_npsi + (m_e1*m_npsi - m_e2)*m_nphi
    end_if    ;-------------------------------------END OF  ZSUB > 0
  END_SECTION

   Case 3
; ---------------------
; Return maximum modulus
; ---------------------
  if m_g = 0.0 then
    m_k     = m_kb  * m_pa
    m_g     = m_kge * m_pa
  end_if
  cm_max = (m_k + 4.0 * m_g / 3.0)
  sm_max = m_g

   Case 4
; --------------------
; Add thermal stresses
; --------------------
  ztsa = ztea * m_k
  ztsb = zteb * m_k
  ztsc = ztec * m_k
  ztsd = zted * m_k
  End_case
end
opt m_mss
set echo=on
```

APPENDIX B

FLAC v4.0 INPUT FILE

```
;DAM BODY
;SEPTEMBER 5 2008
new
config gw dyn ex 5

grid 80 16
gen -400 -72 -400 -24 400 -24 400 -72 i=1,81 j=1,5
gen -400 -24 -400 0 400 0 400 -24 i=1,81 j=5,9
gen -400 0 -400 56 400 56 400 0 i=1,81 j=9,17
gen same -5 56 5 56 same i=30,52 j=9,17


;ROCK
model mohr j=1,4
prop dens 2.2 por=.2 j=1,4
prop bulk 1.7e6 shear 1.2e6 j=1,4
prop cohes 300 fric 43 dilation 11 j=1,4
prop perm = 1e-7

fix x i=1
fix x i=81
fix y j=1
```

```
;ALLUVIUM
model mohr j=5,8
prop dens 1.8 por=.3 j=5,8
prop bulk 3.8e5 shear 8e4 j=5,8
prop cohes 0 fric 38 dilation 6 j=5,8
prop perm = 1e-4 j=5,8

;DAM BODY
model mohr i=30,51 j=9,10
prop dens 1.9 por=.3 i=30,51 j=9,10
prop bulk  9e5 shear 1.9e5 i=30,51 j=9,10
prop cohes 0 fric 35  dilation 3 i=30,51 j=9,10
prop perm = 1e-4  i=30,51 j=9,10



;plot grid hold
set dynamic = off
set flow = off

set gravity = 9.8
ini xdisp = 0 ydisp = 0



solve

;plot hold ydis fill bou

model mohr i=30,51 j=10,11
prop dens 1.9 por=.3 i=30,51 j=10,11
prop bulk  9e5 shear 1.9e5 i=30,51 j=10,11
prop cohes 0 fric 35  dilation 3 i=30,51 j=10,11
```

```
prop perm = 1e-4  i=30,51 j=10,11


solve
;plot hold ydis fill bou

model mohr i=30,51 j=11,12
prop dens 1.9 por=.3 i=30,51 j=11,12
prop bulk  9e5 shear 1.9e5 i=30,51 j=11,12
prop cohes 0 fric 35  dilation 3 i=30,51 j=11,12
prop perm = 1e-4  i=30,51 j=11,12


solve
;plot hold ydis fill bou

model mohr i=30,51 j=12,13
prop dens 1.9 por=.3 i=30,51 j=12,13
prop bulk  9e5 shear 1.9e5 i=30,51 j=12,13
prop cohes 0 fric 35  dilation 3 i=30,51 j=12,13
prop perm = 1e-4  i=30,51 j=12,13


solve
;plot hold ydis fill bou

model mohr i=30,51 j=13,14
prop dens 1.9 por=.3 i=30,51 j=13,14
prop bulk  9e5 shear 1.9e5 i=30,51 j=13,14
prop cohes 0 fric 35  dilation 3 i=30,51 j=13,14
prop perm = 1e-4  i=30,51 j=13,14
```

```
solve
;plot hold ydis fill bou

model mohr i=30,51 j=14,15
prop dens 1.9 por=.3 i=30,51 j=14,15
prop bulk  9e5 shear 1.9e5 i=30,51 j=14,15
prop cohes 0 fric 35  dilation 3 i=30,51 j=14,15
prop perm = 1e-4  i=30,51 j=14,15


solve
;plot hold ydis fill bou

model mohr i=30,51 j=15,16
prop dens 1.9 por=.3 i=30,51 j=15,16
prop bulk  9e5 shear 1.9e5 i=30,51 j=15,16
prop cohes 0 fric 35  dilation 3 i=30,51 j=15,16
prop perm = 1e-4  i=30,51 j=15,16


solve

sav 1a_statik.sav

rest 1a_statik.sav



call c:\flac\1a\ubcsand_sevinc.txt
model m_mss j=1,8
```

```
;ALLUVIUM

prop m_n160 = 20 j=5,8
prop m_n160k=20  j=5,8
prop m_phicv = 38 j=5,8
prop m_pa = 100 j=5,8
prop dens = 1.8 j=5,8

;Rock

prop m_n160 = 50 j=1,4
prop m_n160k=50  j=1,4
prop m_phicv = 45 j=1,4
prop m_pa = 100 j=1,4
prop dens = 2.2 j=1,4


def properties
  loop i (1,izones)
   loop j (1,8)
 ;ELASTIC

   m_n160(i,j) = max(m_n160(i,j),1.0)

   m_p'(i,j)=-syy(i,j)-pp(i,j)         ;mean effective stress assumed that
anisotropic

   ;m_p'(i,j)=max(m_p'(i,j),10)
```

```
  ;m_alfa(i,j)=sxy(i,j)/m_p'(i,j)

  m_alfa(i,j)=min(abs(sxy(i,j))/( m_p'(i,j)),0.3)

  m_Dr(i,j)=(m_n160(i,j)/46)^0.5    ;Idriss and Boulanger

  m_r(i,j)=(1/(10-ln(m_p'(i,j))))-m_Dr(i,j)   ;relative state parameter

  ;m_r(i,j)=max(m_r(i,j),-0.6)

  ;m_r(i,j)=min(m_r(i,j),0.1)

  m_a(i,j)=1267+636*m_alfa(i,j)^2-634*exp(m_alfa(i,j))-632*exp(-
m_alfa(i,j))

  m_b(i,j)=exp(-1.11+12.3*m_alfa(i,j)^2+1.31*ln(m_alfa(i,j)+0.0001))

  m_c(i,j)=0.138+0.126*m_alfa(i,j)+2.52*m_alfa(i,j)^3

  m_Kalfa(i,j)=m_a(i,j)+m_b(i,j)*exp(-m_r(i,j)/m_c(i,j))

  m_Ksigma(i,j)=1-0.185*ln(m_p'/m_pa)

  m_n160k(i,j) =
m_n160(i,j)+13.32*ln(m_Kalfa(i,j))+13.32*ln(m_Ksigma(i,j))     ; new N160

  m_n160k(i,j) = max(m_n160k(i,j),1.0)

 m_kge(i,j) = 21.7*20.*m_n160k(i,j)^.333  ;Shear Mod
  m_kb(i,j) = m_kge(i,j)*.7              ;Bulk mod
  m_me(i,j) = 0.5
```

```
  m_ne(i,j) = 0.5
 ;PLASTIC PROPERTIES
  m_kgp(i,j) = m_kge(i,j)* m_n160k^2*.003 +100.0  ;shear Mod
  m_np(i,j) = .4
  m_phif(i,j) = m_phicv(i,j) + m_n160(i,j)/10.0
 ;plastic modification factors
  m_hfac1(i,j) = 1.0  ;primary hardener
  m_hfac2(i,j) = 1.0  ;Secondary hardener
  m_hfac3(i,j) = 1.0  ;dilation "hardener"
 ;failure ratio --same as in Hyperbolic model
  m_rf(i,j) = 1.0 - m_n160(i,j)/100.
  m_rf(i,j) = max(m_rf(i,j),.5)
  m_rf(i,j) = min(m_rf(i,j),.99)
 ;plastic anisotrophy
  ;m_anisofac(i,j) = .0166*m_n160(i,j)
  ;m_anisofac(i,j) = min(m_anisofac(i,j),1.0)
  ;m_anisofac(i,j) = max(m_anisofac(i,j),0.333)
  m_anisofac(i,j) = 1.0
  ;m_anisofac ;Anisotrophy factor; 1 for isotropic, .333 for loose pluviated
  end_loop
 end_loop
end
properties

prop  m_ratmax = 0.0   j=1,8 ;initializes some plastic properties

set flow = off
;plot hold model fill
solve
```

```
;FLUID PROPERTIES
;water bulk= 5e4
water dens = 1.0
ini pp 720 var   0,-720. j=1,9
prop m_ratmax = 0.0
solve

;***Fill reservoir

apply pressure 560 var 0,-560  from 1,9 to 30,17
prop m_ratmax = 0.0
solve


;***Phreatic surface

water tens=0 bulk=1
apply pp 560 var 0,-560  from 1,9 to 30,17
fix sat i=1,30 j=9
fix sat i=30 j=9,17
fix pp i=30,52 j=17
fix pp i=52 j=9,17
fix pp i=52,81 j=9
fix pp i=81
set flow=on mech=off ncwrite=50


solve
```

```
set flow=off mech=on ncwrite=10
ini fmod = 0

his reset
;1
hist unbal

solve


ini fmod = 5e5
def excess
 loop i (1,izones)
  loop j (1,8)
   ex_1(i,j) = pp(i,j)                ;initial pore pressure
   ex_2(i,j) = -syy(i,j) - pp(i,j)     ;initial effective stress
   ex_2(i,j) = max(ex_2(i,j),.01* m_pa(1,1))
  end_loop
 end_loop
end
excess
solve




;**Dynamic Analysis

set dyn=on  ncwrite=50
```

```
;************************
set dy_damp=local=0.3  ;=pi*FRAC CRIT.
solve
set dy_damp=rayleigh  0.02   1
solve
prop m_ratmax = 0.0
ini xdisp = 0.0 ydisp = 0.0
;set flow = on

set dytime=0.0



def sin_wave

a_reld1=xdisp(1,2)-xdisp(1,1)
a_reld6=xdisp(41,7)-xdisp(41,6)

 loop i (1,izones)
  loop j (1,8)
   ex_3(i,j) = pp(i,j) - ex_1(i,j)  ;excess pore pressure
   ex_3(i+1,j) = ex_3(i,j)
   ex_4(i,j) = ex_3(i,j)/ex_2(i,j)  ; Excess pore pressure ratio
   ex_4(i+1,j) = ex_4(i,j)
   ex_5(i,j) = sxy(i,j)/ex_2(i,j)   ;stress ratio  sxy/esyy0
   ex_5(i+1,j) = ex_5(i,j)
  end_loop
 end_loop
end
sav 1a_dam.sav

rest 1a_dam.sav
```

```
set large

;EARTHQUAKE LOADING
his read 100 c:\flac\1a\1avel.v2                ;***** EARTHQUAKE
apply xvel = 0.01 hist 100 j=1
apply yvel = 0.0 j=1


hist nstep 10
;2
hist dytime

;3
hist xvel i=40 j=15

;4
hist xvel i=40 j=9

;5
hist xvel i=40 j=6

;6
hist xvel i=40 j=4

;7
hist xvel i=40 j=1


;8
his xdisp i=40 j=15
```

;9

his xdisp i=40 j=12

;10

his xdisp i=40 j=9

;11

his xdisp i=40 j=6

;12

his xdisp i=40 j=3

;13

his xdisp i=40 j=1

;14

his xdisp i=1 j=1

;15

hist xacc i=40 j=15

;16

hist xacc i=40 j=9

;17

hist xacc i=40 j=6

;18

hist xacc i=40 j=3

;19

hist xacc i=40 j=1

;20

his a_reld1

;21

his sxy i=40 j=9

;22

his sxy i=40 j=3

;23

his sxy i=41 j=6

;24

his a_reld6

;25 MANSAPDAN UZAKTA

his ex_4 i=20 j=8

;26 MANSAPA YAKIN

his ex_4 i=25 j=8

;27 MANSAP TOPUGU

his ex_4 i=30 j=8

;28 BARAJ ALTI

his ex_4 i=40 j=8

;29 MEMBA TOPUGU

his ex_4 i=52 j=8

;30 MEMBAYA YAKIN

his ex_4 i=65 j=8

;31 MEMBADAN UZAK

his ex_4 i=75 j=8

;32 BARAJ ALTI KAYA

his ex_4 i=40 j=5

;33

his esyy i=40 j=8

;34

his ex_3 i=40 j=12

;35

his ex_3 i=40 j=9

;36

his ex_3 i=40 j=6

;37

his ex_3 i=40 j=3

;38

his ex_3 i=40 j=1

```
;39
his ex_3 i=1 j=1
;40
his esyy i=40 j=9

;41
his xdisp i=20 j=8
;42
his xdisp i=25 j=8
;43
his xdisp i=30 j=8
;44
his xdisp i=40 j=8
;45
his xdisp i=52 j=8
;46
his xdisp i=65 j=8
;47
his xdisp i=75 j=8
;1aff
apply ff
solve dytime = 11.995 step 10000000


Plot hold his 15 16 17 18 19 vs 2    ; Accelerations
plot hold his 8 9 10 11 12 13 14 vs 2      ; Displcements
plot hold his 25 26 27 28 29 30 31 32 vs 2 ; Excess Pore pres ratio,Ru
;plot hold his 23 vs 24
;plot hold his 21 vs -40
save 1avel.sav
```

APPENDIX C

EARTHQUAKE RECORDS

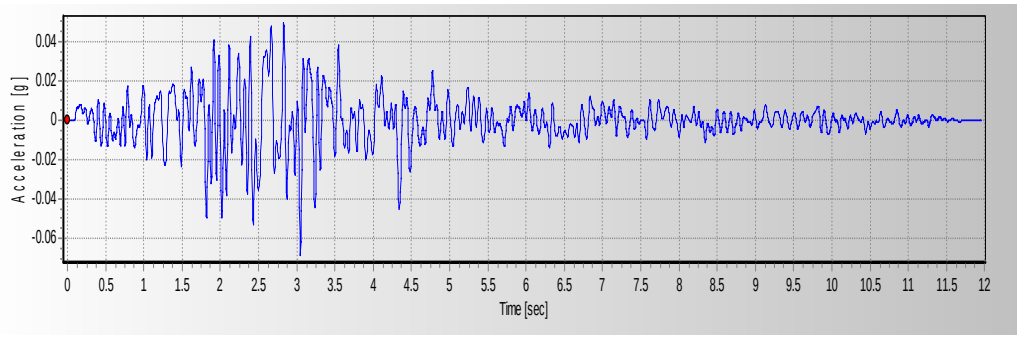

Figure C1: Acceleration vs. Time History for EQ Record Number 1

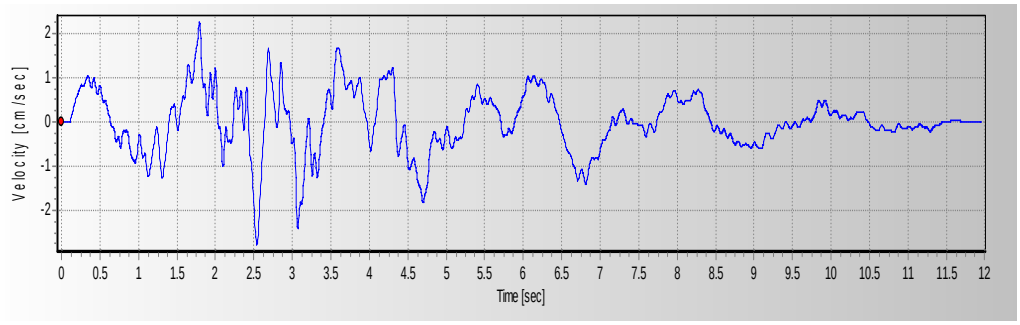

Figure C2: Velocity vs. Time History for EQ Record Number 1

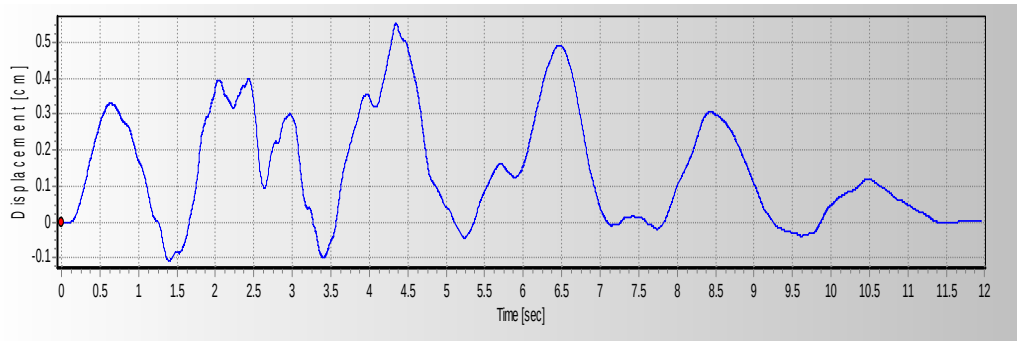

Figure C3: Displacement vs. Time History for EQ Record Number 1

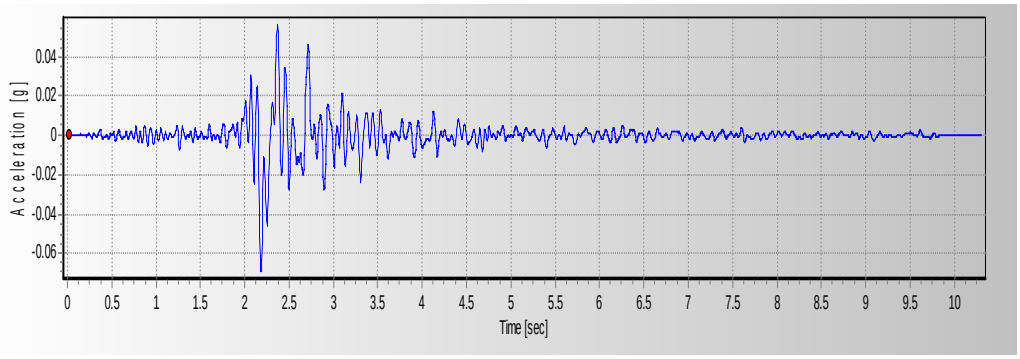

Figure C4: Acceleration vs. Time History for EQ Record Number 2

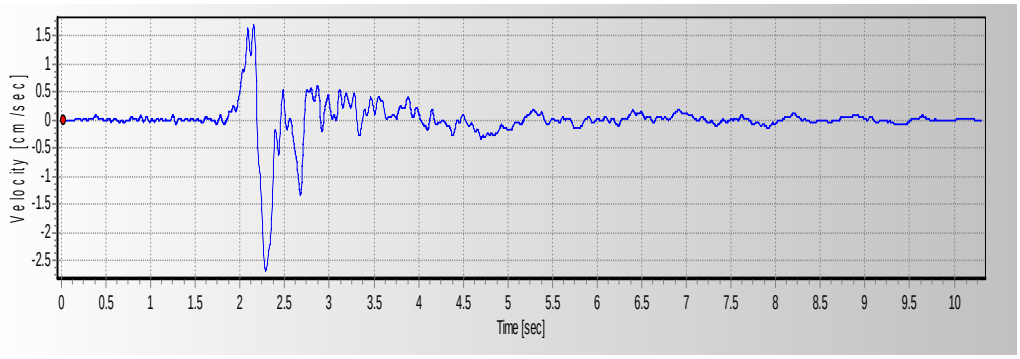

Figure C5: Velocity vs. Time History for EQ Record Number 2

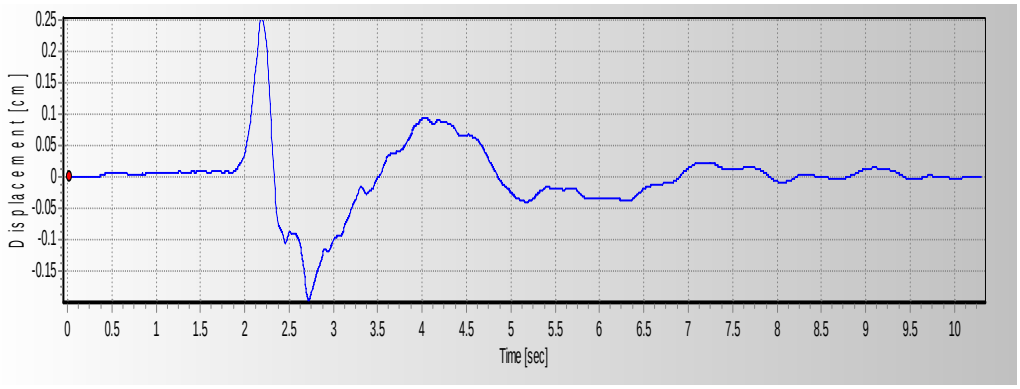

Figure C6: Displacement vs. Time History for EQ Record Number 2

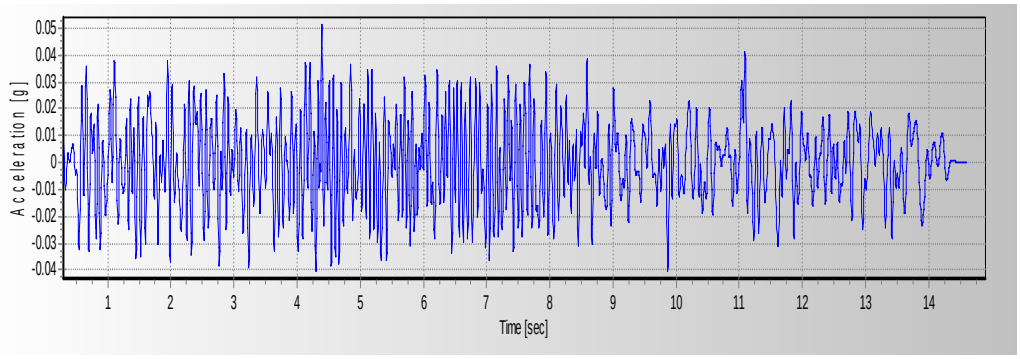

Figure C7: Acceleration vs. Time History for EQ Record Number 3

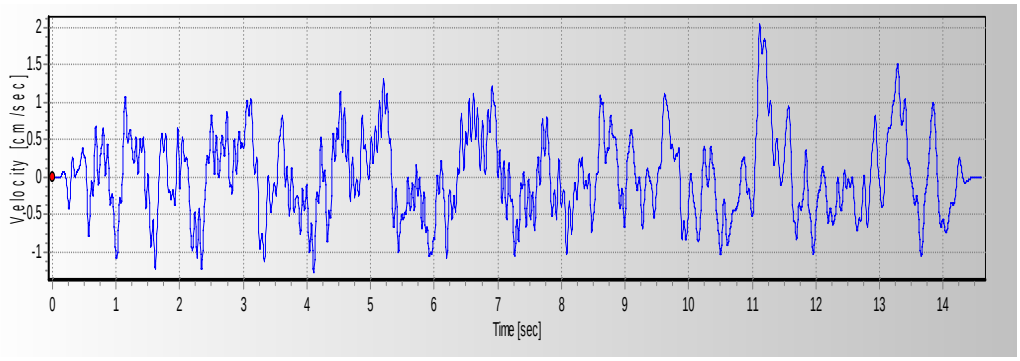

Figure C8: Velocity vs. Time History for EQ Record Number 3

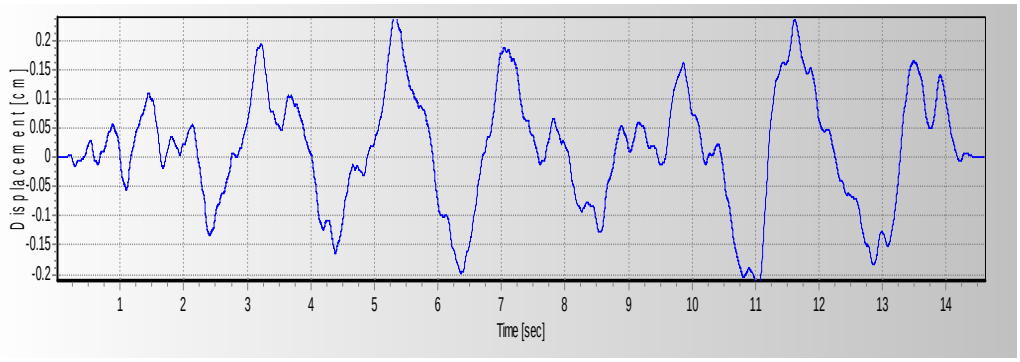

Figure C9: Displacement vs. Time History for EQ Record Number 3

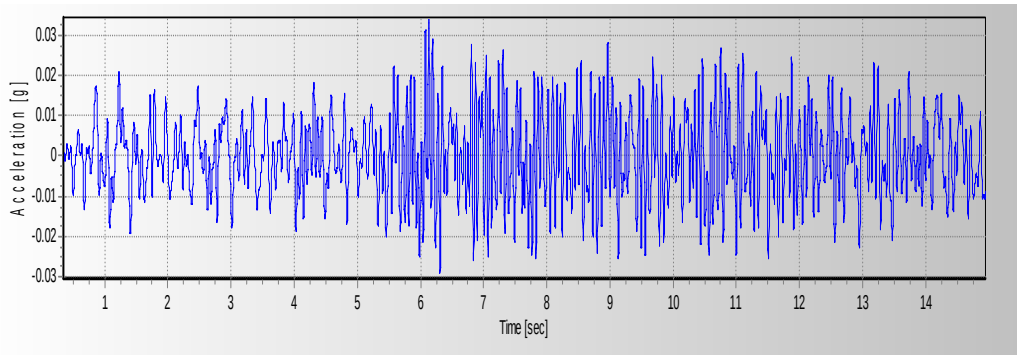

Figure C10: Acceleration vs. Time History for EQ Record Number 4

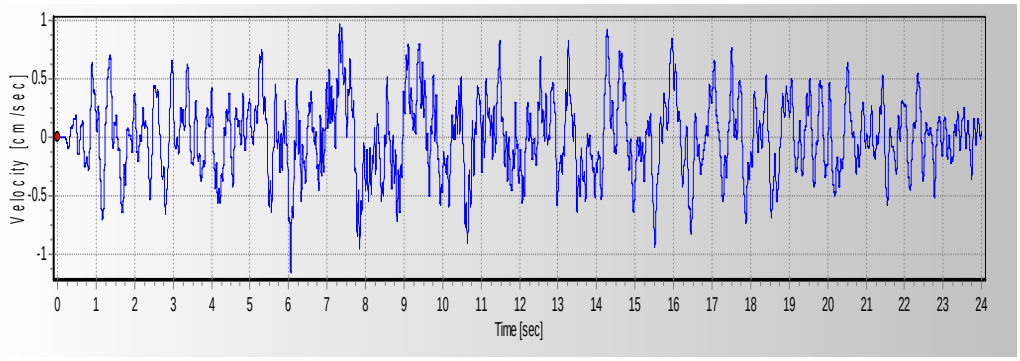

Figure C11: Velocity vs. Time History for EQ Record Number 4

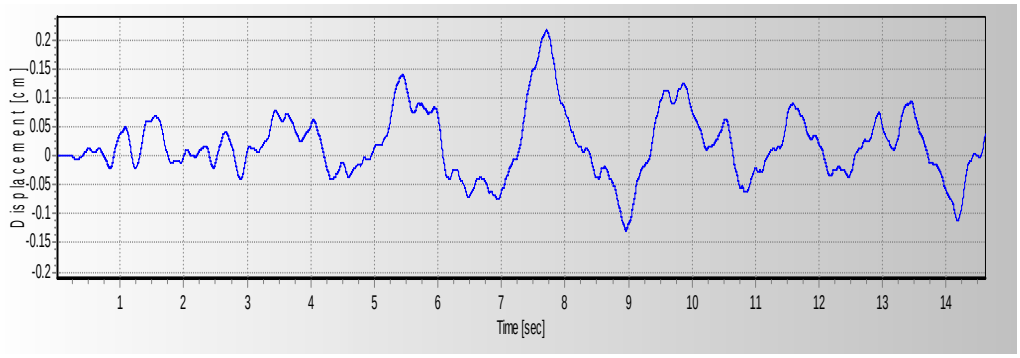

Figure C12: Displacement vs. Time History for EQ Record Number 4

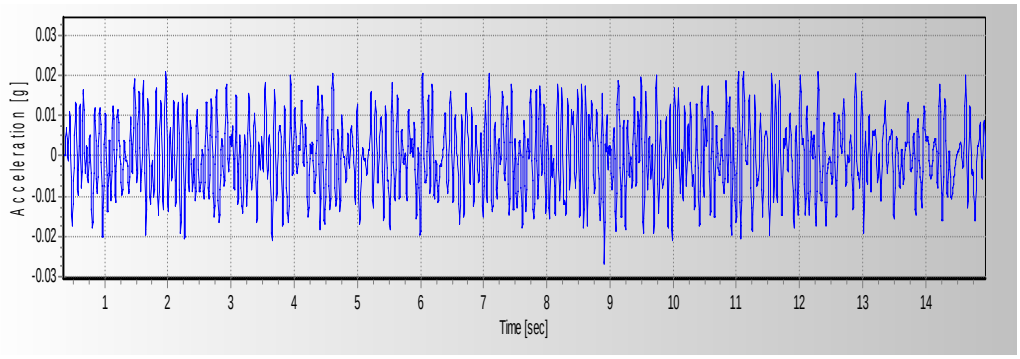

Figure C13: Acceleration vs. Time History for EQ Record Number 5

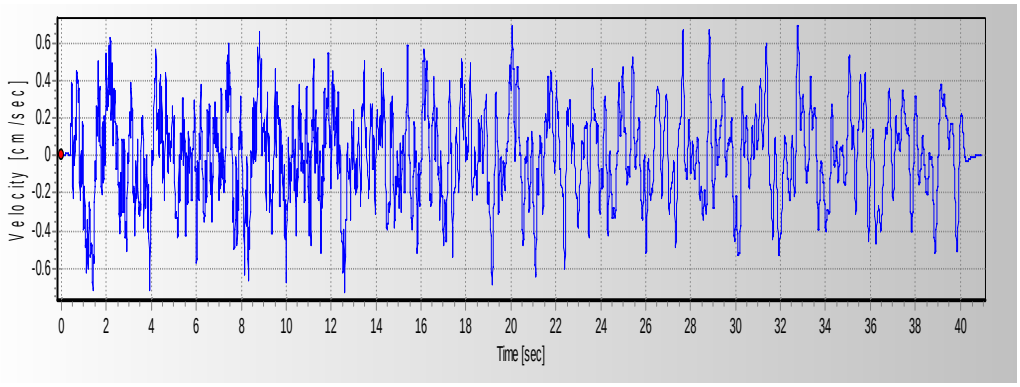

Figure C14: Velocity vs. Time History for EQ Record Number 5

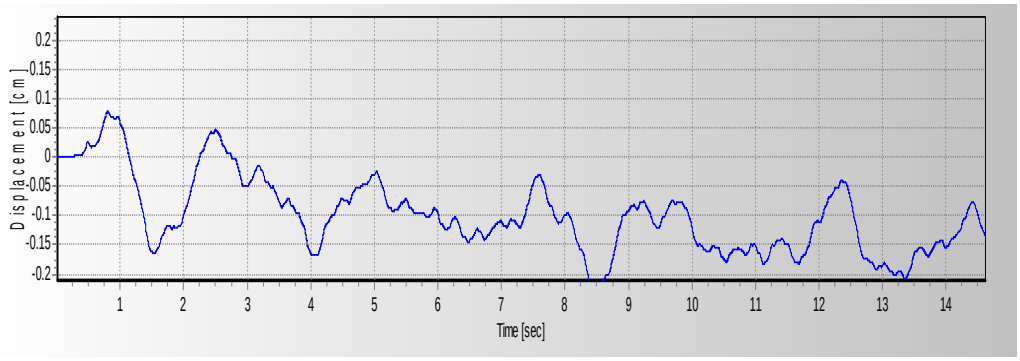

Figure C15: Displacement vs. Time History for EQ Record Number 5

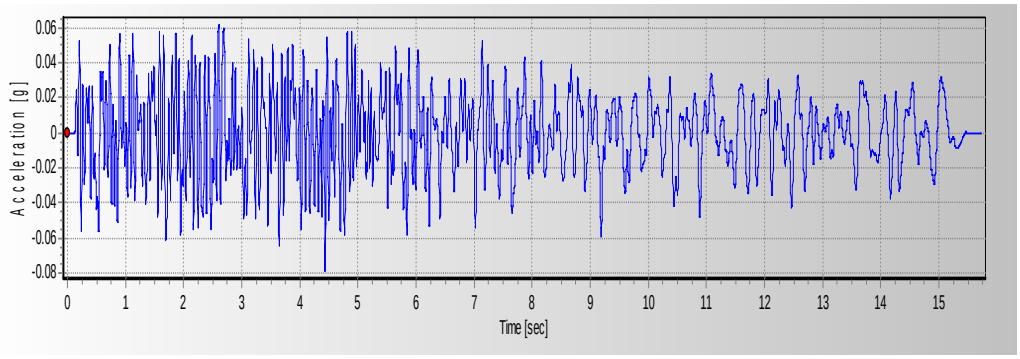

Figure C16: Acceleration vs. Time History for EQ Record Number 6

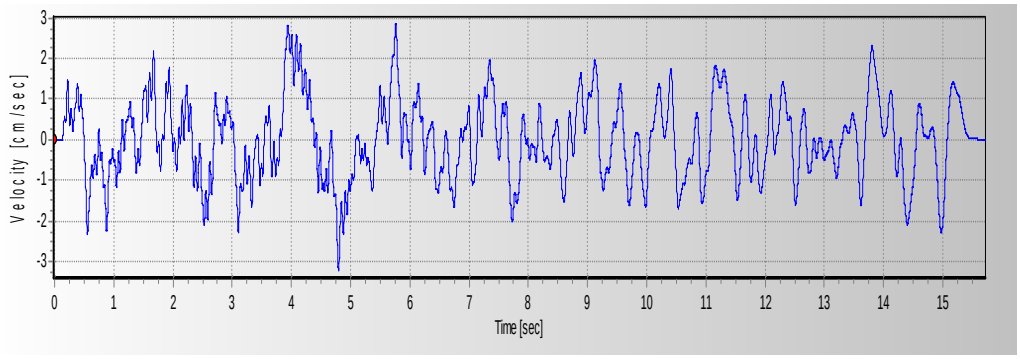

Figure C17: Velocity vs. Time History for EQ Record Number 6

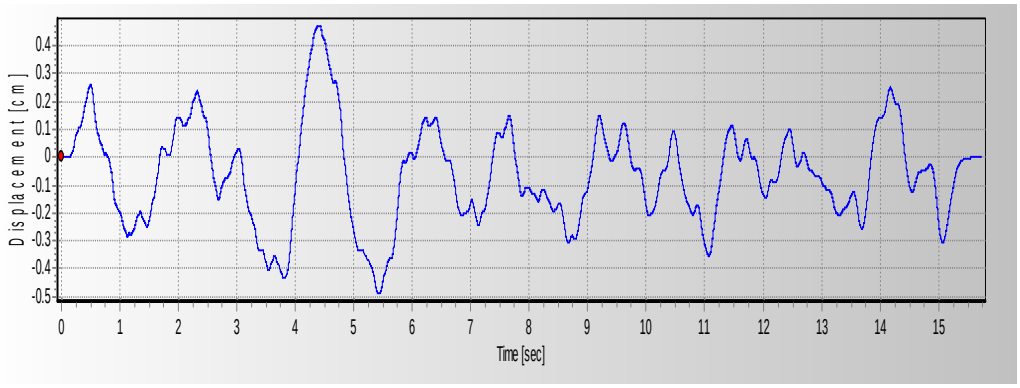

Figure C18: Displacement vs. Time History for EQ Record Number 6

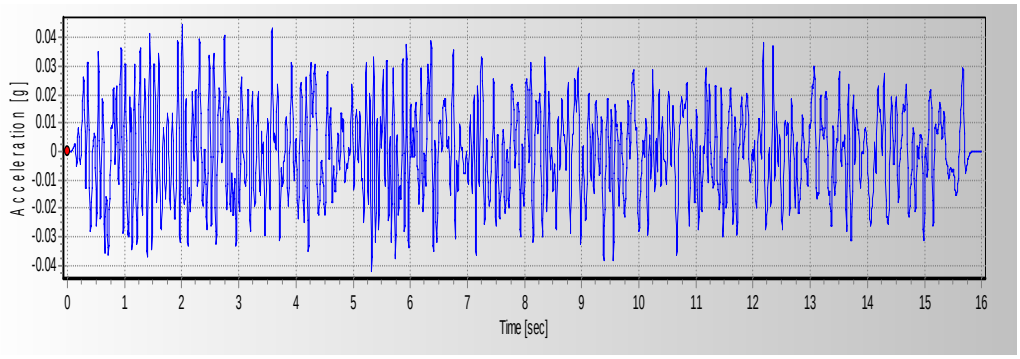

Figure C19: Acceleration vs. Time History for EQ Record Number 7

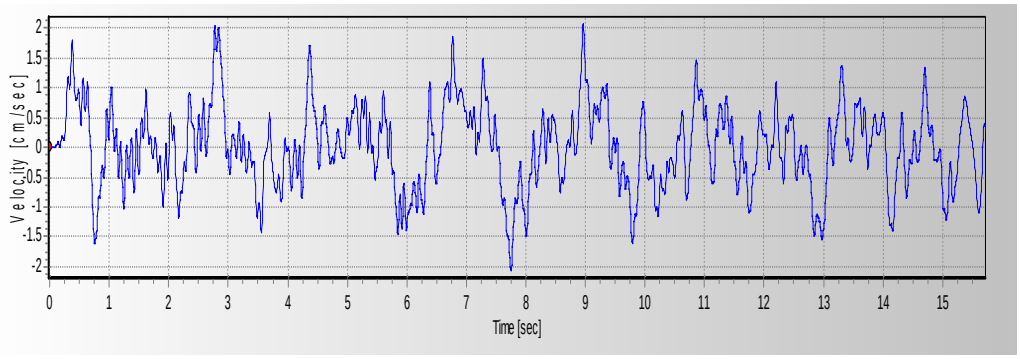

Figure C20: Velocity vs. Time History for EQ Record Number 7

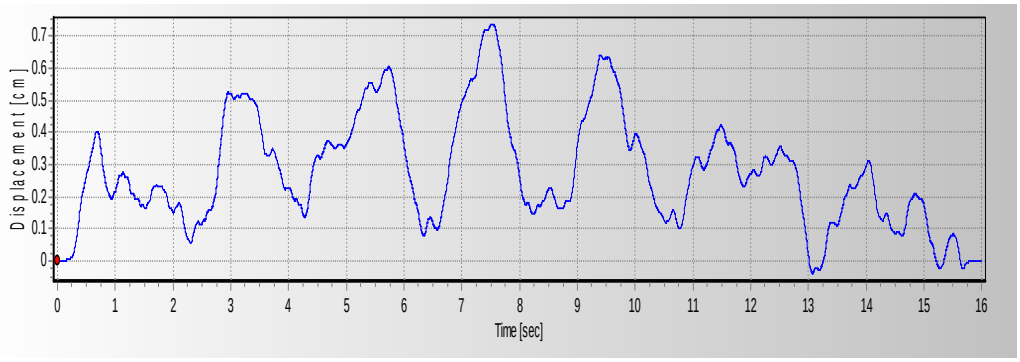

Figure C21: Displacement vs. Time History for EQ Record Number 7

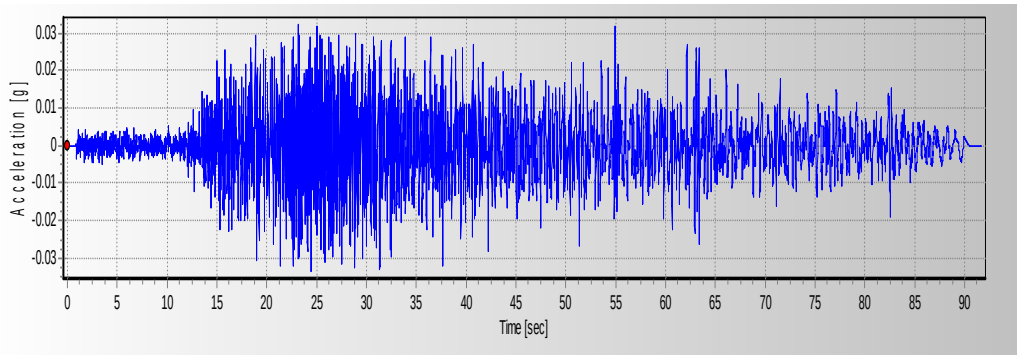

Figure C22: Acceleration vs. Time History for EQ Record Number 8

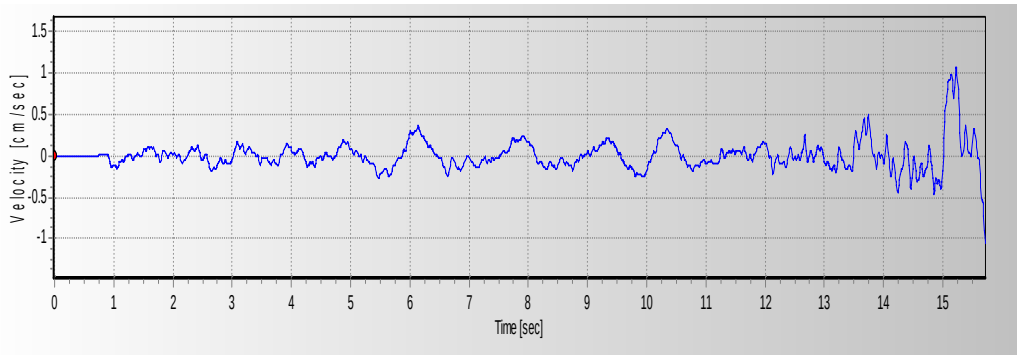

Figure C23: Velocity vs. Time History for EQ Record Number 8

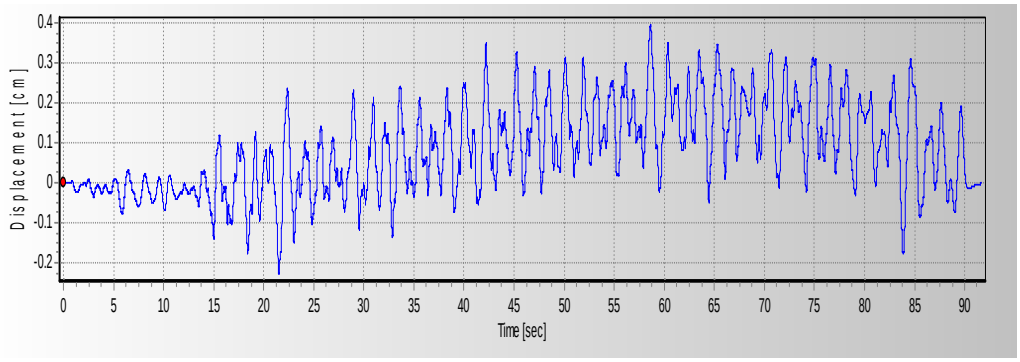

Figure C24: Displacement vs. Time History for EQ Record Number 8

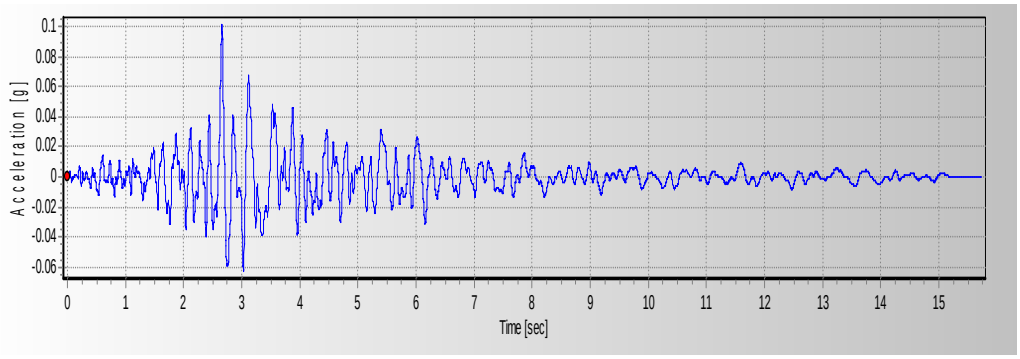

Figure C25: Acceleration vs. Time History for EQ Record Number 9

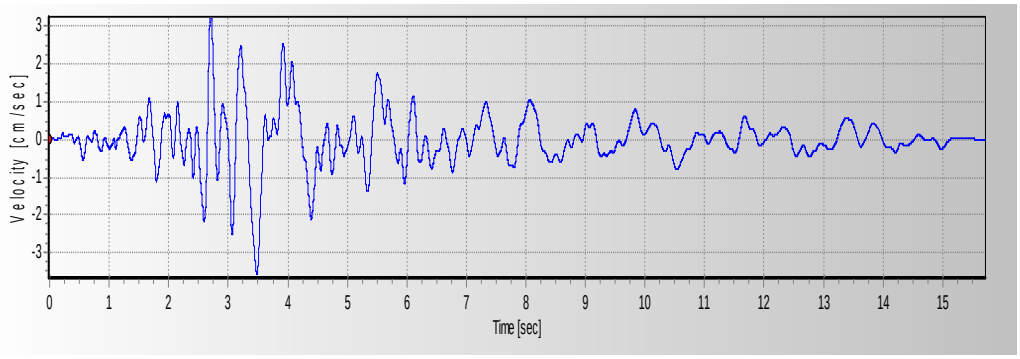

Figure C26: Velocity vs. Time History for EQ Record Number 9

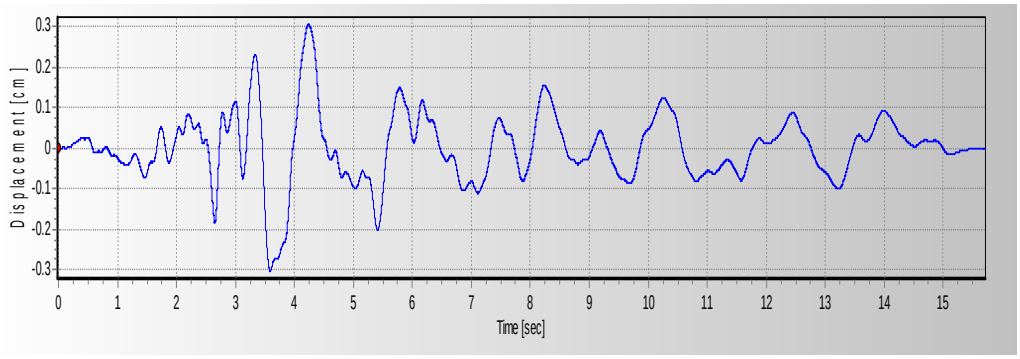

Figure C27: Displacement vs. Time History for EQ Record Number 9

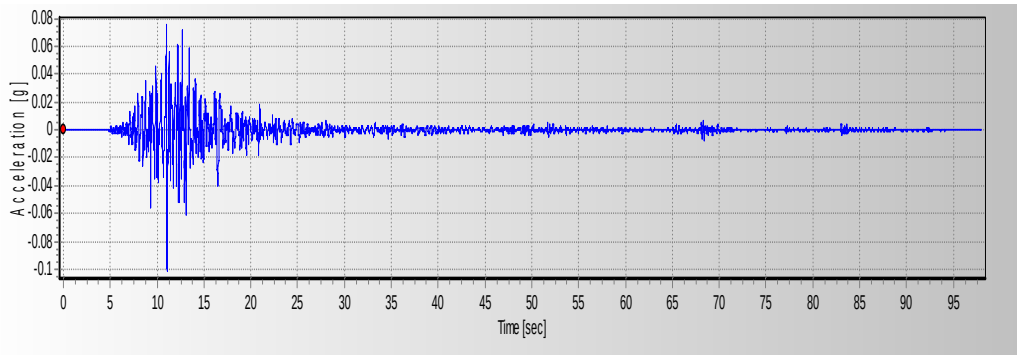

Figure C28: Acceleration vs. Time History for EQ Record Number 10

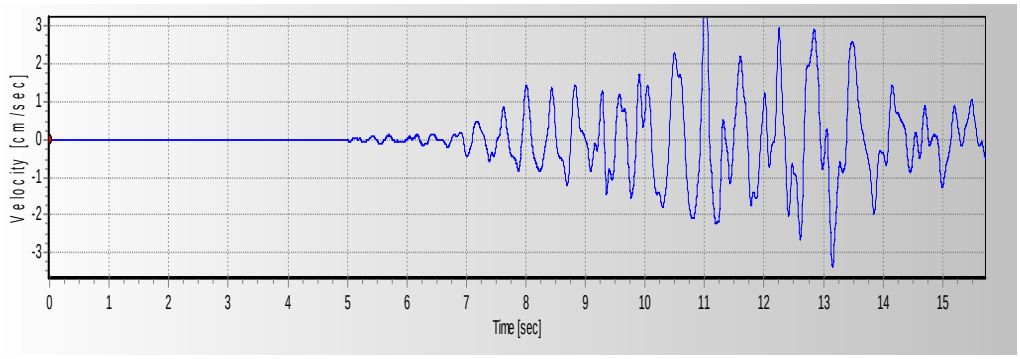

Figure C29: Velocity vs. Time History for EQ Record Number 10

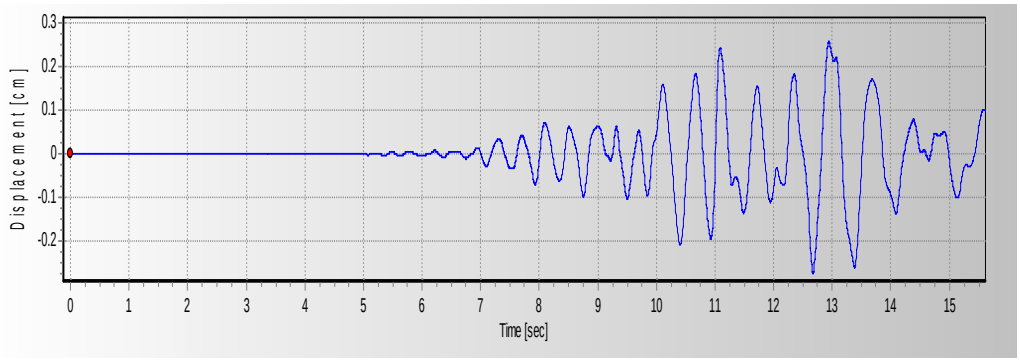

Figure C30: Displacement vs. Time History for EQ Record Number 10

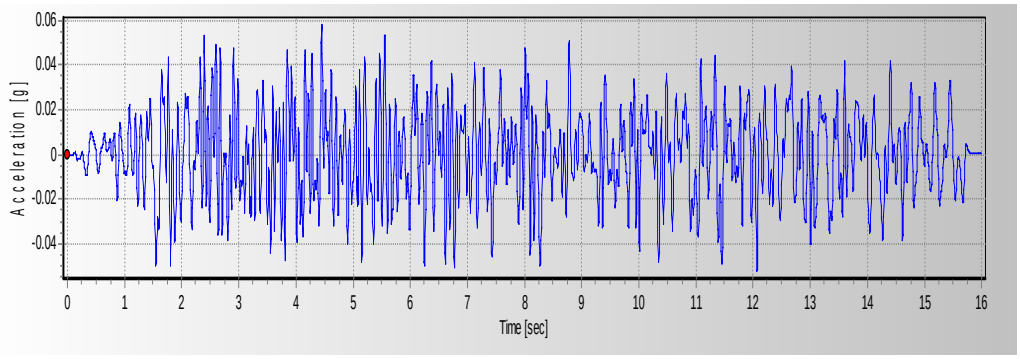

Figure C31: Acceleration vs. Time History for EQ Record Number 11

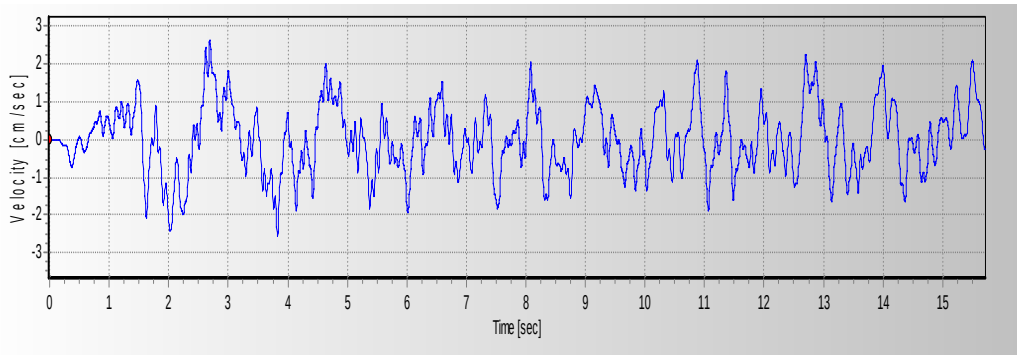

Figure C32: Velocity vs. Time History for EQ Record Number 11

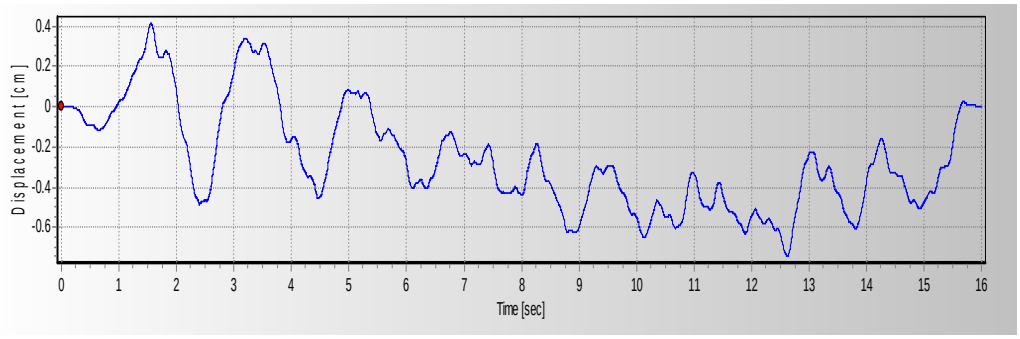

Figure C33: Displacement vs. Time History for EQ Record Number 11

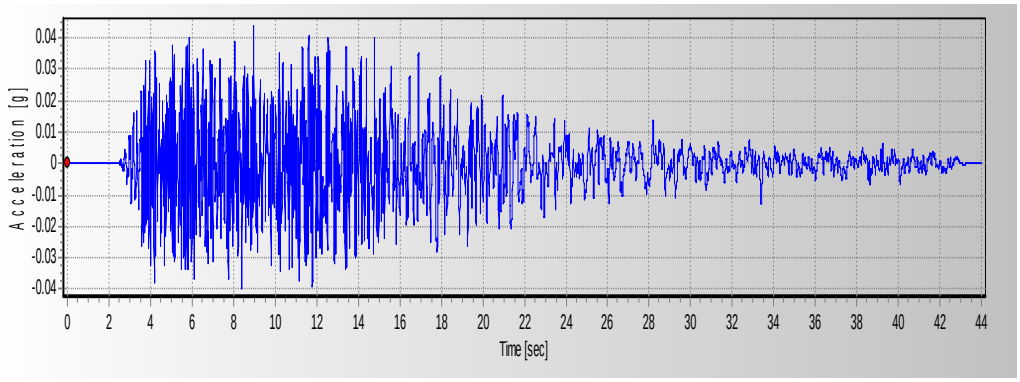

Figure C34: Acceleration vs. Time History for EQ Record Number 12

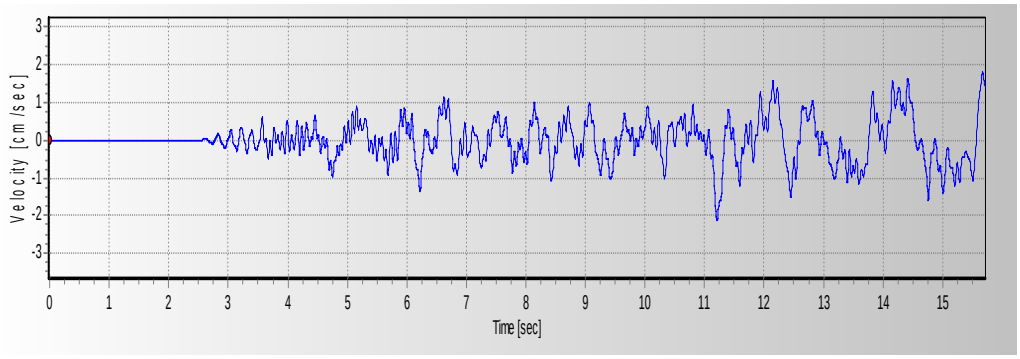

Figure C35: Velocity vs. Time History for EQ Record Number 12

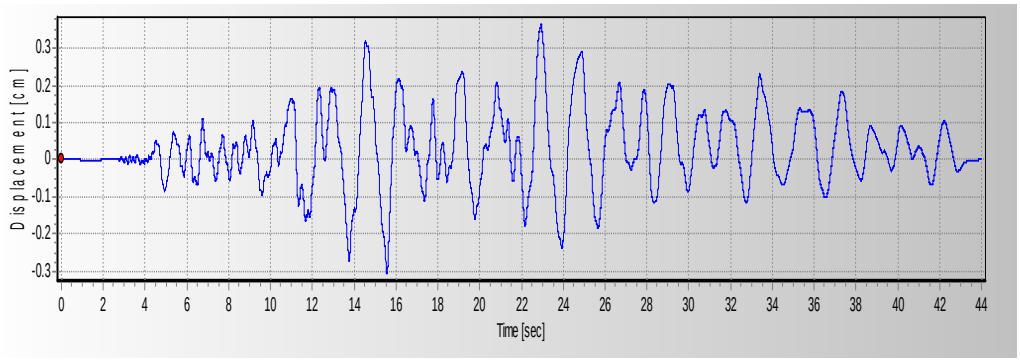

Figure C36: Displacement vs. Time History for EQ Record Number 12

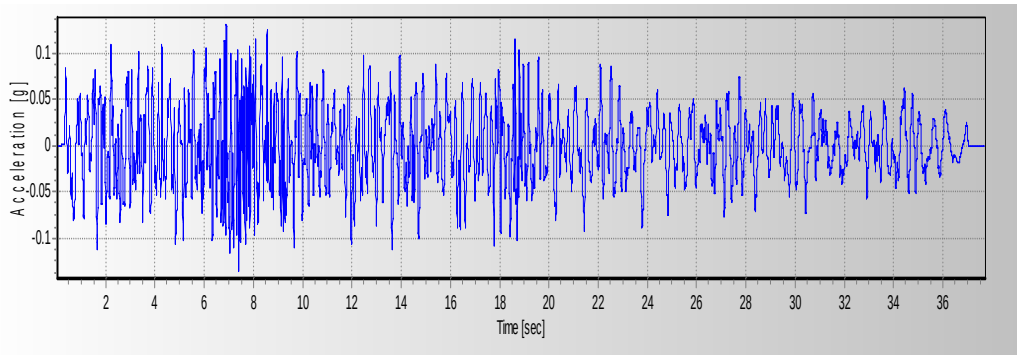

Figure C37: Acceleration vs. Time History for EQ Record Number 13

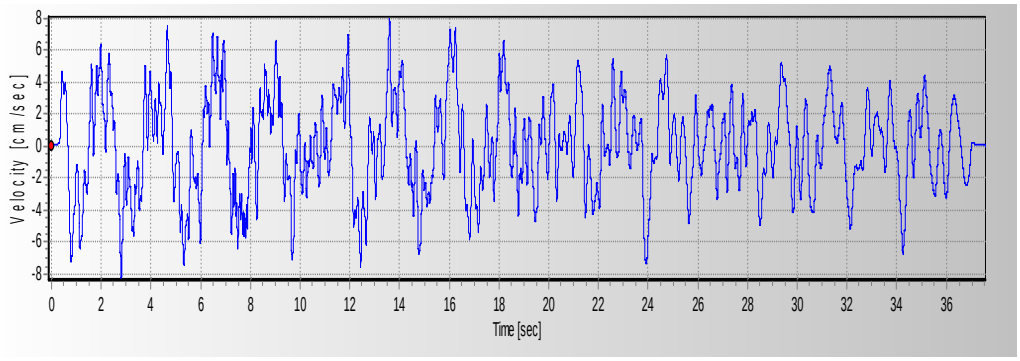

Figure C38: Velocity vs. Time History for EQ Record Number 13

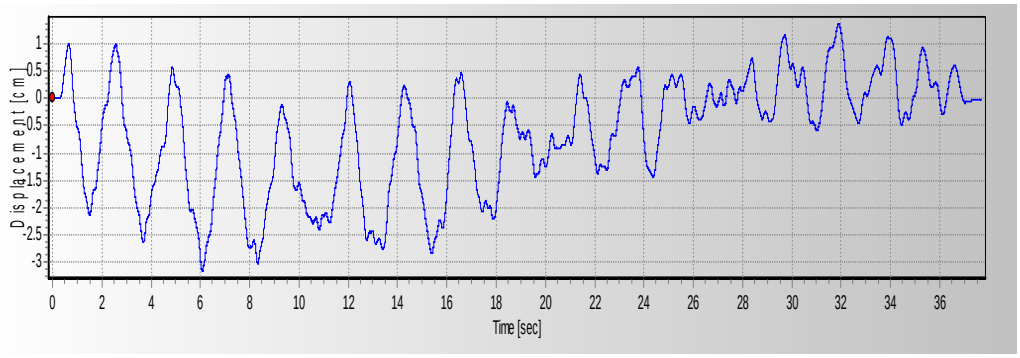

Figure C39: Displacement vs. Time History for EQ Record Number 13

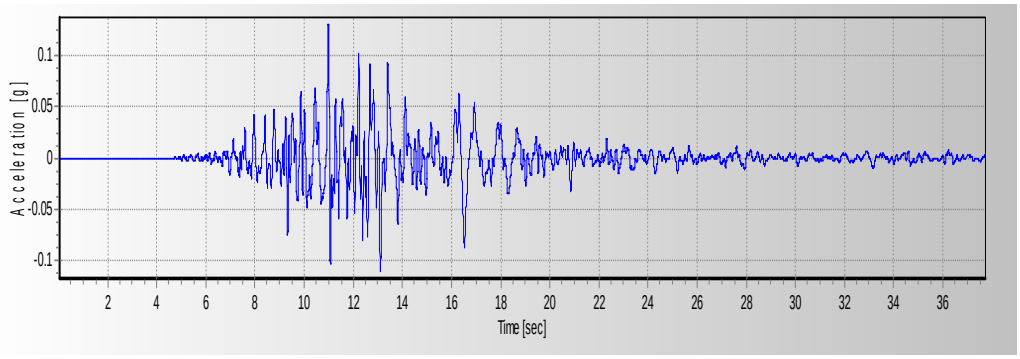

Figure C40: Acceleration vs. Time History for EQ Record Number 14

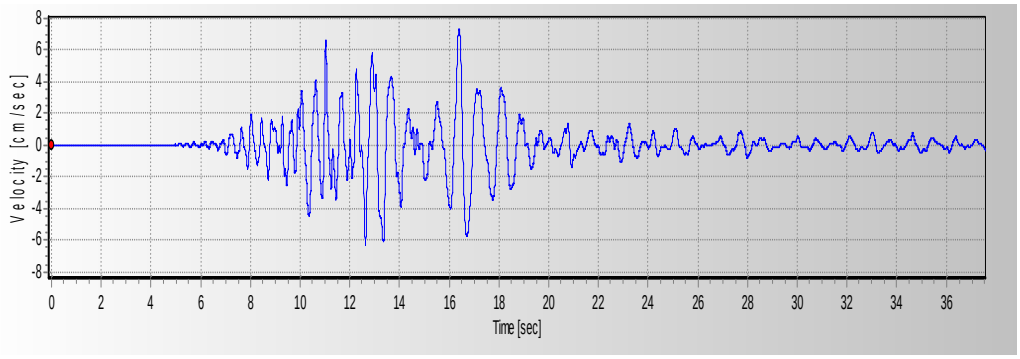

Figure C41: Velocity vs. Time History for EQ Record Number 14

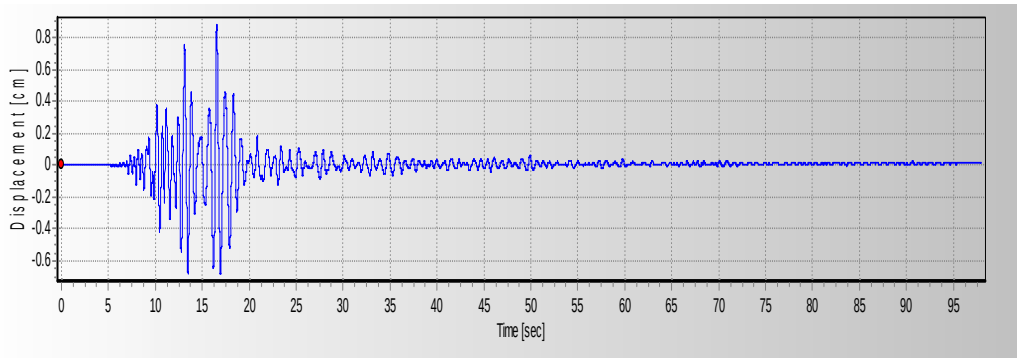

Figure C42: Displacement vs. Time History for EQ Record Number 14

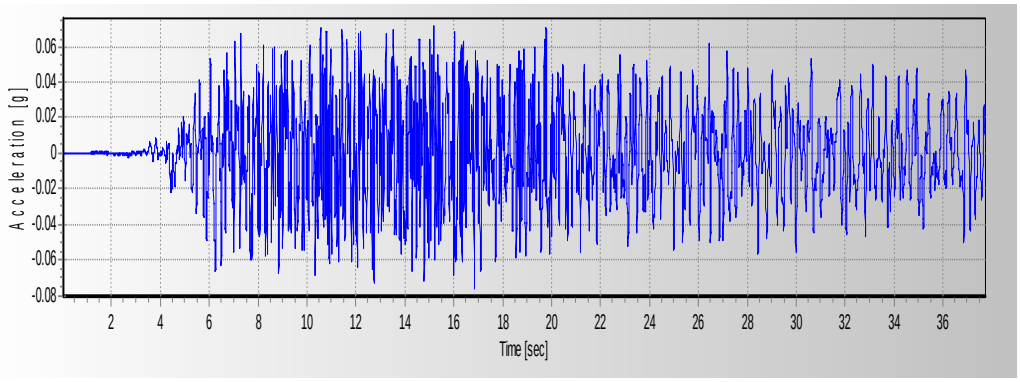

Figure C43: Acceleration vs. Time History for EQ Record Number 15

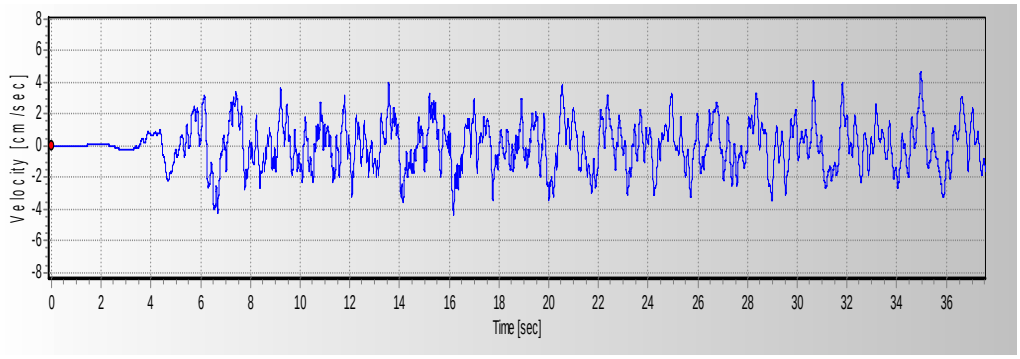

Figure C44: Velocity vs. Time History for EQ Record Number 15

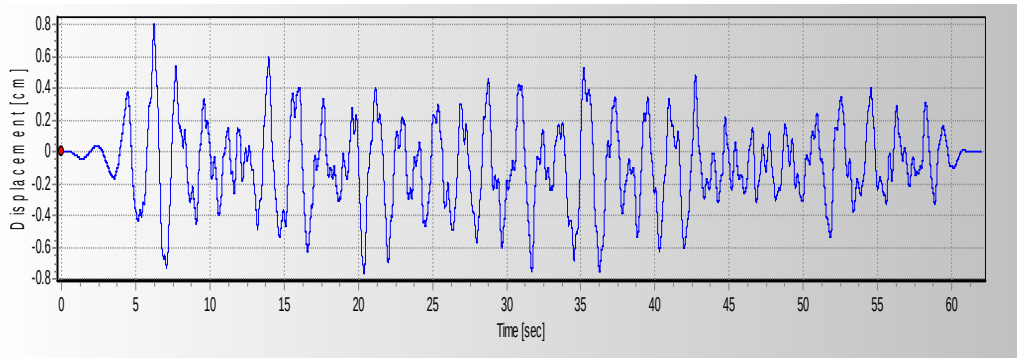

Figure C45: Displacement vs. Time History for EQ Record Number 15

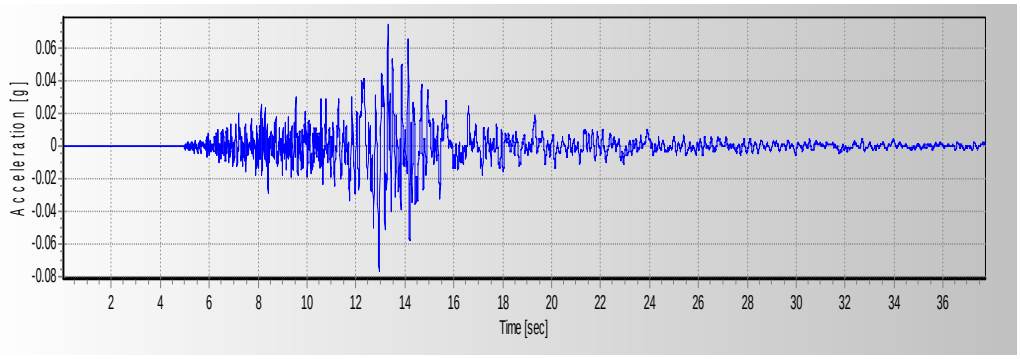

Figure C46: Acceleration vs. Time History for EQ Record Number 16

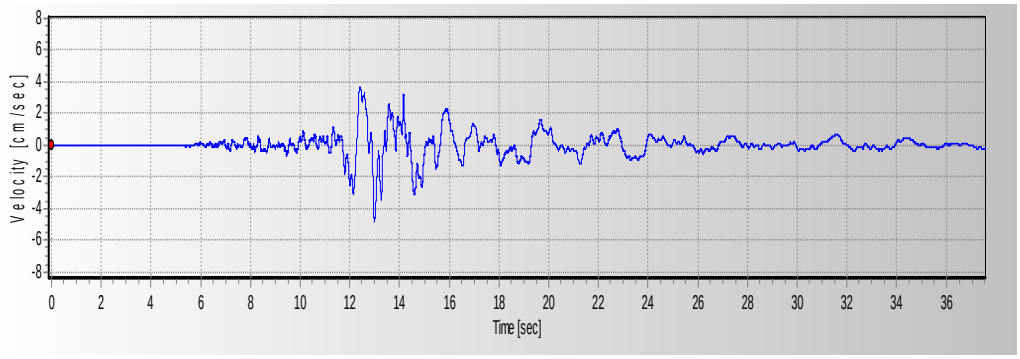

Figure C47: Velocity vs. Time History for EQ Record Number 16

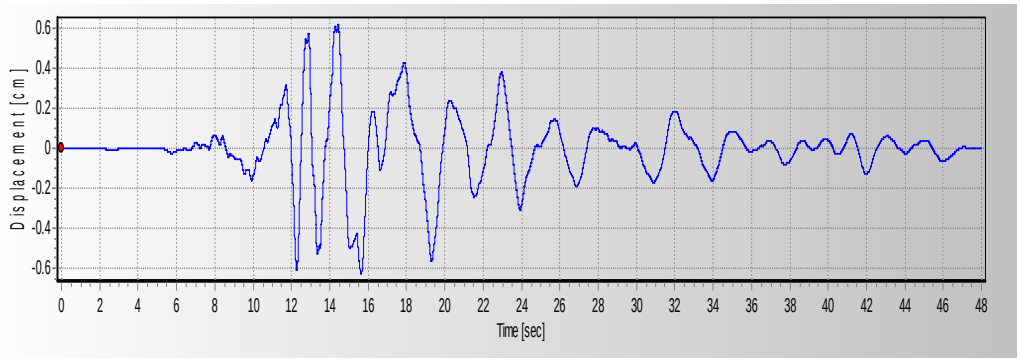

Figure C48: Displacement vs. Time History for EQ Record Number 16

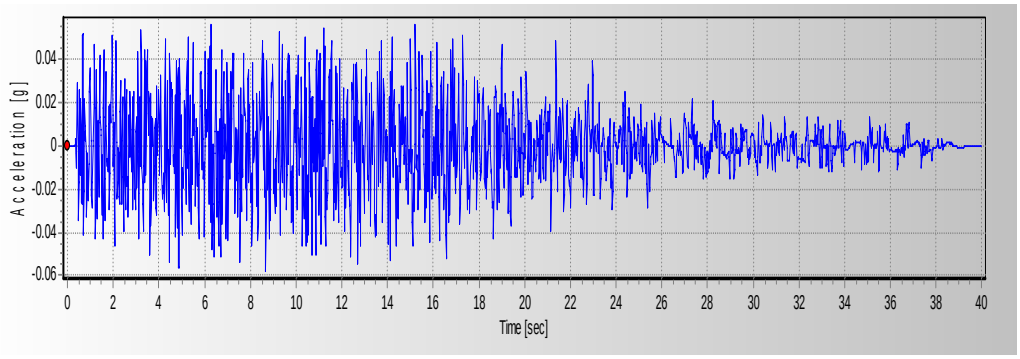

Figure C49: Acceleration vs. Time History for EQ Record Number 17

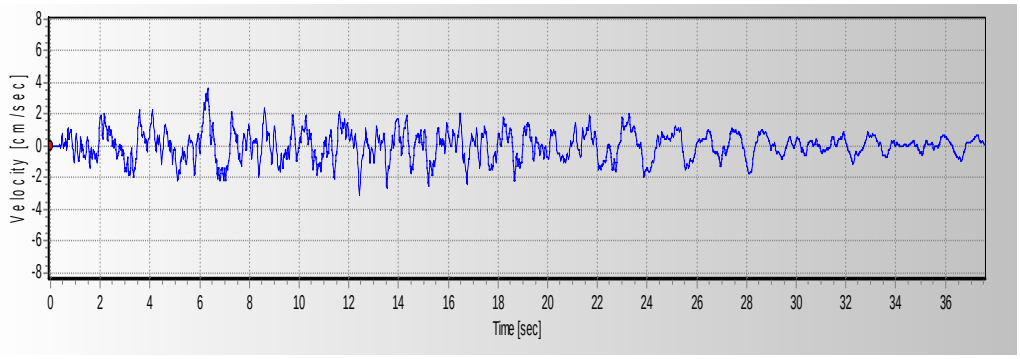

Figure C50: Velocity vs. Time History for EQ Record Number 17

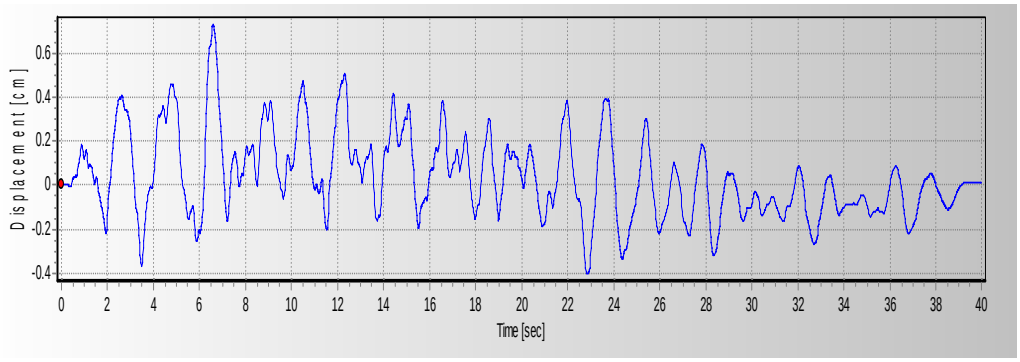

Figure C51: Displacement vs. Time History for EQ Record Number 17

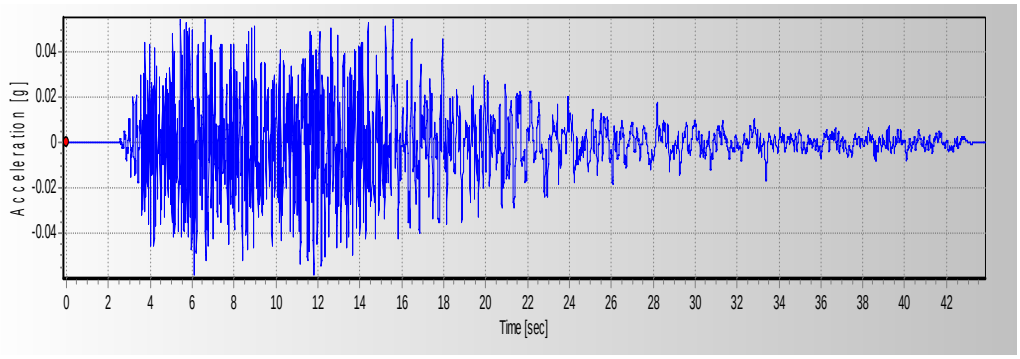

Figure C52: Acceleration vs. Time History for EQ Record Number 18

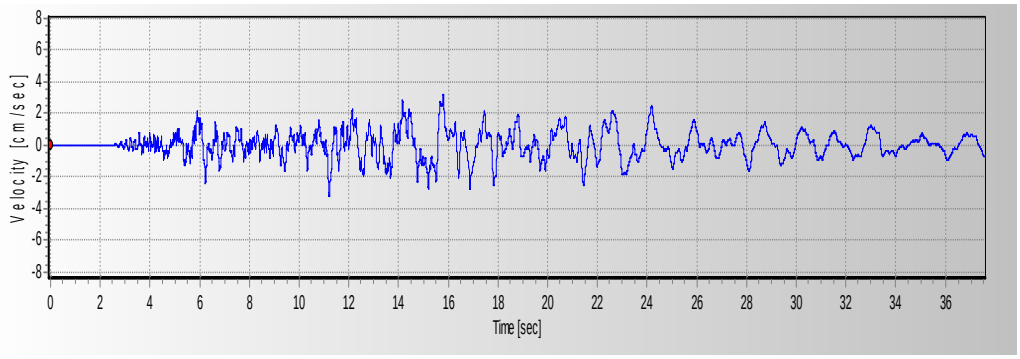

Figure C53: Velocity vs. Time History for EQ Record Number 18

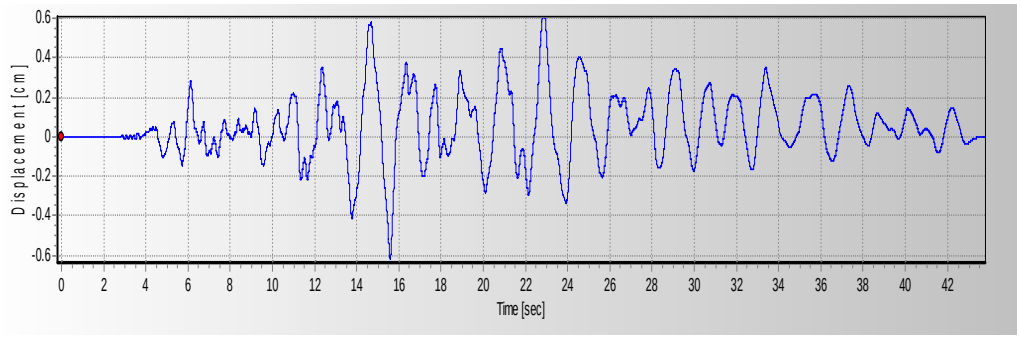

Figure C54: Displacement vs. Time History for EQ Record Number 18

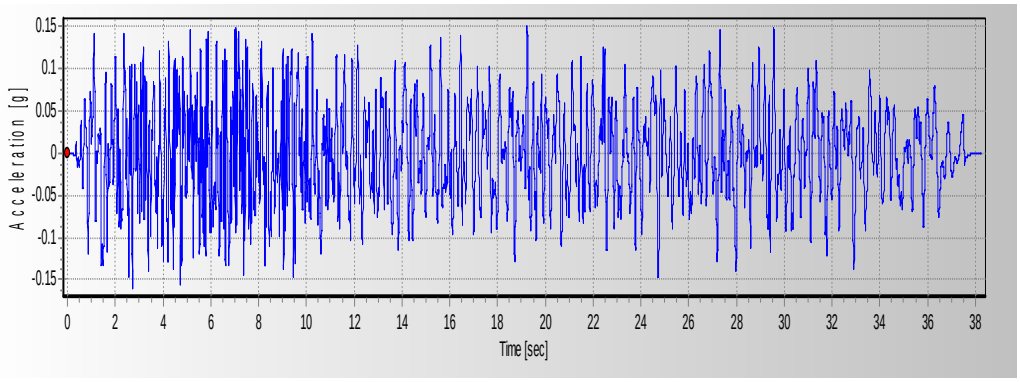

Figure C55: Acceleration vs. Time History for EQ Record Number 19

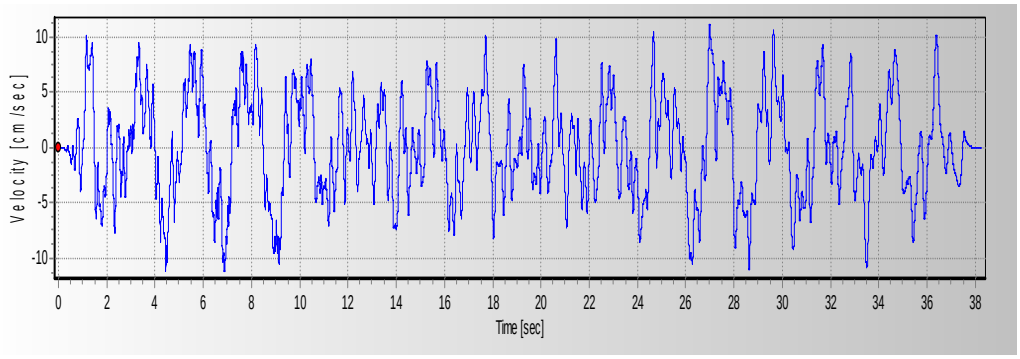

Figure C56: Velocity vs. Time History for EQ Record Number 19

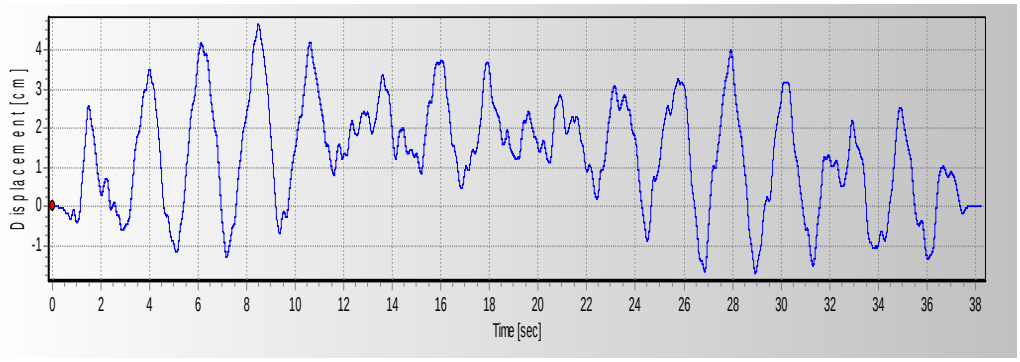

Figure C57: Displacement vs. Time History for EQ Record Number 19

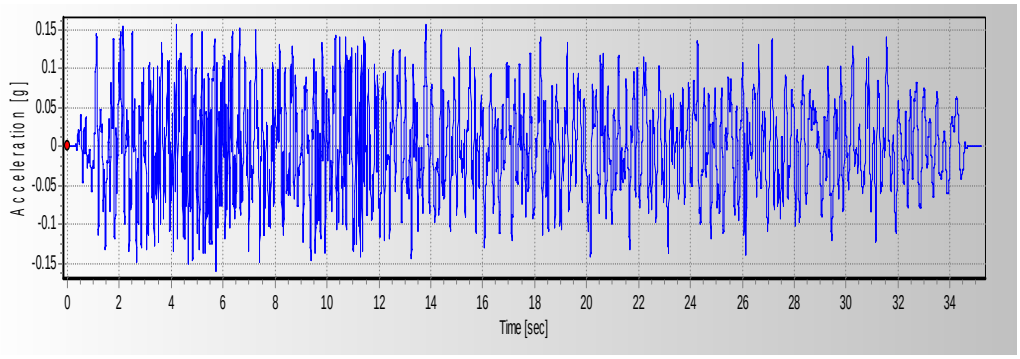

Figure C58: Acceleration vs. Time History for EQ Record Number 20

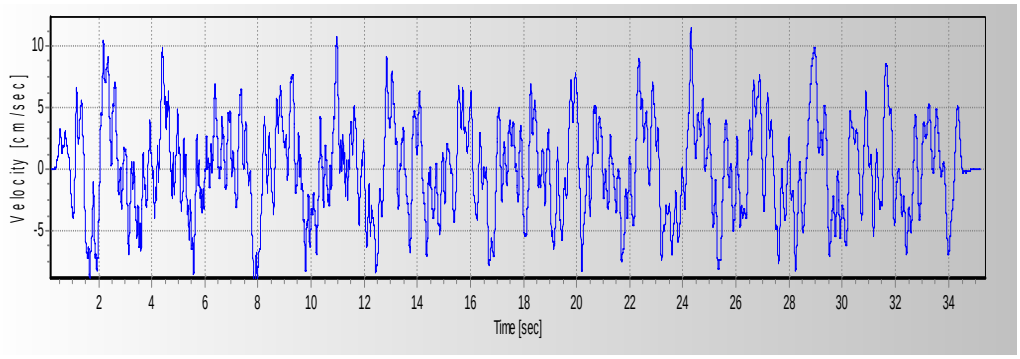

Figure C59: Velocity vs. Time History for EQ Record Number 20

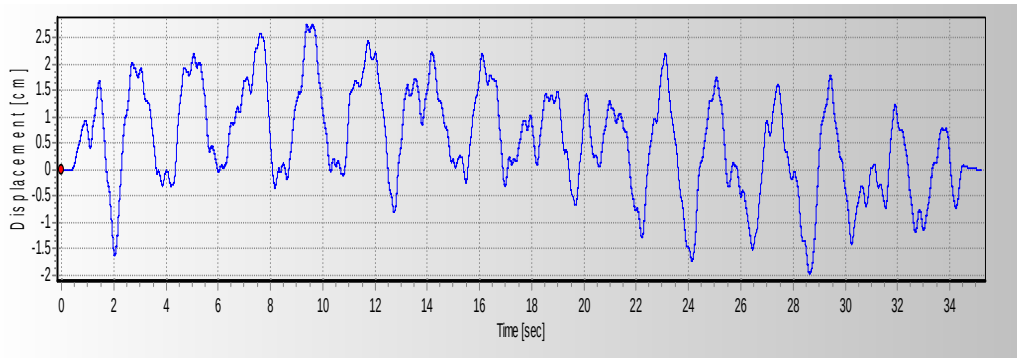

Figure C60: Displacement vs. Time History for EQ Record Number 20

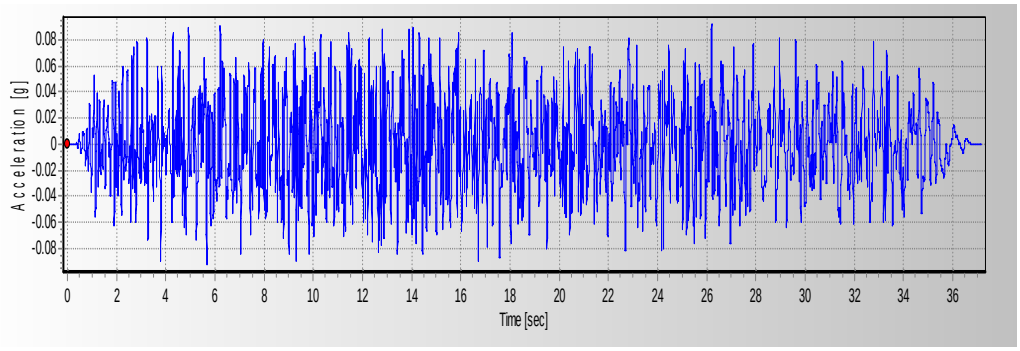

Figure C61: Acceleration vs. Time History for EQ Record Number 21

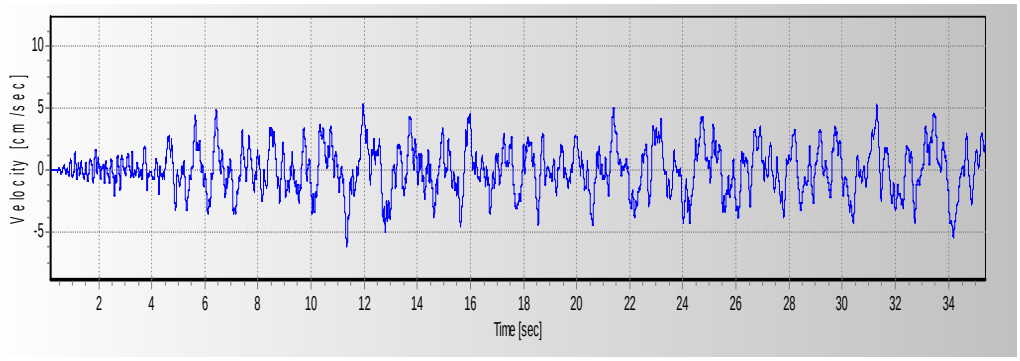

Figure C62: Velocity vs. Time History for EQ Record Number 21

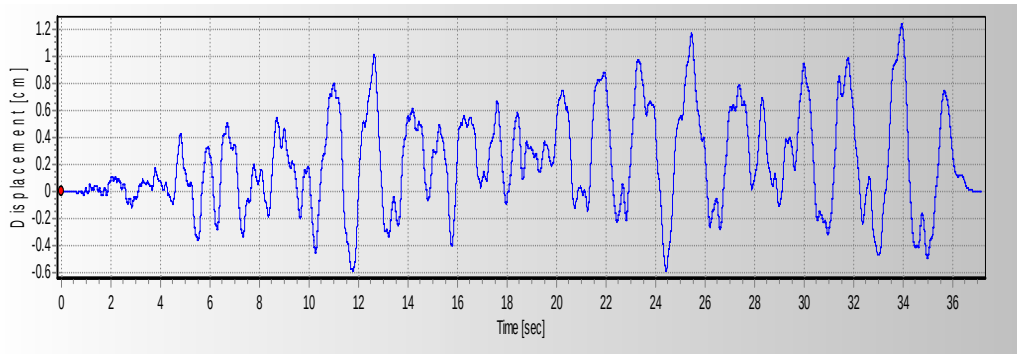

Figure C63: Displacement vs. Time History for EQ Record Number 21

,

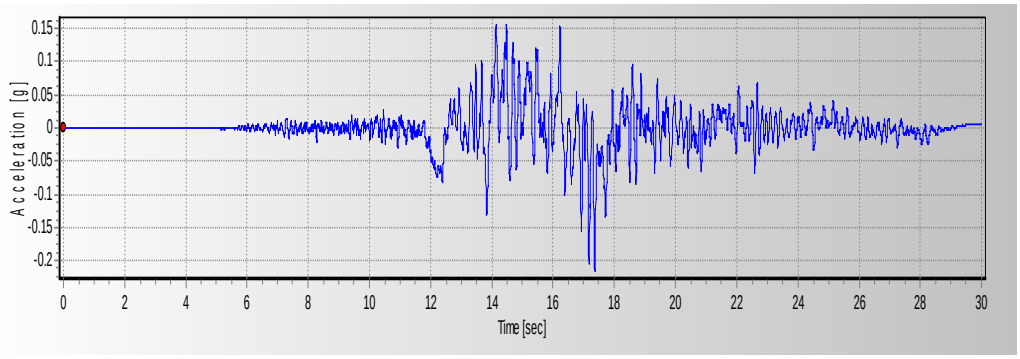

Figure C64: Acceleration vs. Time History for EQ Record Number 22

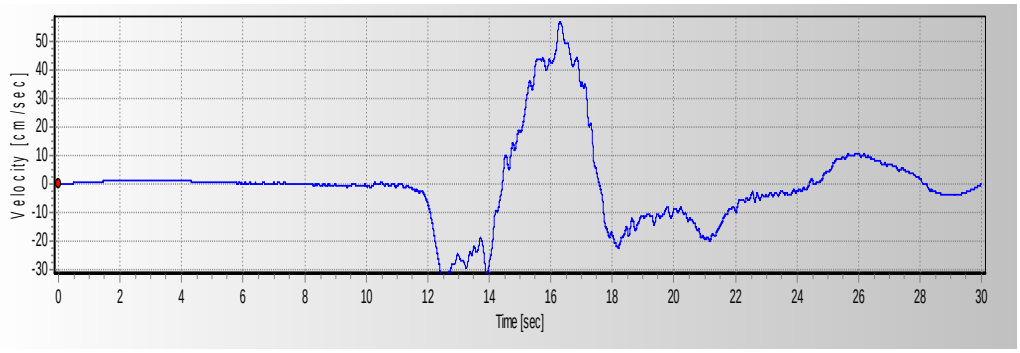

Figure C65: Velocity vs. Time History for EQ Record Number 22

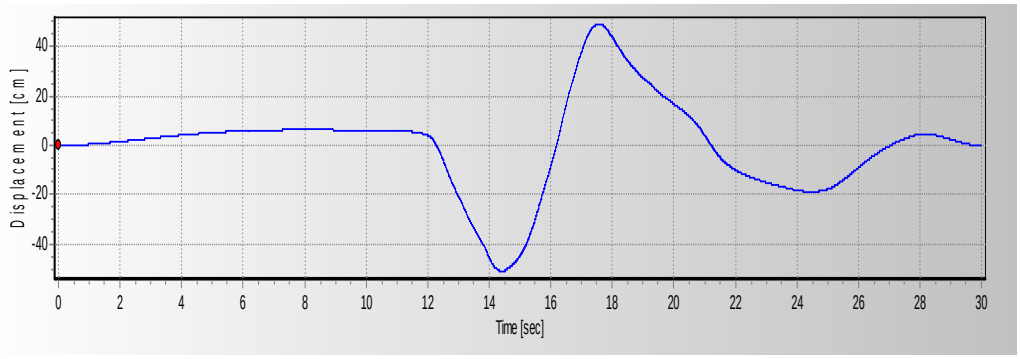

Figure C66: Displacement vs. Time History for EQ Record Number 22

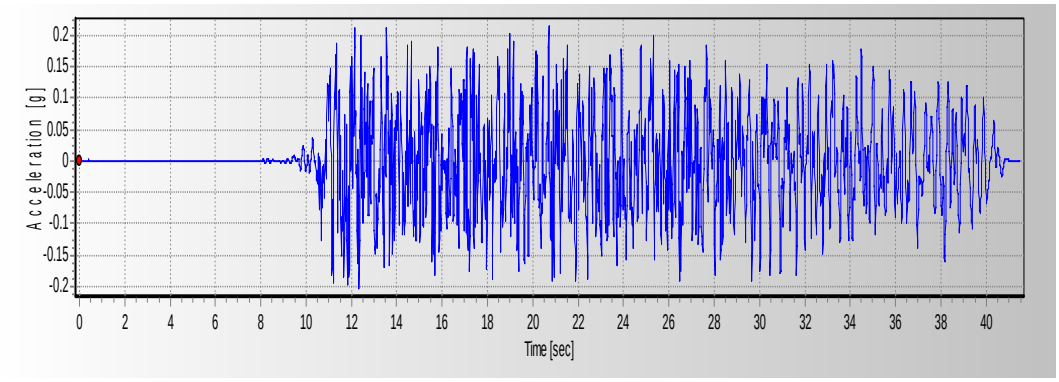

Figure C67: Acceleration vs. Time History for EQ Record Number **23**

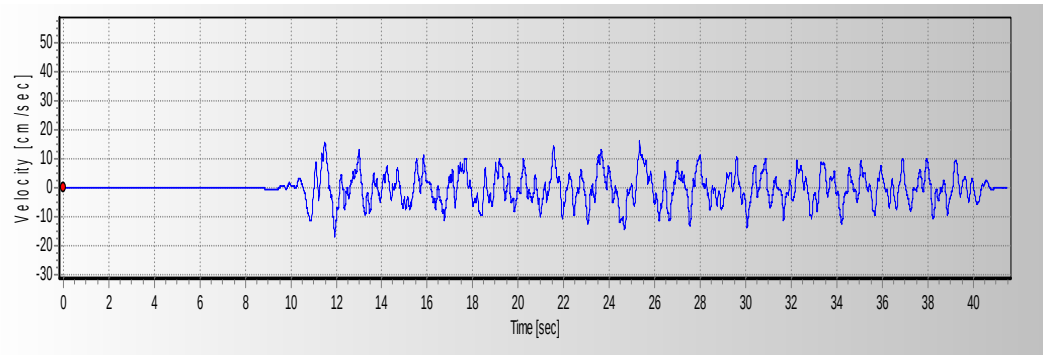

Figure C68: Velocity vs. Time History for EQ Record Number 23

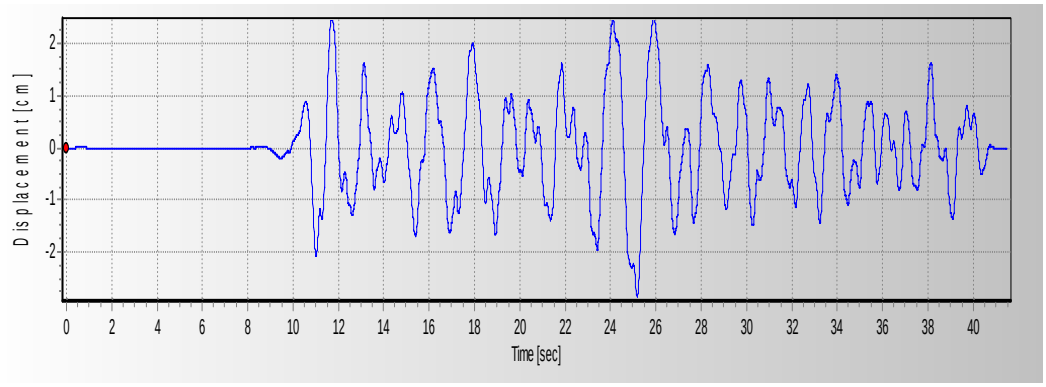

Figure C69: Displacement vs. Time History for EQ Record Number 23

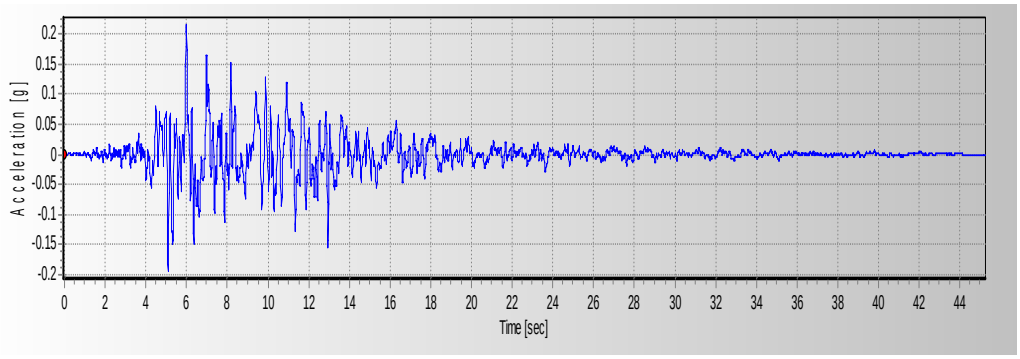

Figure C70: Acceleration vs. Time History for EQ Record Number 24

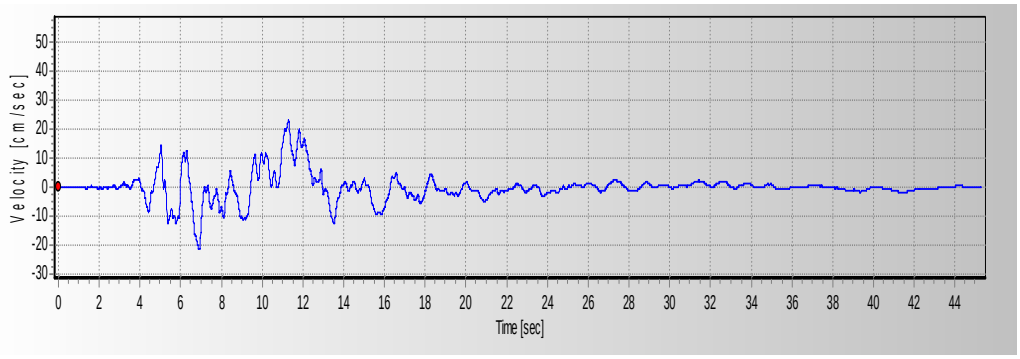

Figure C71: Velocity vs. Time History for EQ Record Number 24

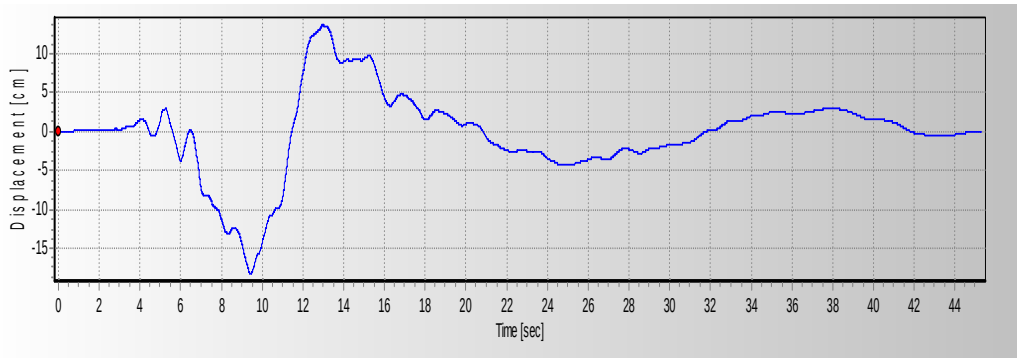

Figure C72: Displacement vs. Time History for EQ Record Number 24